The two-body reactions $K^-p \rightarrow$ Meson + Hyperon at 4.2 GeV/c

G.G.G. MASSARO

EMAN LABORATORIUM
IVERSITEIT VAN AMSTERDAM

THE TWO-BODY REACTIONS

$K^- p \rightarrow$ MESON + HYPERON at 4.2 GeV/c

ACADEMISCH PROEFSCHRIFT

ter verkrijging van de graad van doctor in de Wiskunde en Natuurwetenschappen aan de Universiteit van Amsterdam, op gezag van de Rector Magnificus Dr. G. den Boef, hoogleraar in de faculteit der Wiskunde en Natuurwetenschappen, in het openbaar te verdedigen in de aula der Universiteit (tijdelijk in de Lutherse Kerk, ingang Singel 411, hoek Spui) op 1 maart 1978, des namiddags om 13.30 uur precies.

door

Graziano Guido Giuliano Massaro

geboren te Amsterdam

PROMOTOR : Prof.Dr. J.C. Kluyver

CO-REFERENT: Dr. M.J. Losty

The author performed the work for this thesis at the "Zeeman-Laboratorium" of the "Universiteit van Amsterdam". The investigation is supported by the joint research programs of the "Stichting voor Fundamenteel Onderzoek der Materie (F.O.M.)" and the "Nederlandse Organisatie voor Zuiver Wetenschappelijk Onderzoek (Z.W.O.)".

CONTENTS

Chapter 1

INTRODUCTION

In this thesis results are presented of a study of two-body reactions of the type

$$K^{-}p \rightarrow \text{Meson} + \text{Hyperon} \qquad (1)$$

where the description of the final state includes both particles with a weak or electromagnetic decay as well as strongly decaying resonances. A great variety of $K^{-}p$ reactions, involving different reaction mechanisms, belong to this type. A special feature of these reactions is that often the polarization of the final state baryon can be measured via the analysis of a weak decay in the hyperon decay chain . Combined with the other available information this brings one very near to a complete description of the production amplitudes for these reactions, without the use of models. A list of the reactions of which results will be presented in this thesis is given in table 1, where a classification is made according to the spin-parity of the particles involved.

The data used for this study were collected in a high statistics bubble chamber experiment with a series of exposures of the CERN 2 meter chamber to a K^{-} beam of 4.2 GeV/c nominal momentum. The experiment started in 1967 as a collaboration of two groups from the University of Amsterdam and the University of Nijmegen respectively, with the aim to study $K^{-}p$ interactions at the statistical level of ~ 12 events/μb. Several publications, including two papers on two-body reactions of type (1) [1,2], resulted from that study. In 1971 a new collaboration was set up between these two groups and a group from the CERN Track

Table 1. List of the reactions discussed in this thesis.

Spin-parity group	Reactions
$0^-1/2^+ \rightarrow 0^-1/2^+$	$K^-p \rightarrow \pi^0\Lambda, \eta\Lambda, \eta'\Lambda$ $K^-p \rightarrow \pi^\mp\Sigma^\pm$ $K^-p \rightarrow K^{\overset{+}{0}}\Xi^{\overset{-}{0}}$
$0^-1/2^+ \rightarrow 0^-3/2^+$	$K^-p \rightarrow \pi^\mp\Sigma^\pm(1385)$ $K^-p \rightarrow K^+\Xi^-(1530)$
$0^-1/2^+ \rightarrow 1^-1/2^+$	$K^-p \rightarrow \rho^0\Lambda, \omega\Lambda, \phi\Lambda$ $K^-p \rightarrow \rho^0\Sigma^0, \phi\Sigma^0$
$0^-1/2^+ \rightarrow 1^-3/2^+$	$K^-p \rightarrow \rho^-\Sigma^+(1385)$ $K^-p \rightarrow \phi\Sigma^0(1385)$
$0^-1/2^+ \rightarrow 2^+1/2^+$	$K^-p \rightarrow A_2^0\Lambda, f\Lambda, f'\Lambda$ $K^-p \rightarrow f\Sigma^0, f'\Sigma^0$
$0^-1/2^+ \rightarrow 0^-3/2^-$	$K^-p \rightarrow \pi^0\Lambda(1520), \eta\Lambda(1520), \eta'\Lambda(1520)$
$0^-1/2^+ \rightarrow 1^-3/2^-$	$K^-p \rightarrow \omega\Lambda(1520), \phi\Lambda(1520)$

Chambers division. A group from the University of Oxford joined this collaboration in 1973. The collaboration set out to raise the statistical significance of the 4.2 K^-p experiment to the level of ~ 130 events/μb by analysing a total of 3.10^6 bubble chamber pictures. The measurements were completed in 1976. More details concerning the history of this experiment and the measurement efforts of the different groups are given in ref. [3] and [4].

Most of the results presented in this thesis are obtained from that part of the data which was available for analysis at the end of 1976, and which corresponded to $\sim$ 100 events/μb.

Previous bubble chamber experiments studying reactions of the type (1) above 3 GeV/c incoming momentum have a typical sensitivity of ~ 10 events/μb or less, see fig. 1.

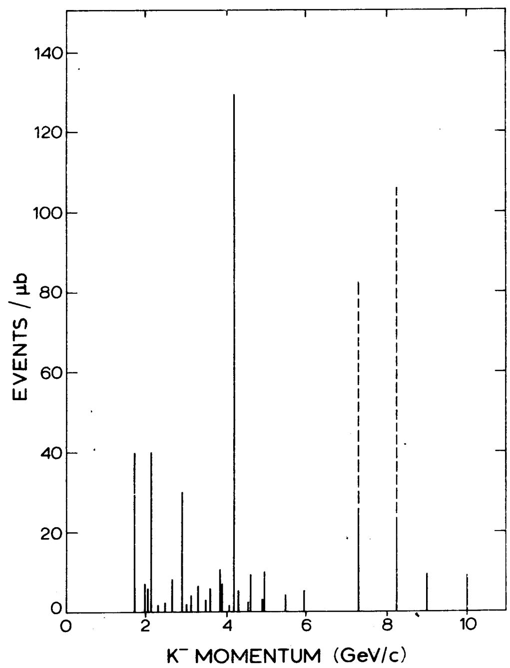

Fig. 1. Exposure sensitivity of K^-p bubble chamber experiments in the range 2-10 GeV/c, completed before 1977. The dashed lines represent experiments in progress.

High statistics data on reactions (1) obtained in counter experiments are scarce and generally limited to a small region of momentum transfer. Although it is possible with a bubble chamber to investigate these reactions over the whole momentum transfer range, the limited statistics of previous experiments restricted a detailed analysis to regions where the differential cross-section is large, which in most cases corresponds to production by meson-exchange. In our experiment we can study this production mechanism in greater detail and moreover we can study other mechanisms which result in small cross-sections like baryon-exchange and exotic-exchange.

In our experiment the two-body reactions are studied at a center-of-mass energy of ~ 3 GeV, which is high enough to neglect in most cases possible efforts of resonance formation in the s-channel, while the contribution of reactions (1) to the total cross-section is still sizable.

Chapter 2 of this thesis contains details of the total data sample and of the methods used to separate the final states of interest. Also in chapter 2 a description is given of the weighting procedures used to correct for scanning losses and of the methods applied for taking background into account.

In chapter 3 the results are presented in the form of tables and figures of differential cross-sections and, where available, the polarization distribution.

In chapter 4 the forward production of reactions (1) is discussed in terms of strange meson exchange and experimental results are compared with predictions of the additive quark model.

Spin density matrix elements have been measured for many of the reactions discussed here. The results are not listed explicitly in this thesis, but they will be used in chapter 4, if this facilitates the discussion of the data.

The results of the model independent amplitude analyses which have been performed in our experiment for some of the reactions, are also not listed explicitly in this thesis. Some of these results will be used in chapter 4 to test quark model predictions.

The main purpose of this thesis is to summarize the results of the work done in our experiment on the analysis of reactions (1). My own contribution to that work has not been of the same importance for all the results presented here. The main effort of my work was concentrated on the study of the reactions $K^-p \to \pi^\mp\Sigma^\pm$ [5], and to a lesser extent, of the reactions $K^-p \to (\pi^o,\eta,\eta')\Lambda$ [6], $K^-p \to \pi^\mp\Sigma^\pm(1385)$ [7], $K^-p \to (\rho,\omega,\phi)(\Lambda,\Sigma^o)$ [2,8] and $K^-p \to \rho^-\Sigma^+(1385)$ [9].

The reactions involving Ξ particles have been studied mainly by the CERN group of our collaboration. These studies are not yet completed and the preliminary results are included here only for comparison with the other reactions.

References Chapter 1.

1) R. Blokzijl et al., Nucl. Phys. B51 (1973) 535.

2) A.J. de Groot et al., Nucl. Phys. B74 (1974) 77.

3) H.G.J.M. Tiecke, Thesis, Universiteit van Nijmegen, 1974.

4) A.J. de Groot, Thesis, Universiteit van Amsterdam, 1975.

5) G.G.G. Massaro et al., Phys. Lett. 66B (1977) 385.

6) F. Marzano et al., Nucl. Phys. B123 (1977) 203.

7) S.O. Holmgren et al., Nucl. Phys. B119 (1977) 261.

8) M.J. Losty et al., Non-strange vector meson production in K^-p interactions at 4.2 GeV/c, CERN/EP/Phys. 77 and to be published.

9) M. Aguilar-Benitez et al., Nucl. Phys. B124 (1977) 189.

Chapter 2

EXPERIMENTAL DETAILS

2.1 Introduction

Detailed descriptions concerning the experimental set up and the processing of bubble chamber pictures have already been given in the seven theses written on this experiment in the past few years [1-7]. Therefore I will restrict myself in the following to those details which are more or less specifically connected to the analysis of the two-body reactions described in this thesis.

2.2 Beam-momentum

The total data sample was acquired during several exposures of the bubble chamber, each having an average beam-momentum between 4.09 and 4.25 GeV/c and a typical momentum spread of 0.05 GeV/c. Events with a beam momentum value too far away from the average of the corresponding exposure, were later removed from the data sample. The beam contamination deduced from a δ ray count was estimated to be $\lesssim$ 2% for π^- and $\lesssim$ 3% for μ^-.

Cross-sections of two-body reactions are expected to depend on the total center-of-mass-energy and thus on the value of the incoming momentum. It is therefore important to know at which average beam-momentum the cross-sections were calculated. The sample of $\sim$ 100 events/μb used for most of the analysis in this thesis has a total average beam-momentum of 4.15 GeV/c corresponding to a center-of-mass-energy of 3.0 GeV. For the sub-sample of events belonging to the reaction

$K^-p \to \pi^-\Sigma^+$ the distribution of the fitted beam-momentum at the chamber entrance is shown in fig. 2.2.1. The final data sample of 130 events/μb has the same average beam-momentum of 4.15 GeV/c, since the latest runs were taken at that value.

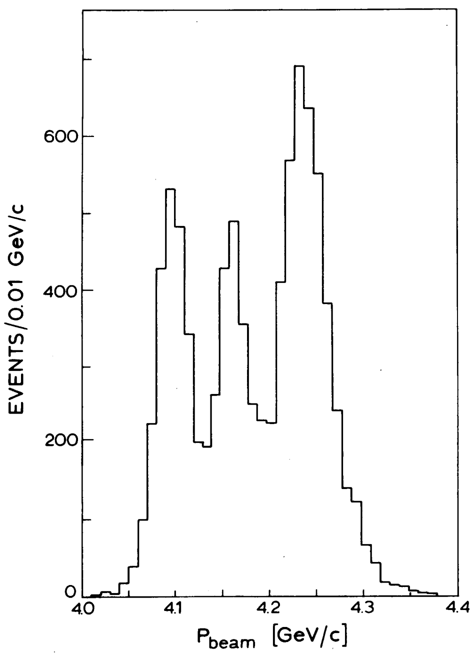

Fig. 2.2.1 Distribution of the fitted beam-momentum at the chamber entrance for a sample of events belonging to the reaction $K^-p \to \pi^-\Sigma^+$.

2.3 Cross section normalization

In order to calculate the cross section corresponding to a certain number of events (N_{ev}) of a given type, one has to know the associated total path length of the K^- beam-tracks in the bubble chamber. In our experiment this is done by counting the number (N_τ) of decays of the type $K^- \to \pi^+\pi^-\pi^-$ observed in the same picture sample. The cross-section is then calculated with the formula

$$\sigma = \frac{N_{ev}}{N_\tau} \frac{2.013}{p_{k^-}} \qquad [\text{mbarn}]$$

where p_{k^-} is the average beam-momentum in GeV/c and N_τ and N_{ev} are corrected for scanning and processing losses. The constant 2.013 is derived from Avogadro's number and the physical properties of the K^- meson and the hydrogen liquid [4].

In practice a certain data sample is characterized by its sensitivity or microbarn equivalent:

$$\frac{N_\tau \times p_{K^-}}{2013.} \quad \text{events}/\mu\text{b},$$

and the reaction cross sections are calculated with that number.

For the samples used in this thesis the statistical error due to N_τ is $\lesssim 0.5\%$ and can be neglected with respect to the statistical error in N_{ev} and the systematical error.

The systematical error comes predominantly from uncertainties in the amount of losses during processing. For a certain reaction it is estimated by comparing the cross-sections obtained from sub-samples, corresponding to different exposures and different processing chains used in each laboratory of the collaboration. For most reactions it is of the order of 5%. In the following this systematic error will only be incorporated in the error quoted for the total cross section of a reaction.

2.4 Scan-types

The events searched for on the bubble chamber pictures are divided into scan-types corresponding to different topologies. These scan-types are denoted by the code: $N^T\ N^{V^{ch}}\ N^{V^o}$, where N^T is the number of outgoing tracks seen, $N^{V^{ch}}$ is the number of these tracks which have a kink, corresponding to a weak decay of a charged strange particle in the chamber, and N^{V^o} is the number of neutral strange particles, coming from the interaction vertex and decaying visibly in the chamber.

The events used for the analyses belong to one of the following scan-types: 001, 002, 003, 201, 210, 211, 401, 410, 411. The scan type 400, processed for only part of the total film sample , is sometimes used for the reactions with a $\Lambda(1520)$ hyperon decaying into pK^-. Scanning efficiencies for different scan types are discussed in reference [3]. For the scan types mentioned above the scanning efficiency varies between 98% and 100% after the film has been scanned twice.

2.5 Separation of final states

After the events have been measured on film *), they are processed through the programming chain **), which does the geometrical reconstruction and fits the measured momenta of the charged particles to different kinematical

---

*) For the measurements we have used automatic machines (Spiral Reader, PEPR, HPD) and conventional film plane digitizers [1,7].

**) Programs used were the standard CERN THRESH/GRIND and the HYDRA GEOM/KIN packages [8].

hypotheses. At the end, one or more possible final states may have passed the corresponding χ^2-criteria of the fit. Events without a satisfactory fit are either remeasured or put into a particular Reject-category. In the calculation of topological cross-sections those Reject-events which have no trivial source of failure (e.g. unacceptable beam-parameters; outside fiducial chamber-volume; misidentified e^+e^- pair) are taken into account on the basis of their scan-type. The measurements of these failed events (where available) have been compared to those of corresponding events which had a good fit. No obvious source of kinematical bias has been found. In order to resolve ambiguities between succesfull fits the predicted track ionisations are compared to the observed bubble densities on the film. For a large fraction of the events a unique solution can be assigned. For the remaining events, which have still more than one possible final state, the procedure of preferring the fit with the highest number of constraints was followed in nearly all cases.

To illustrate this procedure we list below the most important final states for the events which belong to the topology 201 with a visible Λ-decay. (This sample provides a large part of the events used for this thesis)

		number of constraints
(i)	$K^-p \rightarrow \Lambda\pi^+\pi^-$	4C
(ii)	$\rightarrow \Sigma^o\pi^+\pi^-$	2C
(iii)	$\rightarrow \Lambda\pi^+\pi^- + \pi^o$	1C
(iv)	$\rightarrow \Lambda\pi^+\pi^-$ + neutrals	0C

Ambiguities between these final states occur frequently, especially between (i) and (ii), or between (ii) and (iii). As can be seen from the listed constraint-numbers, the final state which is higher up in the list is preferred. Also for the "multistrange" final states

$$K^-p \rightarrow \Lambda K^+K^- \quad (4C)$$

$$K^-p \rightarrow \Sigma^oK^+K^- \quad (2C)$$

which are frequently ambiguous with final state (iii) of the list above, this simple rule gives a good separation.

Ambiguities may occur however for which this procedure gives no solution, e.g. between the following hypotheses:

$$\begin{aligned} K^-p &\rightarrow \Lambda\pi^+\pi^- && + \text{ neutral(s)} && (a) \\ &\rightarrow \Lambda K^\pm\pi^\mp && + \quad '' && (b) \\ &\rightarrow \Lambda K^+K^- && + \quad '' && (c) \end{aligned}$$

Since reactions of the type $K^-p \rightarrow$ Hyperon + K-meson(s) + ... have relatively small cross-sections the final state without K-meson(s) is preferred. This will only give a small contamination in the samples of final states like (a), but of course it can not be applied bluntly when studying reactions which involve "multistrange" final states like (b) and (c).

To further increase the purity of the samples one demands in addition a χ^2-probability of > 1% for 4C and 2C-fits, and of > 5% for 1C-fits. Checks on the selection criteria are performed by looking at missing-mass distributions and Σ^o-decay distributions, as shown for example in fig. 2.5.1.

More detailed descriptions of the selection criteria for a particular final state can be found in the references quoted in the tables of chapter 3.

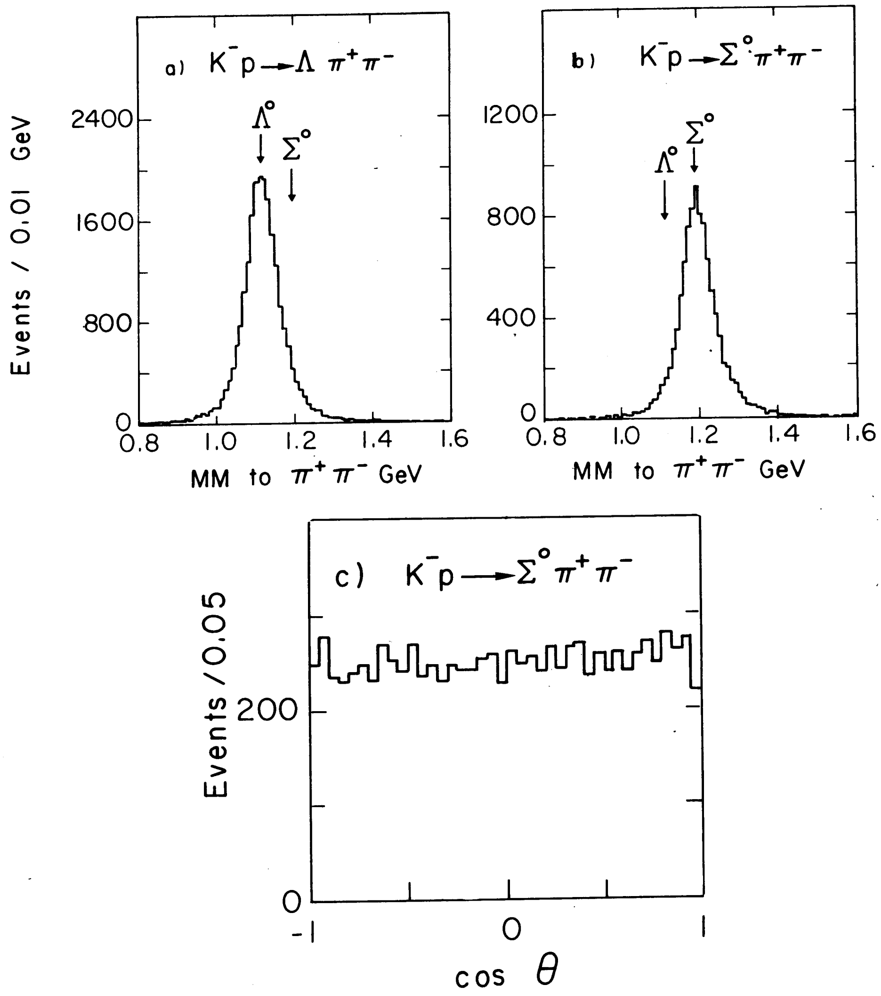

Fig. 2.5.1. Examples of checks on final state separation. The missing mass to the $\pi^+\pi^-$ system (calculated with unfitted momenta) is plotted for events assigned to the final states $\Lambda\pi^+\pi^-$ (a) and $\Sigma^o\pi^+\pi^-$ (b). The distributions show symmetric peaks which are well centered at the proper hyperon masses. In fig. (c) the cosine of the angle between the Λ direction in the Σ^o rest frame and the Σ^o line-of-flight is plotted for the $\Sigma^o\pi^+\pi^-$ sample. For the electromagnetic decay $\Sigma^o \to \Lambda\gamma$ this distribution should be flat. Contamination from $\Lambda\pi^+\pi^-$ events would show up as a peak near $\cos\,\theta = 1$.

2.6 Background problems

The two-body reactions $K^-p \to$ Meson + Hyperon discussed in this thesis can be separated into the following three classes, which present different problems when trying to obtain pure samples of events:

A) Reactions in which both the Meson and the Hyperon are "stable", i.e. they do not decay via the strong interaction. Examples of this kind are:

$$K^-p \to \pi^o\Lambda$$

$$K^-p \to \pi^{\pm}\Sigma^{\mp}$$

In this case the reaction sample is identified directly as those events which have a succesfull fit to the corresponding final state and the background problems are limited to the ones discussed in the previous section.

B) Reactions in which either the Meson or the Hyperon is a resonance, for example

$$K^-p \to \eta\Lambda \to (\pi^+\pi^-\pi^o)\Lambda$$

$$K^-p \to \omega\Lambda \to (\pi^+\pi^-\pi^o)\Lambda$$

$$K^-p \to \rho^o\Lambda \to (\pi^+\pi^-)\Lambda$$

$$K^-p \to \pi^-\Sigma^+(1385) \to \pi^-(\pi^+\Lambda)$$

$$K^-p \to \pi^+\Sigma^-(1385) \to \pi^+(\pi^-\Lambda)$$

Evidence for these reactions generally shows up in the appropriate invariant mass distributions of the corresponding final state samples, as indicated by the particle combinations between the parentheses in the above list. As an example fig. 2.6.1 shows the invariant mass distribution $M(\pi^+\pi^-\pi^o)$ for the final state $\Lambda\pi^+\pi^-\pi^o$.

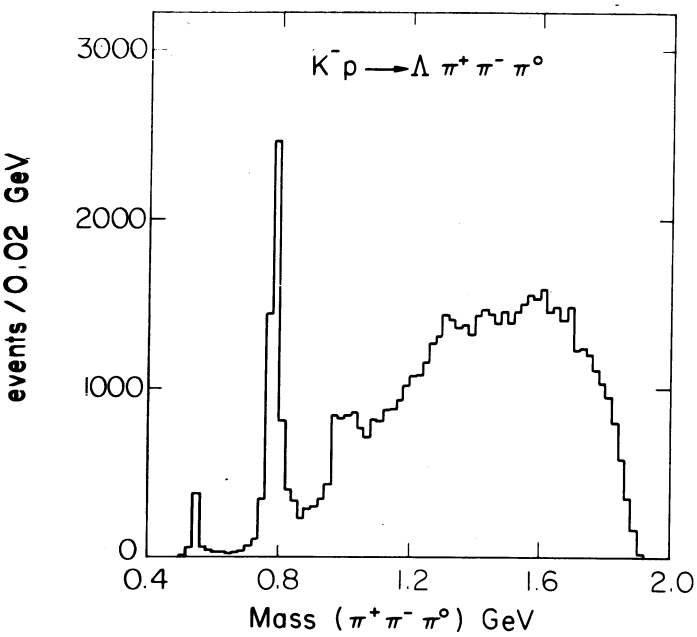

Fig. 2.6.1. The invariant mass of the $\pi^+\pi^-\pi^o$ system for the final state $\Lambda\pi^+\pi^-\pi^o$

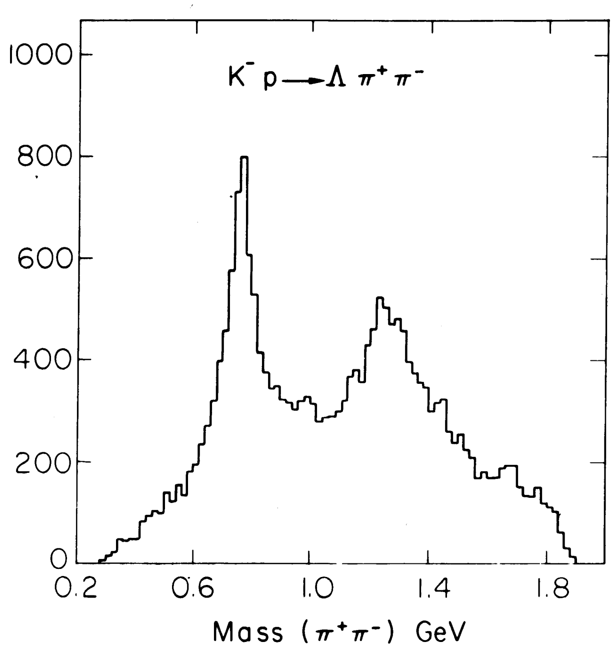

Fig. 2.6.2. The invariant mass of the $\pi^+\pi^-$ system for the final state $\Lambda\pi^+\pi^-$

The peaks at ~ 0.55 GeV and ~ 0.78 GeV correspond to production of the first two reactions listed above. The plot shows that these reactions are produced with little background. This fortunate situation does not exist for all two-body reactions, as can be seen in fig. 2.6.2, where the $M(\pi^+\pi^-)$ distribution of the $\Lambda\pi^+\pi^-$ final state sample is plotted. The broad peaks at ~ 0.77 GeV and ~ 1.28 GeV correspond to the two-body reactions $K^-p \rightarrow \rho^o\Lambda$ and $K^-p \rightarrow f^o\Lambda$ and the background under these peaks is substantial.

In fig. 2.6.4 the Dalitz plot $M^2(\Lambda\pi^+)$ -vs.- $M^2(\Lambda\pi^-)$ for events assigned to the final state $\Lambda\pi^+\pi^-$ is shown. Clear evidence for production of two-body reactions is provided in this plot by the dark bands which run parallel to the axes for $(\Lambda\pi)$ resonances and diagonally for $(\pi^+\pi^-)$ resonances. The plot shows that these bands often overlap.

From the examples presented above, it is clear that for this kind of two-body reactions the complete separation of events belonging only to one particular reaction is often made impossible by the occurrence of competing processes. For most of the reactions in this thesis the cross-sections are estimated by fitting the invariant mass distribution in the resonance region with a Breit-Wigner function and a polynomial background. The result of such a fit is shown in fig. 2.6.3 for the reaction $K^-p \rightarrow \omega\Lambda$.

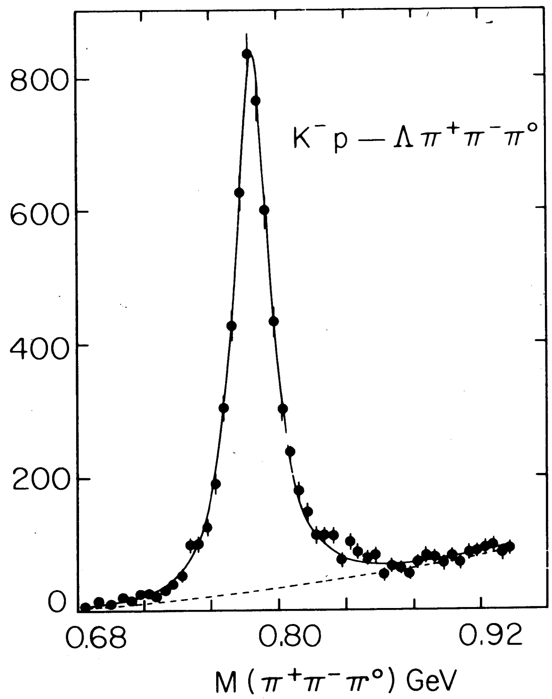

Fig. 2.6.3. Plot showing the result of the fit (solid line) to the invariant mass spectrum $M(\pi^+\pi^-\pi^o)$ in the ω region for the final state $\Lambda\pi^+\pi^-\pi^o$.

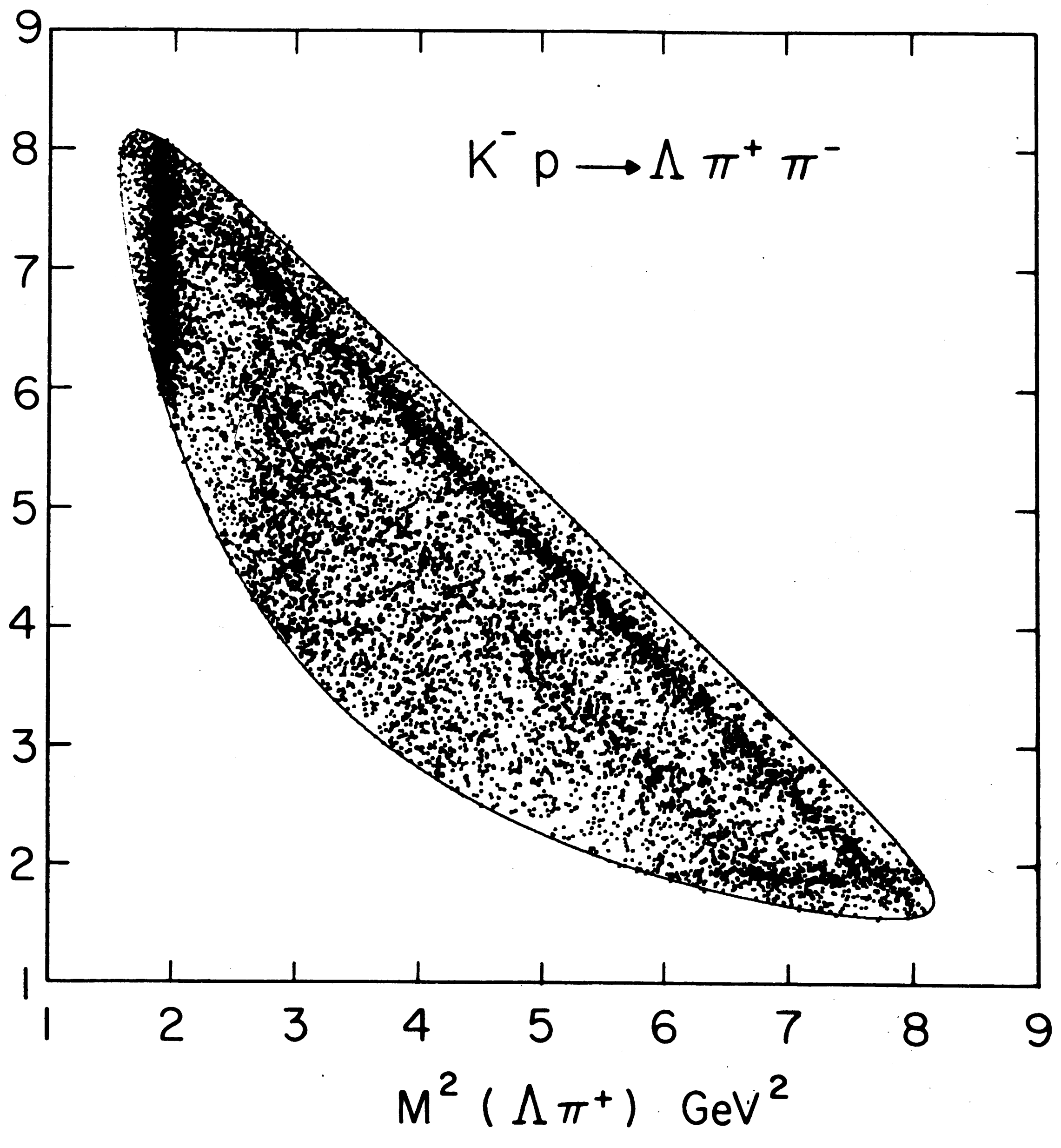

Fig. 2.6.4. Dalitz plot showing the distribution of the invariant mass squared of the $\Lambda\pi^+$ system and $\Lambda\pi^-$ system plotted against each other for the final state $\Lambda\pi^+\pi^-$.

For further analysis the reaction sample is defined by cuts in the invariant mass distribution, sometimes combined with cuts in other distributions (e.g. momentum-transfer) to reduce the amount of background in the sample. When the available statistics allow this, more sophisticated procedures are applied.

If the resonance decays via different channels one can sometimes use several final states to study the same two-body reaction, for example

$$K^-p \to \phi\Lambda \to (K^+K^-)\Lambda$$

and $$K^-p \to \phi\Lambda \to (K^o\overline{K^o})\Lambda$$

Comparison of total and differential cross-sections and other observables obtained from the different samples can be used as a check on the treatment of background or on the presence of other biases in these samples.

C) Reactions in which both the Meson and the Hyperon are resonances, for example

$$K^-p \to \rho^-\Sigma^+(1385) \to (\pi^-\pi^o)(\pi^+\Lambda)$$

In this case the associated production of the two resonances must be separated from single resonance production and other background processes. In fig. 2.6.5 the scatterplot $M(\pi^-\pi^o)$ vs. $M(\pi^+\Lambda)$ for the $\Lambda\pi^+\pi^-\pi^o$ final state shows the accumulation of events in the region where the ρ^- band ($M(\pi^-\pi^o)$ ~ 0.77 GeV) and the $\Sigma^+(1385)$ band ($M(\pi^+\Lambda)$ ~ 1.38 GeV) overlap. Cross-section estimates are obtained in this case by a "slicing-technique" [9] or similar fitting procedures [10]. The results of these fits yield background estimates for reaction samples defined by mass cuts. On the basis of these estimates one can decide whether further analysis of such a sample is useful.

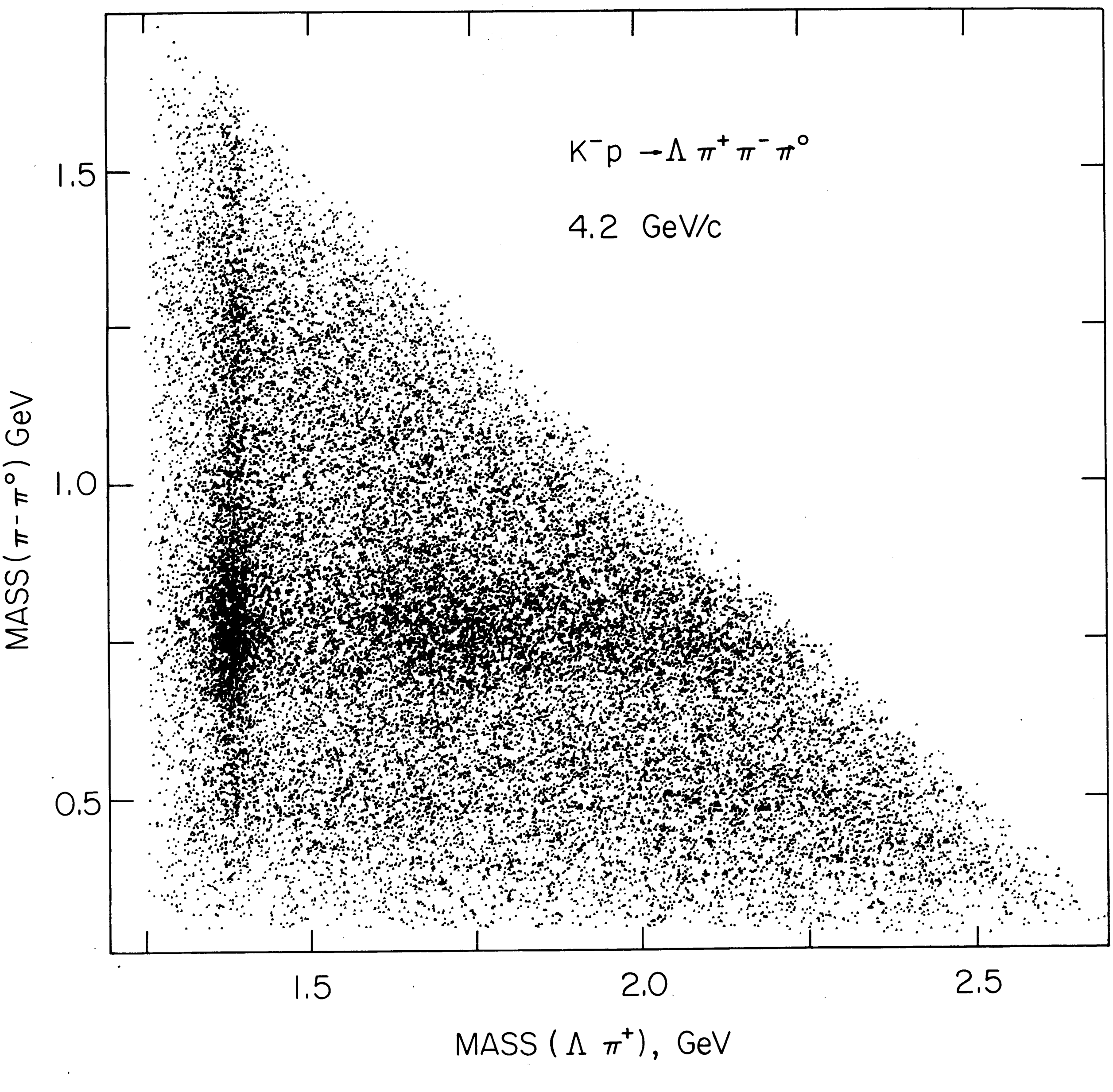

Fig. 2.6.5. Scatterplot showing the distribution of $M(\Lambda\pi^+)$ versus $M(\pi^-\pi^0)$ for the final state $\Lambda\pi^+\pi^-\pi^0$.

Detailed descriptions of the definitions of the reaction samples, the fitting procedures used, and the amount of background can be found in the references quoted in chapter 3 for each of the two-body reactions discussed there.

2.7 Event weighting

Most of the events used for this thesis have scan types involving the visible decay of a strange particle (see 2.4). When calculating cross-sections one must correct for the loss of events due to decays outside the visible region of the bubble chamber and due to decays which for geometrical reasons have not been recognized. These geometrical losses are caused by:

A) Decays which occur very near the interaction vertex.

B) Decays with a short secondary track.

C) Charged particle decays in which the projected angle between the primary and the secondary track is small.

These losses are accounted for by cuts on the projected lengths of the primary tracks, on the momenta of the charged decay products, and on the projected angles mentioned in C). The remaining events are given a weight to compensate for these cuts.

Extensive discussions on the various weighting procedures and appropriate cut-off values for our experiment are given in ref. [3] and [11]. For the event samples used in this thesis the average weight ranges from ~ 1.1 for the reaction $K^- p \to \eta\Lambda$, to ~ 1.5 for the reaction $K^- p \to \pi^- \Sigma^+$. A maximum value of 5 is allowed for an individual event weight, but very few events are rejected for this reason.

References Chapter 2

1) H. Voorthuis, Thesis, Universiteit van Amsterdam, 1973.

2) H.G.J.M. Tiecke, Thesis, Universiteit van Nijmegen, 1974.

3) A.J. de Groot, Thesis, Universiteit van Amsterdam, 1975.

4) J.J.M. Timmermans, Thesis, Universiteit van Nijmegen, 1976.

5) P.M. Heinen, Thesis, Universiteit van Nijmegen, 1976.

6) R. Blokzijl, Thesis, Universiteit van Amsterdam, 1977.

7) Th.E. Schouten, Thesis, Universiteit van Nijmegen, 1977.

8) CERN Program Library, CERN, Geneva.

9) M. Aguilar-Benitez et al., Phys. Rev. D6 (1972) 29.

10) G.G.G. Massaro, Internal Report 4.2 no. 85, Zeeman-laboratorium, Amsterdam 1977.

11) J.B. Gay Internal Report, X42-Note 75-1,2, CERN, Geneva, 1975.

Chapter 3.

CROSS SECTIONS AND POLARIZATIONS

3.1 Introduction

In this chapter the differential cross section and the hyperon polarization for the reactions

$$K^{-}p \rightarrow M(eson) + H(yperon) \qquad (1)$$

studied in our experiment will be presented. In this section the expressions used in the presentation are introduced and the variables are defined.

For the total center of mass (c.m.) system the situation in the reaction plane is plotted in fig. 3.1.1, which also defines the scattering angle θ^*.

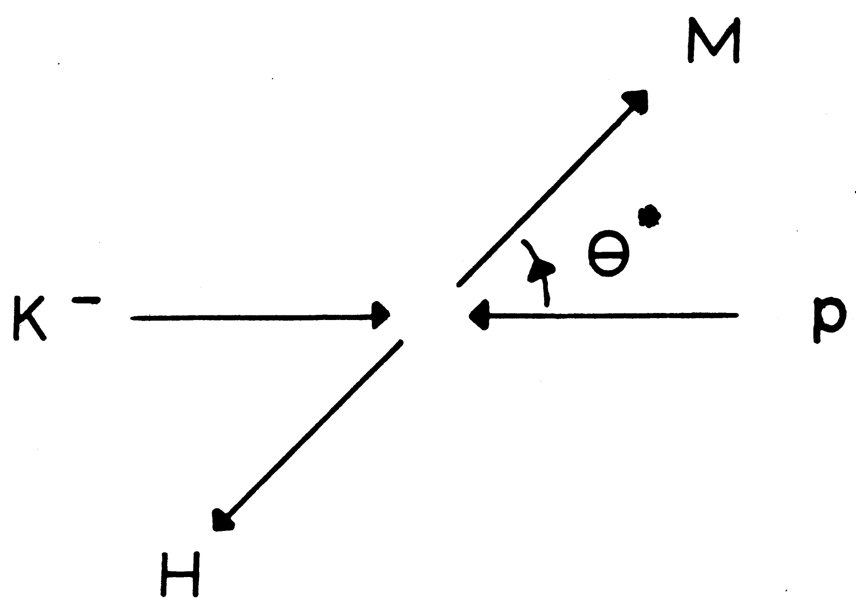

Fig. 3.1.1.

The reaction can be described in terms of three different production mechanisms, one of which proceeds via the formation of a resonance, and the other two via the exchange of virtual intermediaries. The Feynman diagrams corresponding to these so-called s-, t-, and u-channel interactions are plotted in fig. 3.1.2, together with the expression used later on for the corresponding mechanism and the region of the c.m. scattering angle θ^*, where this mechanism dominates. In addition the baryon (B), strangeness (S) and isospin (I) numbers of the possible intermediate or exchanged states are given.

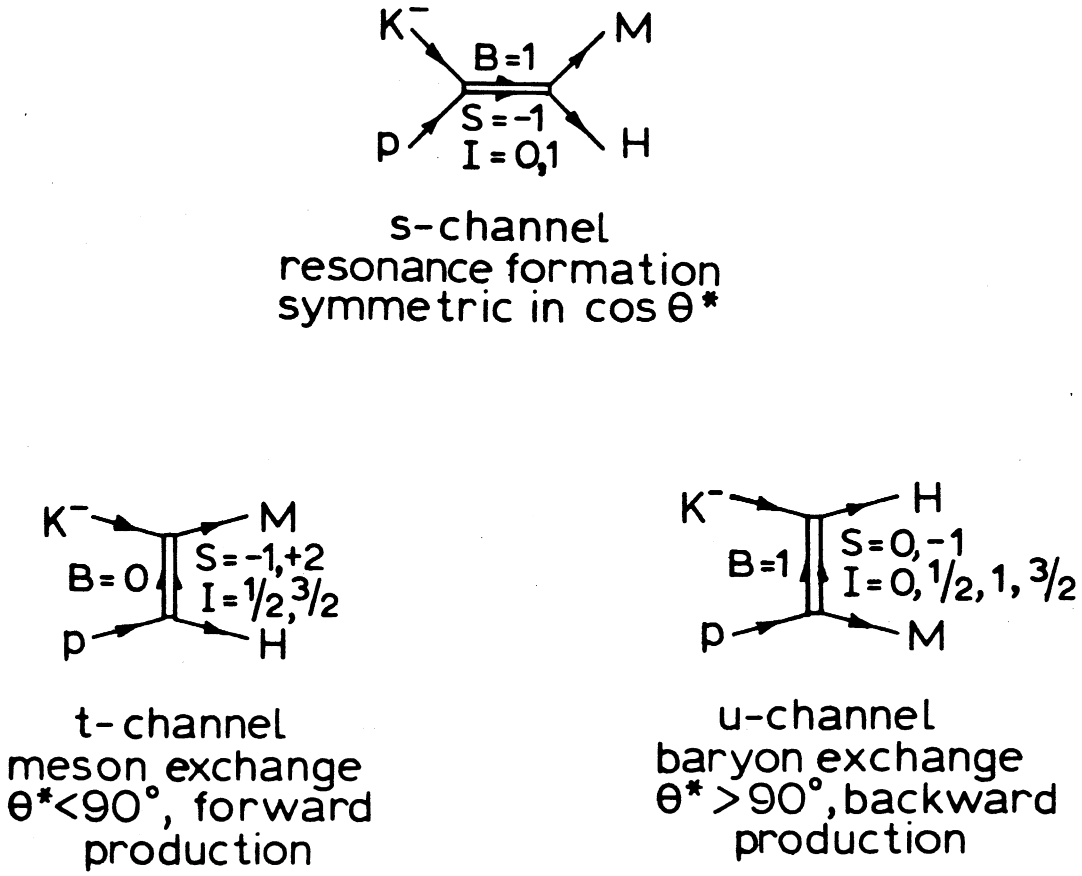

Fig. 3.1.2 Feynman diagrams for the reactions
$K^- p \to$ Meson + Hyperon.

At our c.m. energy (~ 3.0 GeV) the dominant contribution comes from meson exchange, while in general the baryon exchange cross sections are an order of magnitude smaller. Resonance formation is negligible at this energy and will only be taken into consideration when the other processes are expected to be absent for reasons discussed below. This situation is reflected in the differential cross section presented in the figures of this chapter, where in general a large forward peak and a smaller backward peak are seen.

The exchanged objects in the t- and u-channel processes are thought to be connected with real particles found in nature. This idea is supported by the fact that the absence of significant forward or backward production in a reaction often coincides with "exotic" quantum numbers in the corresponding t- or u-channel. In this thesis the term "exotic" is used for a combination of quantum numbers for which so far no bound state has been found. Examples of these exotic states are mesons with $S = 2$ or $I = 3/2$ and baryons with positive S. The absence of these states is predicted by classification schemes like SU(3) and by the quark model. Another conspicuous feature in the data is the absence of ϕ meson production by baryon exchange. This is also predicted by the quark model and will be discussed in section 3.11.

The differential cross sections and polarizations will be presented as functions of t' or u', which are defined as (see fig. 3.1.2)

$$t' = t_{max} - t \qquad , \qquad u' = u_{max} - u$$

with $t = (P_K - P_M)^2 = (P_p - P_H)^2$

$$u = (P_K - P_H)^2 = (P_p - P_M)^2$$

where P_i is the four-momentum vector of particle i and $t_{max} = t(\theta^* = 0^o)$ and $u_{max} = u(\theta^* = 180^o)$.

With these definitions t' and u' are positive numbers. The values of t_{max} and u_{max} and the maximal value of t' and u' depend on the c.m. energy and the mass of the particles. In table A1 of the appendix these values are listed for the reactions described here.

In order to facilitate the comparison of differential cross sections and polarizations for different reactions the horizontal and vertical axes of all the figures in this chapter have the same scales. The change from t' to u' on the horizontal scale is made at the point corresponding to a c.m. scattering angle of 90^o at an average beam momentum of 4.15 GeV/c.

The polarization of the hyperon is measured relative to the direction of the normal to the reaction plane defined by,

$$\hat{n} = \hat{p}_K \times \hat{p}_M = \hat{p}_p \times \hat{p}_H$$

in the c.m. system (see fig. 3.1.1). As a consequence of parity conservation in the production process, the polarization relative to a direction in the reaction plane should be zero for a two-body reaction with an unpolarized target (this can be used as a check on the purity of the reaction sample). The hyperon polarization can be measured only for those reaction samples where sufficient statistics are available and where the final state hyperon has a large asymmetry parameter α. Thus only large samples with a $\Lambda \rightarrow p\pi$ decay ($\alpha \simeq 0.65$), a $\Sigma^+ \rightarrow p\pi^o$ decay ($\alpha \simeq -0.98$) or a $\Xi^- \rightarrow \Lambda\pi^-$ decay ($\alpha \simeq -0.39$) can be used.

In the presentation the reactions will be grouped together according to the spin-parity of the particles involved.

The bulk of the data comes from reactions which belong to one of the following groups:

$$0^-1/2^+ \rightarrow 0^-1/2^+$$
$$" \quad \rightarrow 0^-3/2^+$$
$$" \quad \rightarrow 1^-1/2^+$$
$$" \quad \rightarrow 1^-3/2^+$$

In the quark model approach, where mesons are $q\bar{q}$ and baryons are qqq systems, the spin-parity combinations in the list above correspond to the multiplets with zero quark orbital angular momentum.

In addition, data will be presented on reactions belonging to one of the following groups:

$$0^-1/2^+ \rightarrow 2^+1/2^+$$
$$" \quad \rightarrow 0^-3/2^-$$
$$" \quad \rightarrow 1^-3/2^-$$

For each group of reactions the presentation will consist of a table listing the reactions together with some sample descriptions, and a table with cross sections. The differential cross sections and polarizations are presented in the figures and listed in tables in the appendix. For each reaction some comment will be given on specific features in the distributions. Table A10 in the appendix summarizes the cross sections of all the reactions presented in this chapter.

For reactions where a hyperon with spin > 1/2 and/or a meson with spin > 0 is produced, there are more observables than the differential cross section and the hyperon polarization. The spin orientation of these particles can be studied (in more detail) by analyzing the decay

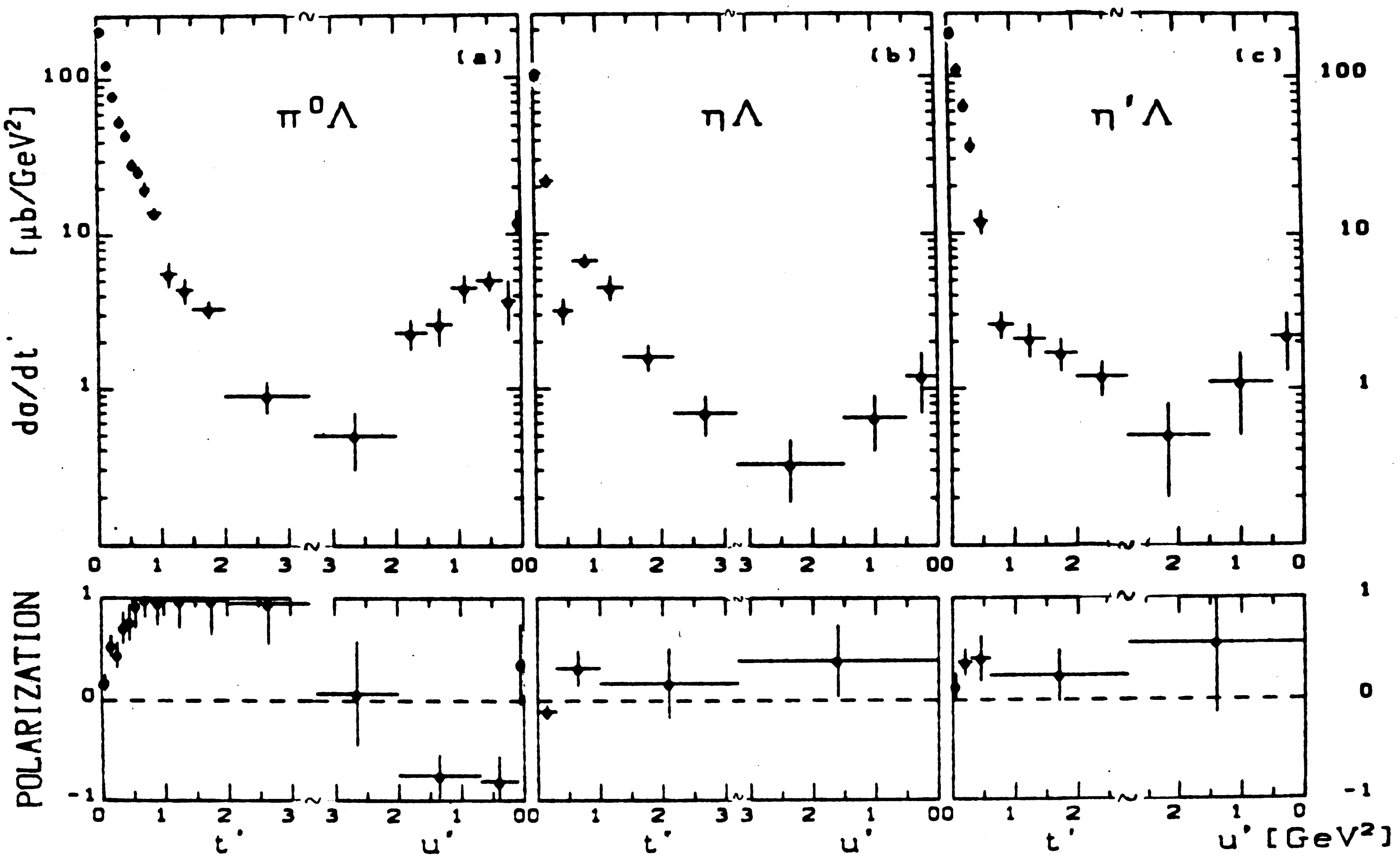

Fig. 3.2.1 Differential cross sections and polarizations for the reactions (1), (2) and (3) of the $0^-1/2^+$ group.

distributions of the strong decays. Section 3.10 contains a brief discussion on how this information can be used to obtain an almost complete description of the production amplitudes of reactions of type (1). Also in section 3.10 some examples will be given of the measurement of spin density matrix elements of the resonances produced in this reactions.

3.2 Reactions of the type $0^-1/2^+ \to 0^-1/2^+$

The reactions of this type analysed in our experiment are listed in table 3.2A and B, together with sample descriptions and cross sections. The differential cross sections and polarizations are shown in figures 3.2.1-3 and listed in table A2 in the appendix.

As can be seen in the figures the reactions (1) - (4) have a large forward peak (small t'), while in reactions (5) - (7) this peak is small or absent. Backward production (small u') is present for all reactions, although relatively small cross sections are found for reactions (2) and (3). Where measured, the hyperon polarization is often significantly different from zero and sometimes maximal.

The differential cross section of reaction (1) decreases smoothly over the forward region (fig. 3.2.1a). For backward production the distribution shows a dip at $u' \sim 0.2$ GeV^2. The Λ polarization for this reaction rises sharply with t' and is maximal over the whole forward region, while large and negative values are found for backward production.

For reaction (2) $d\sigma/dt'$ (fig. 3.2.1b) falls steeply from $t' = 0$ to a minimum at $t' \sim 0.4$ GeV^2. After a maximum at $t' \sim 0.8$ GeV^2 the decrease is more gradual. Backward production is small but peaked near $u' = 0$. The Λ-polarization

Table 3.2A Sample description for $0^-1/2^+$ reactions

	Reaction [a)]	Decay-modes [b)]	No. of events [c)]	Final state [d)]	ev/μb [e)]
(1)	$\pi^o\Lambda$	-	4000 (<1)	$\Lambda\pi^o$ (4000)	103
(2)	$\eta\Lambda$	$\eta \to \pi^+\pi^-\pi^o$	370 (<2)	$\Lambda\pi^+\pi^-\pi^o$ (56000)	103
		$\eta \to$ neutrals	1100 (40)	Λ + neutrals (54000)	
(3)	$\eta'\Lambda$	$\eta' \to \pi^+\pi^-\eta$, $\eta \to \pi^+\pi^-\pi^o$	300 (5)	$\Lambda\pi^+\pi^-\pi^+\pi^-\pi^o$ (24000)	103
		$\eta' \to \pi^+\pi^-$ + neutrals	900 (5)	$\Lambda\pi^+\pi^-$ + neutrals (96000)	
(4)	$\pi^-\Sigma^+$	-	6000 (<1)	$\Sigma^+\pi^-$ (6000)	95
(5)	$\pi^+\Sigma^-$	-	600 (<1)	$\Sigma^-\pi^+$ (600)	95
(6)	$K^+\Xi^-$	-	1000 (<1)	Ξ^-K^+ (1000)	103
(7)	$K^o\Xi^o$	-	80 (5)	K^o + neutrals (65000)	103

a) In all the tables of this chapter only the final state of the reaction is denoted. The initial state is of course K^-p.

b) The column lists the decay-modes of the resonances used in the analysis of the two-body reaction.

c) The approximate number of events in a reaction sample defined by reasonable mass cuts is listed. The number between brackets is the estimated percentage of background in this sample. This number can change significantly when a momentum transfer cut is applied.

d) The approximate number of events assigned to the final state is listed between brackets.

e) The sensitivity of the data sample, available at the time the reaction was studied.

Table 3.2B Cross sections for $0^- 1/2^+$ reactions

	Reaction	σ_T a)	σ_F b)	σ_B c)	Reference
(1)	$\pi^o \Lambda$	74.5 ± 4.2	66.0 ± 4.1	8.5 ± 0.7	[2]
(2)	$\eta \Lambda$	24.8 ± 1.3	22.9 ± 1.2	1.9 ± 0.4	"
(3)	$\eta' \Lambda$	50.5 ± 2.9	47.6 ± 2.8	2.9 ± 0.8	"
(4)	$\pi^- \Sigma^+$	154 ± 8	137 ± 7	16.0 ± 1.0	[3]
(5)	$\pi^+ \Sigma^-$	10.4 ± 0.7	1.3 ± 0.2	9.0 ± 0.6	"
(6)	$K^+ \Xi^-$	14.5 ± 1.0	1.4 ± 0.2	13.2 ± 1.0	[4]
(7)	$K^o \Xi^o$	-	-	6.1 ± 0.8 (u'<1.0)	"

a) The total cross section. All cross sections in the tables are in μb. The cross sections have been corrected for unobserved decay modes using the branching ratios of reference [1].

b) The cross section for the forward hemisphere. Sometimes a smaller region is used to get a better background separation. In this case the momentum transfer cut is indicated in GeV^2 between brackets.

c) The cross section for the backward hemisphere, see note b).

is much smaller than found in reaction (1) and of opposite sign in the backward region.

Reaction (3) shows a break in the dσ/dt' distribution at $t' \sim 0.8$ GeV^2 (fig. 3.2.1c). Backward production resembles that of reaction (2). In the forward direction the polarization is ~30% of that of reaction (1).

Reaction (4) shows interesting structures both in the differential cross section and the polarization distribution (fig. 3.2.2a). Dips or breaks are seen at $t' \sim 0.6$, $u' \sim 1.0$ and $t' \sim u' \sim 3.2$ GeV^2. In the forward direction the polarization is negative and large. For backward production the polarization is positive on average. There are remarkable correlations between the structures in the differential cross section and those in the polarization distribution of this reaction.

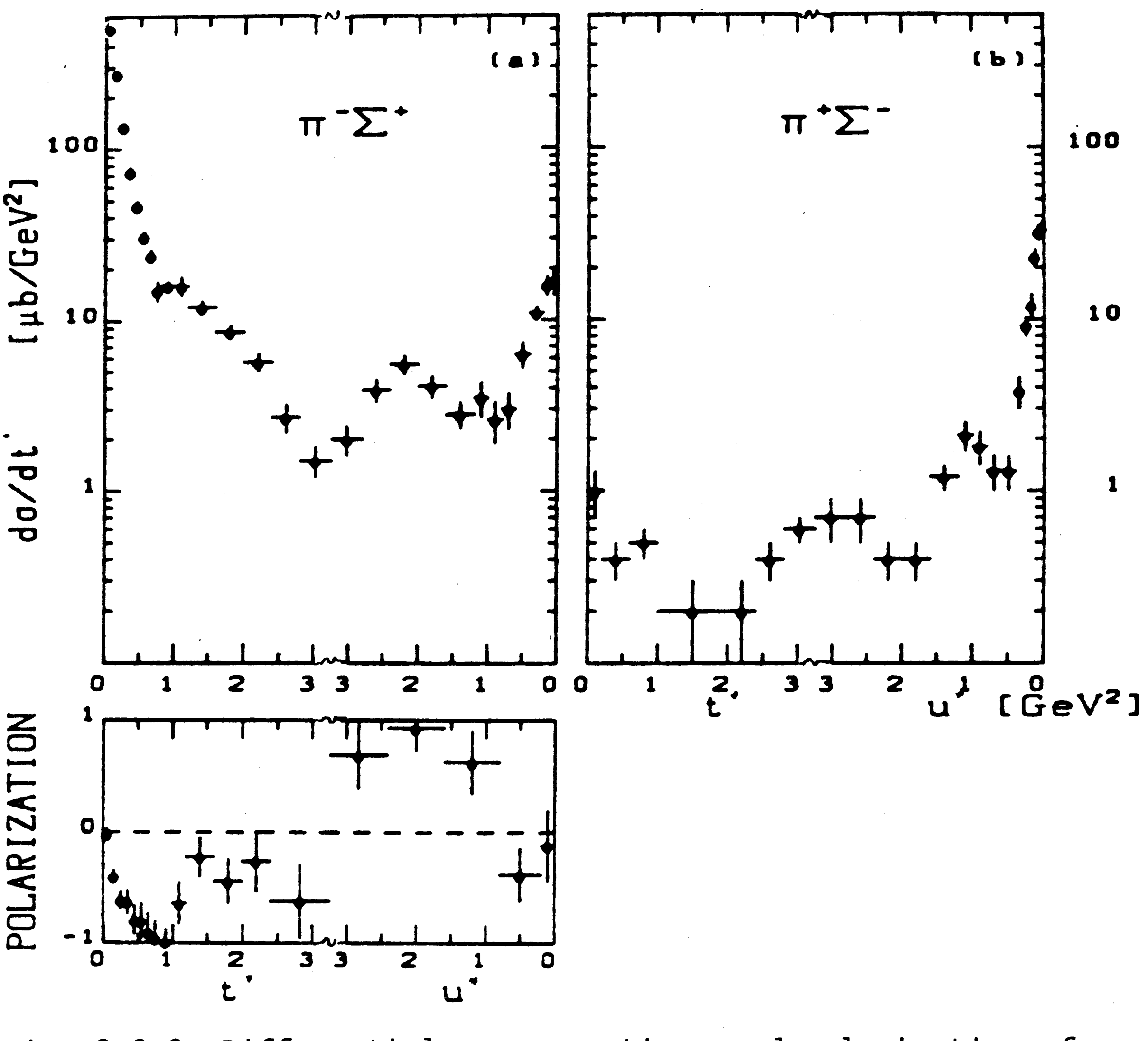

Fig. 3.2.2 Differential cross sections and polarizations for the reactions (4) and (5) of the $0^-1/2^+$ group.

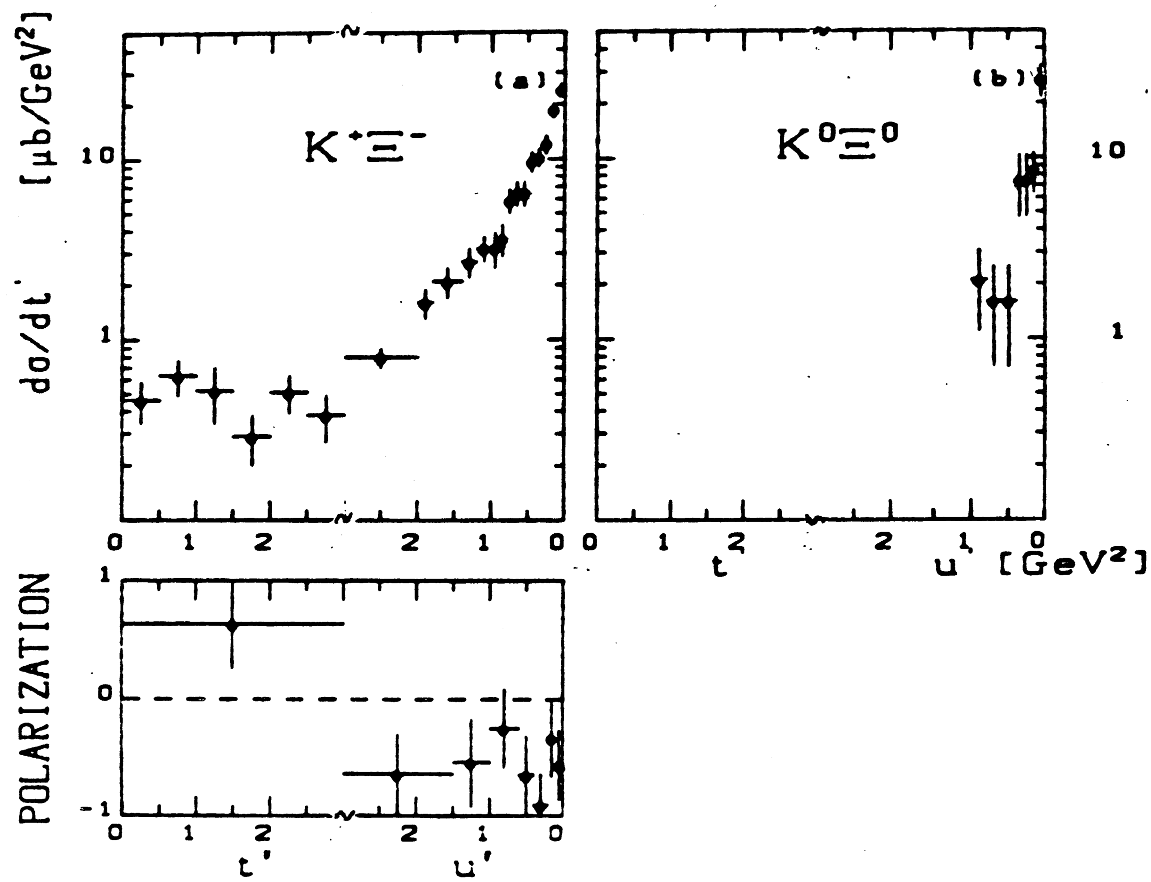

Fig. 3.2.3 Differential cross sections and polarizations for the reactions (6) and (7) of the $0^-1/2^+$ group.

For reaction (5) forward production is small (exotic t-channel) but with the available statistics one can show that the distribution is peaking near t' = 0 (see fig. 3.2.2b). In the backward region the dσ/du' distribution is much steeper than that of reaction (4). Dips are seen at $u' \sim 0.6$ and $u' \sim 2.0$ GeV^2.

Reaction (6) has some (exotic) forward production, but no peaking is seen near t' = 0 (fig. 3.2.3a). The backward peak has a rather smooth dσ/du' distribution. The Ξ^- polarization is large and negative for backward production.

Due to background problems reaction (7) could be studied only in the extreme backward direction ($u' \sim 1.0$ GeV). In this region the differential cross section (fig. 3.2.3b) is steeper than that of reaction (6).

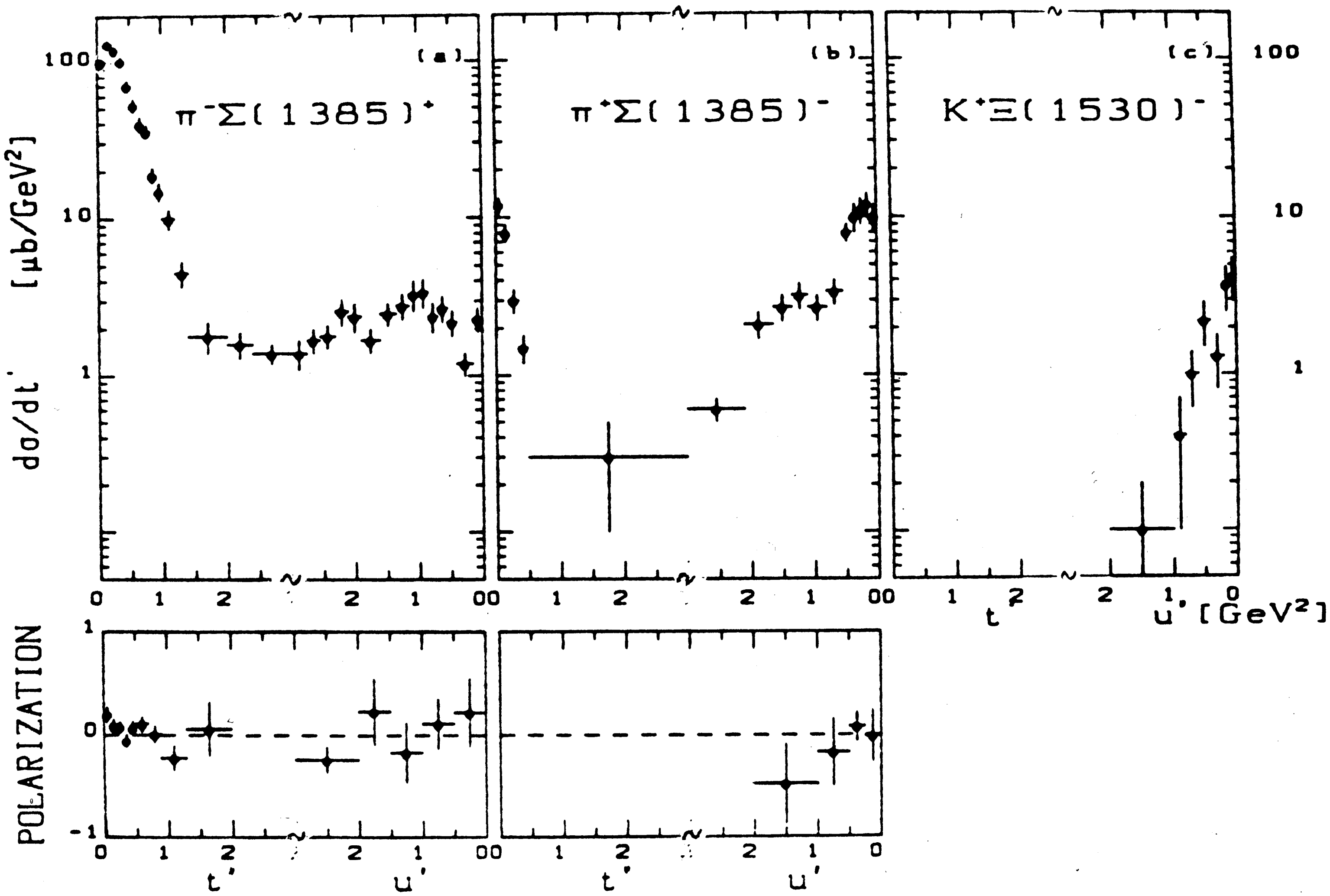

Fig. 3.3.1 Differential cross sections and polarizations for the reactions (1), (2) and (3) of the $0^{-}3/2^{+}$ group.

The most conspicuous feature of the data presented above is the variety of structures found in the differential cross sections and hyperon polarization distributions. Although the reactions all belong to the same spin-parity group, the distributions differ considerable from reaction to reaction. This is especially true for forward production (for those reactions having non exotic t-channel quantum numbers), where the data is most precise, even though the exchanged quantum numbers always correspond to those of K* or K** mesons.

3.3 Reactions of the type $0^-1/2^+ \to 0^-3/2^+$

The reactions of this type studied in our experiment are listed in table 3.3A and B together with the experimental details and cross sections. The differential cross sections and polarizations are shown in figure 3.3.1 and listed in table A3 in the appendix.

The differential cross section of reaction (1) (fig. 3.3.1a) shows a large forward peak with a dip at t' = 0 and a smooth exponential decrease up to $t' \sim 2.0$ GeV^2. Although the integrated cross section for backward production is not particularly small for a baryon-exchange process, the distribution is surprisingly flat, with possible structures near $u' \sim 0.3$ and $u' \sim 1.7$ GeV^2. The difference compared with backward production of $K^-p \to \pi^-\Sigma^+$ (fig. 3.2.2a) is striking, considering the u-channel has the same quantum numbers in both reactions. Apart from the region near t' = 0 the polarization is consistent with zero.

The $d\sigma/dt'$ distribution of reaction (2) (fig. 3.3.1b) shows a sharp forward peak, although the t-channel is exotic. In the backward direction there is some structure at $u' \sim 1.0$ GeV and a turnover near u' = 0. The polarization is small on average.

Table 3.3A Sample description for $0^-3/2^+$ reactions (see footnotes to table 3.2A)

	Reaction	Decay-modes	No. of events	Final state	ev/μb
(1)	$\pi^-\Sigma(1385)^+$	$\Sigma(1385)^+ \to \Lambda\pi^+$	3400(13)	$\Lambda\pi^+\pi^-$(14000)	80
(2)	$\pi^+\Sigma(1385)^-$	$\Sigma(1385)^- \to \Lambda\pi^-$	760(46)	$\Lambda\pi^+\pi^-$(14000)	80
(3)	$K^+\Xi(1530)^-$	$\Xi(1530)^- \to \Xi^-\pi^o$	70(10)	$\Xi^-K^+\pi^o$(500)	103

Table 3.3B Cross sections for $0^-3/2^+$ reactions (see footnotes to table 3.2B)

	Reaction	σ_T	σ_F	σ_B	Reference
(1)	$\pi^-\Sigma(1385)^+$	81 ± 4	75 ± 4	6.6 ± 0.6	[5]
(2)	$\pi^+\Sigma(1385)^-$	12.0 ± 1.6	3.0 ± 0.7	9.0 ± 1.1	[5]
(3)	$K^+\Xi(1530)^-$	-	-	1.9 ± 0.4 (u' < 2.0)	[4]

Table 3.4A Sample descriptions for $1^{-}1/2^{+}$ reactions (see footnotes of table 3.2A)

Reaction	Decay-modes	No. of events	Final state	ev/μb
(1) $\rho^{o}\Lambda$	$\rho^{o} \rightarrow \pi^{+}\pi^{-}$	4100(30)	$\Lambda\pi^{+}\pi^{-}$(19000)	120
(2) $\omega\Lambda$	$\omega \rightarrow \pi^{+}\pi^{-}\pi^{o}$	4500(6)	$\Lambda\pi^{+}\pi^{-}\pi^{o}$(59000)	120
(3) $\phi\Lambda$	$\phi \rightarrow K^{+}K^{-}$	1600(2)	$\Lambda K^{+}K^{-}$(4000)	120
	$\phi \rightarrow K^{o}\overline{K^{o}}$	800(1)	$\Lambda K^{o}\overline{K^{o}}$(1500)	120
(4) $\rho^{o}\Sigma^{o}$	$\rho^{o} \rightarrow \pi^{+}\pi^{-}$	2000(25)	$\Sigma^{o}\pi^{+}\pi^{-}$(10000)	120
(5) $\phi\Sigma^{o}$	$\phi \rightarrow K^{+}K^{-}$	900(2)	$\Sigma^{o}K^{+}K^{-}$(2000)	120

Table 3.4B Cross sections for $1^{-}1/2^{+}$ reactions (see footnotes to table 3.2B)

Reaction	σ_T	σ_F	σ_B	Reference
(1) $\rho^{o}\Lambda$	82 ± 8	57 ± 5	25 ± 3	[6]
(2) $\omega\Lambda$	91 ± 8	60 ± 5	31 ± 3	[6]
(3) $\phi\Lambda$	66 ± 4	66 ± 4	0.4 ± 0.2	[6]
(4) $\rho^{o}\Sigma^{o}$	30 ± 3	19 ± 2	11 ± 1	[6]
(5) $\phi\Sigma^{o}$	34 ± 3	33 ± 3	0.3 ± 0.2	[6]

Reaction (3) has not yet been studied completely. The preliminary results show a rather steep backward peak (fig. 3.3.1c). The t-channel of this reaction is exotic.

3.4 Reactions of the type $0^- 1/2^+ \rightarrow 1^- 1/2^+$

The reactions analyzed are listed in table 3.4A and B together with the experimental details and the cross sections. The differential cross sections and polarizations are shown in figures 3.4.1-2 and listed in table A4.

As the background in the samples of reaction (1) and (4) is rather large (see also fig. 2.6.2) the differential cross sections and polarizations for these reactions have been obtained from amplitude fits (such as described in section 3.10), which included an interfering s-wave background contribution.

Reactions (1), (2) and (4) have a large contribution from backward production, while for the reactions (3) and (5) the backward peak is completely absent (no events have been found for these reactions with $u' \lesssim 1.0$ GeV^2).

The forward peaks of reactions (1) and (2) exhibit a rather smooth distribution (fig. 3.4.1a and b) with a dip at $t' = 0$ for reaction (2). The backward cross sections are relatively large and the distributions show a dip around $u' \sim 0.3$ GeV^2 for both reactions. The Λ polarization behaves similarly for both reactions, being positive in the forward and negative in the backward region.

The differential cross section for reaction (3) (fig. 3.4.1c) has a dip at $t' = 0$ and an exponential fall-off into the backward region. The polarization is negative on average.

Reaction (4) has a smooth forward differential cross section, while in the backward direction the distribution peaks sharply near $u' = 0$ (fig. 3.4.2a). The polarization

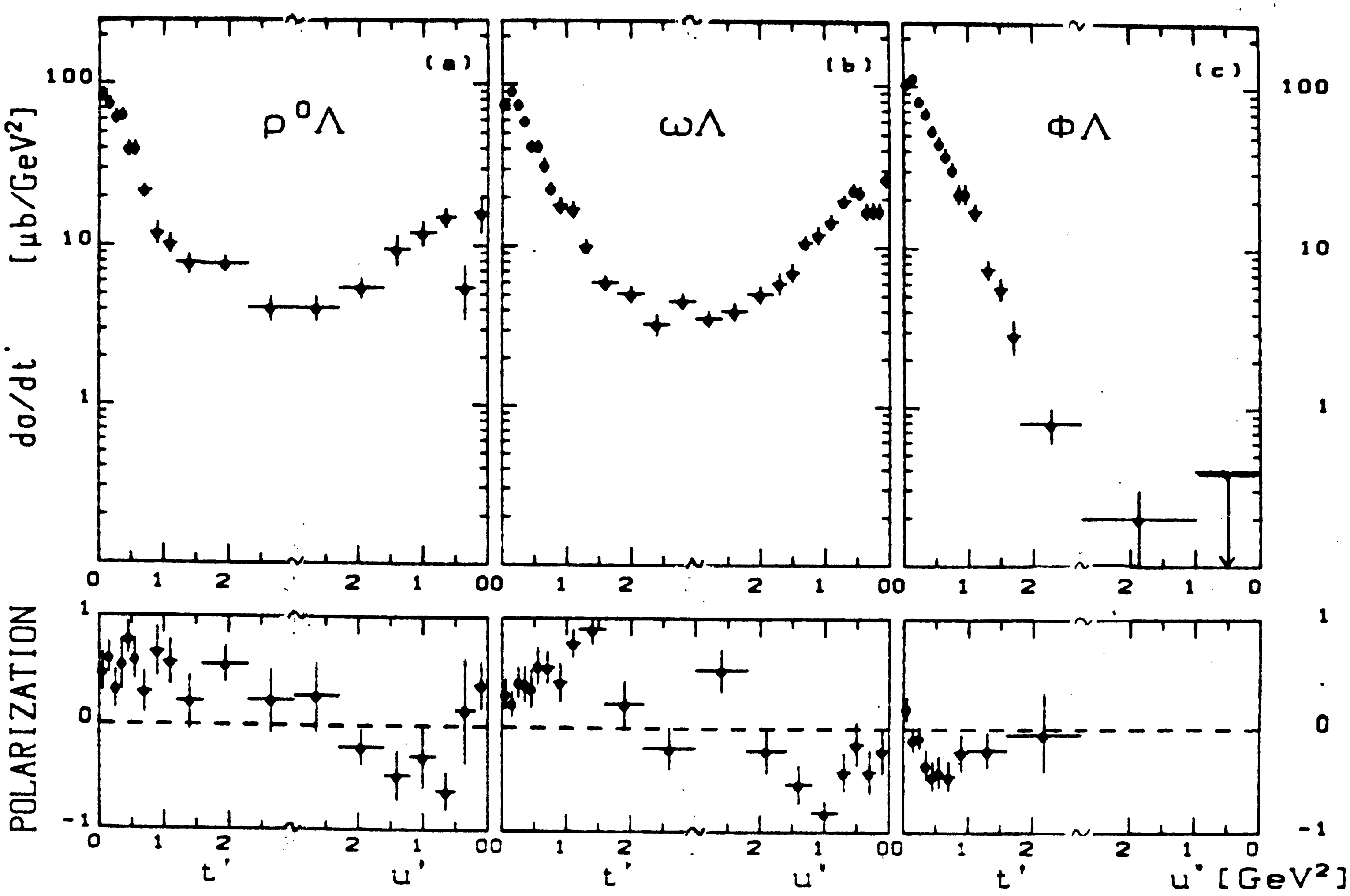

Fig. 3.4.1 Differential cross sections and polarizations for the reactions (1), (2) and (3) of the $1^-1/2^+$ group.

distribution shows large fluctuations. On average the polarization would appear to be small and negative in the forward direction, and positive in the backward direction.

Reaction (5) has a dip at t' = 0 and a large positive polarization (fig. 3.4.2b).

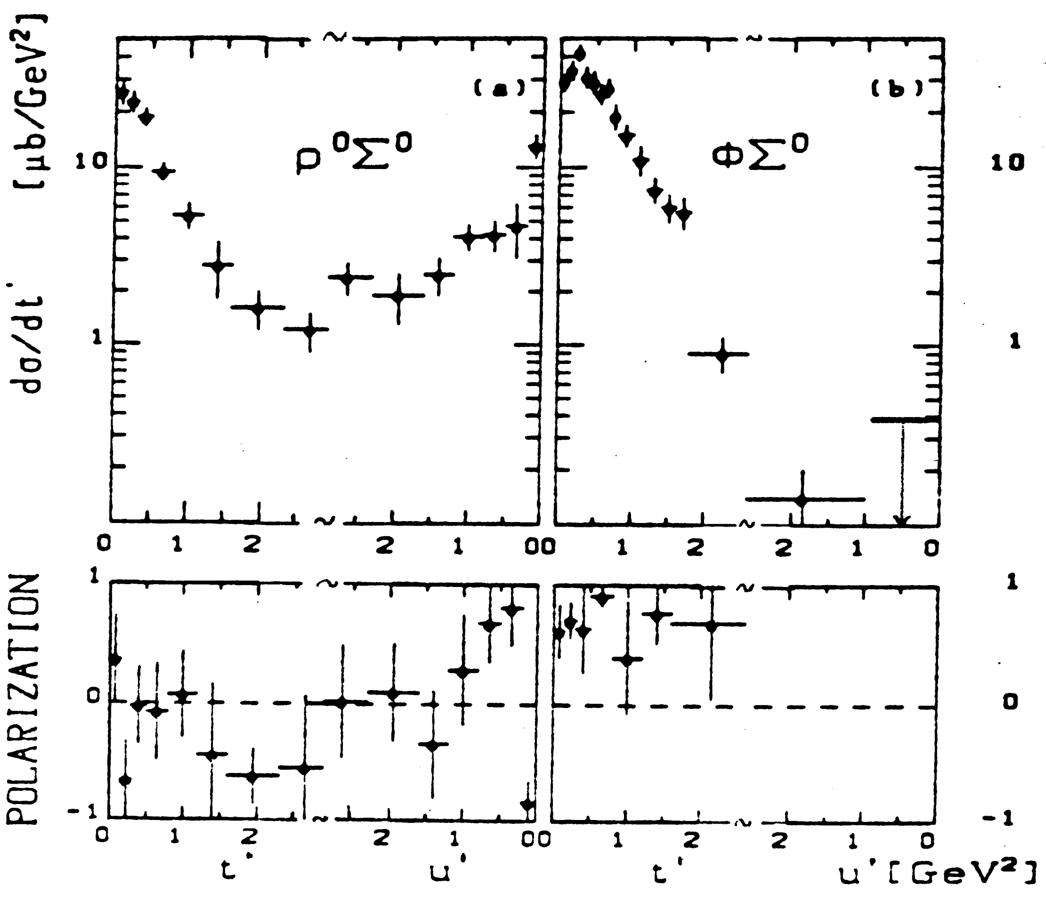

Fig. 3.4.2 Differential cross sections and polarizations for the reactions (4) and (5) of the $1^-1/2^+$ group.

3.5 Reactions of the type $0^-1/2^+ \rightarrow 1^-3/2^+$

Table 3.5A, B lists the sample descriptions and cross sections for the reactions studied in our experiment at the statistical level of ~ 65 events/μb. The differential cross sections and polarizations are shown in figure 3.5.1 and listed in table A5.

Reaction (1) shows both forward and backward production. The $d\sigma/dt'$ is sharply peaked near $t' = 0$ and dips are seen at $t' \sim 0.3$ and $t' \sim 0.6$ GeV^2. For backward production the errors are too large to say anything about the structure. The hyperon polarization measured for forward production is small and positive on average.

Reaction (2) has no significant backward cross section as expected for a ϕ-reaction. The $d\sigma/dt'$ is smooth and the polarization is small.

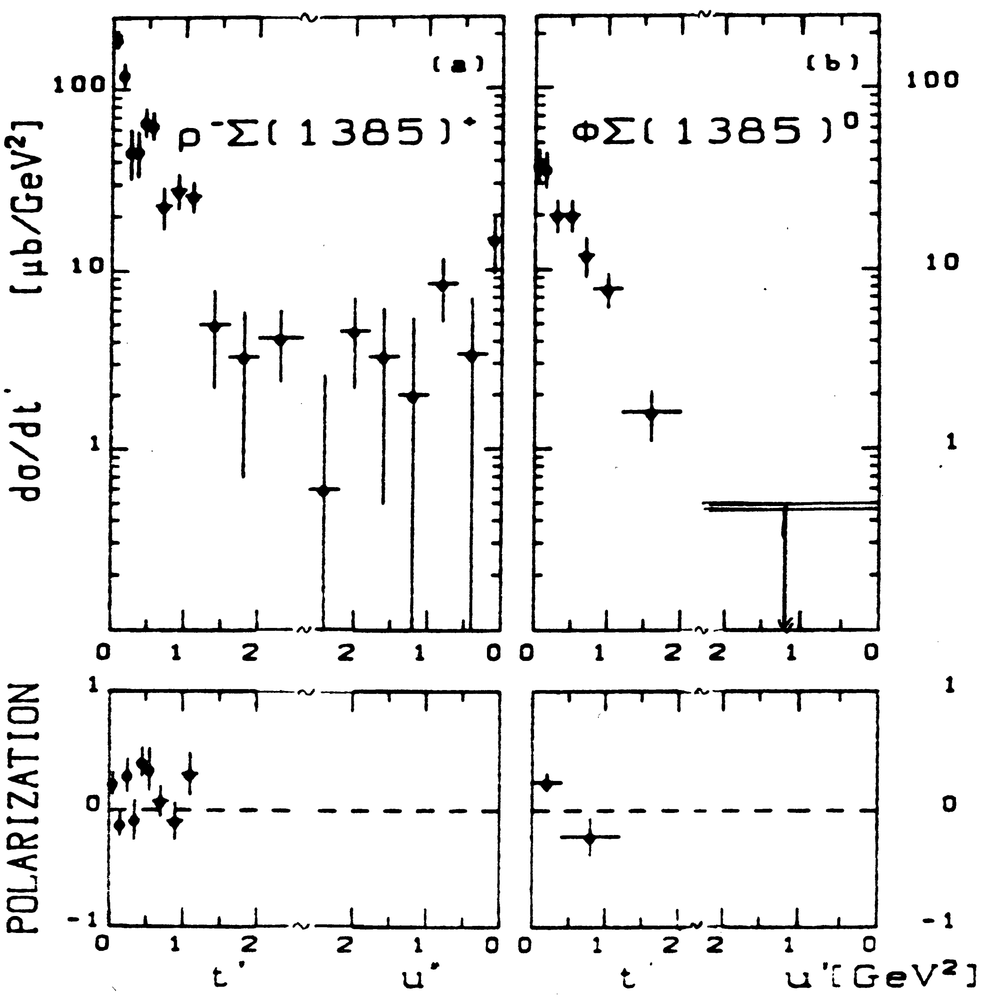

Fig. 3.5.1 Differential cross sections and polarizations for the reactions (1) and (2) of the $1^-3/2^+$ group.

3.6 Reactions of the type $0^-1/2^+ \to 2^+1/2^+$

The sample description and cross sections for the reactions of this type are listed in tables 3.6A, B. The data on reactions (2) and (4) come from a preliminary study. The simple treatment of the large background in this study is accounted for in the errors quoted. The differential cross sections and polarizations are shown in figure 3.6.1 and listed in table A6.

The data for reaction (1) have been obtained via a partial-wave analysis of the 3π system in the final state $\Lambda\pi^+\pi^-\pi^o$ with $t' < 1.0$ GeV^2. The $d\sigma/dt'$ distributions (fig. 3.6.1a) appears to level off near $t' = 0$. The polarization is positive in this region. Backward production of this reaction has not yet been analysed.

The forward and the backward cross section for reaction (2) are about equal. The $d\sigma/du'$ distribution (fig. 3.6.1b) shows a dip near $u' \sim 0.4$ GeV^2. The polarization is positive at small t' and negative in the backward region.

In reaction (3) the backward peak is absent (fig. 3.7.1c). This is predicted by the quark model, as will be discussed in section 3.11.

Backward f production in reaction (4) is not as large as found in reaction (2). In both reactions the $d\sigma/dt'$ distribution levels off near $t' = 0$ (fig. 3.6.1b,d).

In these reactions the cross sections for f' productions are small compared to those for f production. This is rather different from the situation found for ϕ and ω production in similar reactions (see table 3.4B).

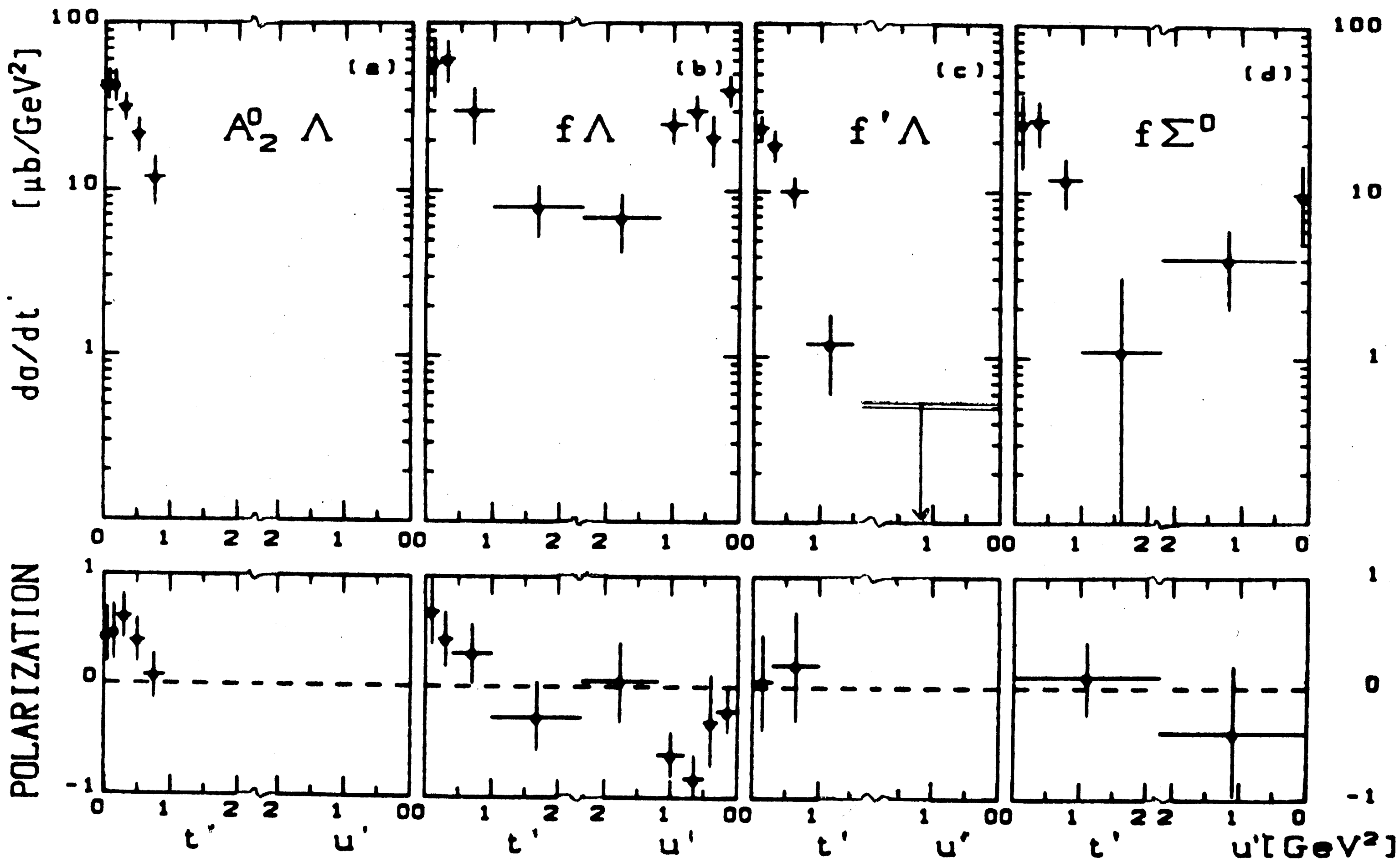

Fig. 3.6.1 Differential cross sections and polarizations for the reactions (1), (2), (3) and (4) of the $2^+1/2^+$ group.

Table 3.5A Sample description for $1^-3/2^+$ reactions (see footnotes to table 3.2A)

	Reaction	Decay-modes	No. of events	Final state	ev/μb
(1)	$\rho^-\Sigma(1385)^+$	$\rho^- \rightarrow \pi^-\pi^o$ $\Sigma(1385)^+ \rightarrow \Lambda\pi^+$	2400(33)	$\Lambda\pi^+\pi^-\pi^o$ (30000)	65
(2)	$\phi\Sigma(1385)^o$	$\phi \rightarrow K^+K^-$ $\Sigma(1385)^o \rightarrow \Lambda\pi^o$	240(13)	$\Lambda K^+K^-\pi^o$ (2300)	65

Table 3.5B Cross sections for $1^-3/2^+$ reactions (see footnotes to table 3.2B)

	Reaction	σ_T	σ_F	σ_B	Reference
(1)	$\rho^-\Sigma(1385)^+$	88 ± 6	74 ± 6	14 ± 3	[7]
(2)	$\phi\Sigma(1385)^o$	22 ± 4	21 ± 4	0.6 ± 0.3	[7]

Table 3.6A Sample description for $2^+1/2^+$ reactions (see footnotes to table 3.2A)

Reactions	Decay-modes	No. of events	Final state	ev/μb
(1) $A_2^o\Lambda$	$A_2^o \to \pi^+\pi^-\pi^o$	2000(60)	$\Lambda\pi^+\pi^-\pi^o$(47000)	95
(2) $f\Lambda$	$f \to \pi^+\pi^-$	8000(65)	$\Lambda\pi^+\pi^-$(22000)	128
(3) $f'\Lambda$	$f' \to K_s^o\overline{K_s^o}$	120(20)	$\Lambda K_s^o\overline{K_s^o}$(300)	100
(4) $f\Sigma^o$	$f \to \pi^+\pi^-$	4000(70)	$\Sigma^o\pi^+\pi^-$(10000)	128
(5) $f'\Sigma^o$	$f' \to K_s^o\overline{K_s^o}$	50(20)	$\Sigma^o K_s^o\overline{K_s^o}$(100)	100

Table 3.6B Cross sections for $2^+1/2^+$ reactions (see footnotes to table 3.2B)

Reactions	σ_T	σ_F	σ_B	Reference
(1) $A_2^o\Lambda$	-	22 ± 3 (t' < 1.0)	-	[8]
(2) $f\Lambda$	89 ± 10	47 ± 7	41 ± 7	[9]
(3) $f'\Lambda$	13 ± 2	13 ± 2	0.1 ± 0.3	[10]
(4) $f\Sigma^o$	33 ± 7	23 ± 6	10 ± 5	[9]
(5) $f'\Sigma^o$	5.0 ± 1.1	-	-	[10]

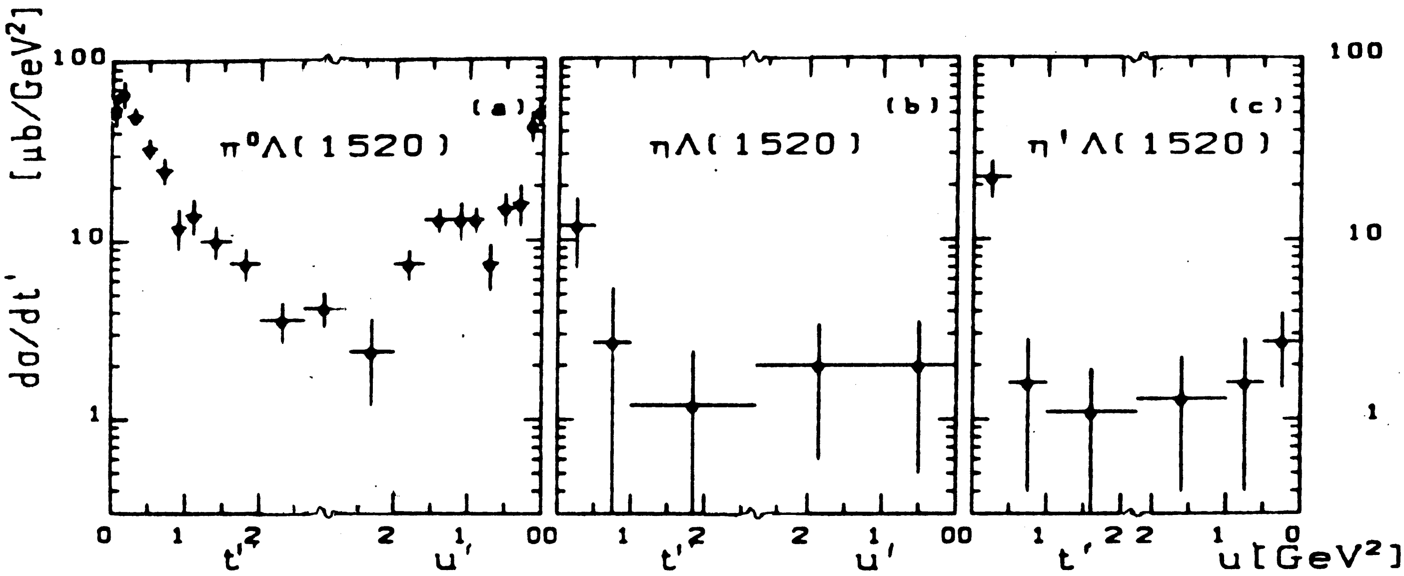

Fig. 3.7.1 Differential cross sections for the reactions (1), (2) and (3) of the $0^-3/2^-$ group.

3.7 Reactions of the type $0^-3/2^-$

In this section (and the next one) results are presented of two-body reactions in which a $\Lambda(1520)$ hyperon is produced. This resonance is the only hyperon with a well established $3/2^-$ spin-parity for which the corresponding two-body reactions are reasonably accessible for analysis. For some reactions however the decay mode $\Lambda(1520) \rightarrow pK^-$ has to be used, since the other channels lead to unfavourable final states (large background, bad resolution). Consequently the event samples for these reactions are small, because the final states corresponding with the topology 400, were scanned for in only part of the total picture sample. The sample descriptions and the cross sections are listed in tables 3.7A, B. The differential cross sections are shown in figure 3.7.1 and listed in table A7.

The analyses of reactions (2) and (3) are based on marginal statistics. The main reason for including the results here, is to be able to compare the set of reactions (1) - (3) with the corresponding set of reactions $K^-p \rightarrow \pi^0, \eta, \eta'\Lambda$ presented in section 3.2. Comparing figure 3.7.1 with figure 3.2.1 one can make the following observations:

The forward peak of reaction (1) is of a size comparable to that of the $\pi^o\Lambda$ reaction. The distribution in reaction (1) is somewhat less steep however and shows a dip at $t' = 0$, which is not seen for $\pi^o\Lambda$. The backward cross section for reaction (1) is much larger than that for $\pi^o\Lambda$ and here a structure is seen around $u' \sim 0.7$ GeV^2 instead of $u' \sim 0.2$ GeV^2, as seen in $\pi^o\Lambda$(the corresponding u-values are $u \sim -0.5$ GeV^2 and $u \sim -0.1$ GeV^2 respectively).

For reactions (2) and (3) there are not enough events to look for the same structures as found in the forward peaks of the $\eta\Lambda$ and $\eta'\Lambda$ reactions, but the t' depences are roughly comparable. However the forward cross section for reaction (3) is much smaller than that for the $\eta'\Lambda$ reaction, and the difference cannot be explained by phase-space differences.

Within the large errors the backward peaks for reactions (2) and (3) are comparable to those for the $\eta\Lambda$ and $\eta'\Lambda$ reactions.

3.8 Reactions of the type $1^-3/2^-$

Two reactions of this type have been analysed at a time when about half of the final statistics was available. Both reactions involve the production of a $\Lambda(1520)$. The sample description and the cross sections are listed in tables 3.8A, B. The differential cross sections are shown in figure 3.8.1 and listed in table A8.

Comparing these reactions with the reactions $K^-p \to \omega,\phi\Lambda$ presented in section 3.4 (fig. 3.4.1), one can make the following remarks:

The largest difference is seen in the forward peaks of the ω reactions, where reaction (1) has a smaller cross

Table 3.7A Sample description for $0^-3/2^-$ reactions (see footnotes to table 3.2A)

Reaction	Decay-modes	No. of events	Final state	ev/μb
(1) $\pi^o\Lambda(1520)$	$\Lambda(1520) \to \Sigma^\pm\pi^\mp$	1700 (40)	$\Sigma^\pm\pi^\mp\pi^o$ (32000)	110
	$\Lambda(1520) \to \Lambda\pi^+\pi^-$	400 (30)	$\Lambda\pi^+\pi^-\pi^o$ (60000)	128
(2) $\eta\Lambda(1520)$	$\Lambda(1520) \to pK^-$ $\eta \to \pi^+\pi^-\pi^o$	34 (30)	$pK^-\pi^+\pi^-\pi^o$ (24000)	33
(3) $\eta'\Lambda(1520)$	$\Lambda(1520) \to pK^-$ $\eta' \to \pi^+\pi^-\eta$ $\eta \to \pi^+\pi^-\pi^o$	43 (25)	$pK^-\pi^+\pi^-\pi^+\pi^-\pi^o$ (3000)	100
	$\eta \to$ neutrals	40 (25)	$pK^-\pi^+\pi^-$neutrals (15000)	33

Table 3.7B Cross sections for $0^-3/2^-$ reactions (see footnotes to table 3.2B)

Reaction	σ_T	σ_F	σ_B	Reference
(1) $\pi^o\Lambda(1520)$	82 ± 8	50 ± 6	32 ± 5	[11]
(2) $\eta\Lambda(1520)$	15 ± 5	9.4 ± 3.5	5.4 ± 2.8	[11]
(3) $\eta'\Lambda(1520)$	17 ± 3	13 ± 3	3.7 ± 1.4	[11]

Table 3.8A Sample description for $1^-3/2^-$ reactions
(see footnotes to table 3.2A)

Reaction	Decay modes	No. of events	Final state	ev/μb
(1) $\omega\Lambda(1520)$	$\omega \rightarrow \pi^+\pi^-\pi^o$	1500(35)	$\Sigma^\pm\pi^\mp\pi^+\pi^-\pi^o$ (27000)	65
	$\Lambda(1520) \begin{cases} \rightarrow \Sigma^\pm\pi^\mp \\ \rightarrow pK^- \end{cases}$		$pK^-\pi^+\pi^-\pi^o$ (13000)	18
(2) $\phi\Lambda(1520)$	$\phi \rightarrow K\bar{K}$	260(20)	$\Sigma^\pm\pi^\mp K^+K^-$ (2300)	65
	$\Lambda(1520) \rightarrow \Sigma^\pm\pi^\mp$		$\Sigma^\pm\pi^\mp K^o\overline{K^o}$ (1000)	

Table 3.8B Cross sections for $1^-3/2^+$ reactions
(see footnotes to table 3.2B)

Reaction	σ_T	σ_F	σ_B	Reference
(1) $\omega\Lambda(1520)$	57 ± 6	27 ± 4	29 ± 4	[7]
(2) $\phi\Lambda(1520)$	31 ± 9	31 ± 9	0.5 ± 0.4	[7]

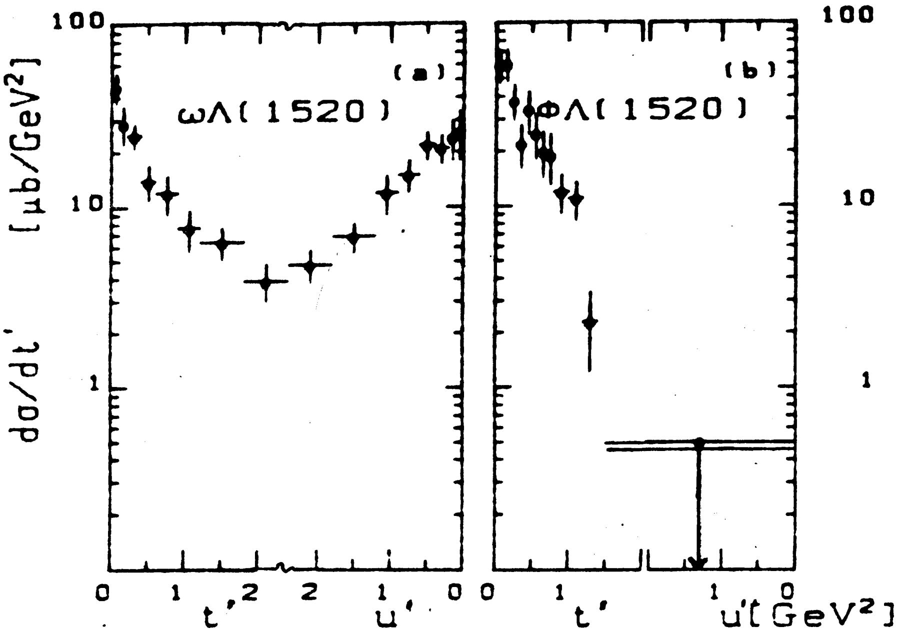

Fig. 3.8.1 Differential cross sections for the reactions (1) and (2) of the $1^-3/2^-$ group.

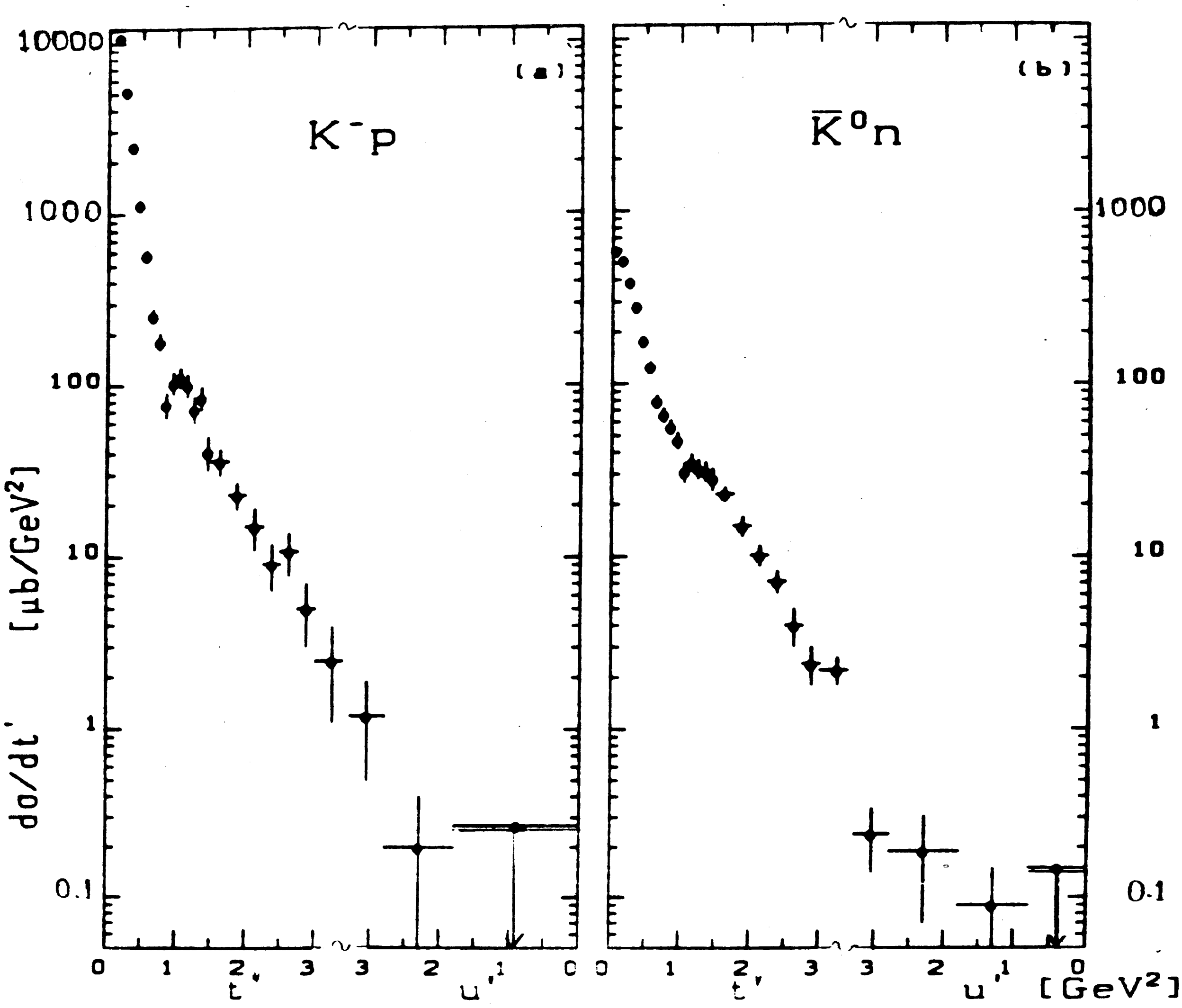

Fig. 3.9.1 Differential cross sections for the reactions $K^-p \rightarrow K^-p$ and $K^-p \rightarrow \overline{K^0}n$.

cross section and a sharp peak near $t' = 0$, while $\omega\Lambda$ has a dip at $t' = 0$. The large backward peaks in the ω-reactions are very similar in size and shape.

The cross section for reaction (2) is smaller than that for $\phi\Lambda$, but the distributions are very much the same. Again no backward peak is found for a reaction in which a ϕ meson is produced.

3.9 The reactions $K^-p \to K^-p$ and $K^-p \to \bar{K}^0 n$.

For comparison we show in this section the total and differential cross sections for two important two-body reactions which are not of the type $K^-p \to$ Meson + Hyperon. The sample descriptions and the cross sections for these two $0^-1/2^+ \to 0^-1/2^+$ reactions are listed in table 3.9. The elastic scattering reaction corresponds to the topology 200, which was scanned for in only a small part of the total picture sample.

Table 3.9 Sample descriptions and cross sections (see footnotes to tables 3.2A,B)

Reaction	No. of events	ev/μb	σ_T	σ_F	σ_B	Reference
(1) K^-p	13000	5	4500 ± 240	4500 ± 240	0.85 ± 0.43	[12]
(2) $\bar{K}^0 n$	5400	80	266 ± 11	266 ± 11	0.40 ± 0.15	[12]

The differential cross sections are shown in fig. 3.9.1 and the values are listed (for smaller t' bins) in table A9.

The much larger differential cross sections in the forward direction ($t' < 1$ GeV^2) make it clear that the production mechanism for reaction (1) in this region must be quite different from the one which is responsible for the reactions discussed in the previous sections. For reaction (2) on the other hand the production mechanism is similar and the somewhat larger cross section can be ascribed to the fact that no hypercharge exchange is required in the t-channel. At larger t' values the two reactions show a remarkably similar behaviour.

The u-channel has exotic quantum numbers for both reactions. In the backward region the differential cross sections show no evidence for any excess of events above the tails of the forward peaks. No events were found with $t' > 6$ GeV^2 ($u' < 0.8$ GeV^2) for reaction (1), or with $t' > 5$ GeV^2 ($u' < 1.8$ GeV^2) for reaction (2). The corresponding upper limits (at 90% confidence level) are 0.48 μb and 0.12 μb respectively. These small numbers again indicate that s-channel effects are relatively unimportant in our experiment.

3.10 Production amplitudes and spin density matrix elements

The production amplitudes for the reaction

$$K^- p \rightarrow M + H$$

can be defined by

$$T^M_{H\,p}(s,t) = \langle M\,H | T(s,t) | K^- p \rangle$$

where the indices of T^M_{Hp} denote the spin components along the quantization axis of the corresponding particles (the K^- index is omitted since the K^- has spin 0). The number of independent (complex) amplitudes is given by the total number of possible combinations of the spin indices, divided by 2. This reduction is a consequence of parity conservation in the production process. For the direction of the quantization axis one generally chooses between one of the following frames:

a) s-channel helicity frame; for each particle the quantization axis is along the direction of the particle in the total c.m. frame.

b) t-channel helicity frame; for the mesons (baryons) the quantization axis is along the direction of the incoming meson (baryon) in the rest frame of the outgoing meson (baryon).

c) transversity frame; the quantization axis is along the normal to the production plane.

In the transversity frame parity conservation implies

$$T^{M}_{H\,p} = \eta(-1)^{M-H+p}\, T^{M}_{H\,p}$$

where η is the product of the intrinsic parities of the four particles in the reaction. Thus for a given reaction half of the transversity amplitudes are zero and the remaining ones are independent.

The presence of a weakly decaying hyperon in the final state of the reactions discussed here, allows one to obtain an almost complete description of the production amplitudes of these reactions. I will illustrate this for the reaction $K^- p \to \rho^- \Sigma^+(1385)$ which belongs to the spin-parity group $0^- 1/2^+ \to 1^- 3/2^+$, and has 12 independent production amplitudes. I chose this reaction because it has the most general set of decay angles, defined in fig. 3.10.1. The six angle joint decay distribution for the decay chains $\Sigma^+(1385) \to \Lambda\pi^+$, $\Lambda \to p\pi^-$, and $\rho^- \to \pi^-\pi^o$ (see fig. 3.10.1) is expressed in terms of the production amplitudes as [7]:

$$W(\Omega_Y,\Omega_\Lambda,\Omega_\rho) = C \sum_{\substack{MM'HH' \\ \lambda\lambda'\nu}} \rho^{MM'}_{HH'}\, D^{1^*}_{M0}(\Omega_\rho)\, D^{1}_{M'0}(\Omega_\rho)$$

$$\times\, D^{3/2^*}_{H\lambda}(\Omega_Y)\, D^{3/2}_{H'\lambda'}(\Omega_Y)\, D^{1/2^*}_{\lambda\nu}(\Omega_\Lambda)\, D^{1/2}_{\lambda'\nu}(\Omega_\Lambda)\, \left|F^{1/2}_\nu\right|^2$$

where the density matrix $\rho^{MM'}_{HH'}$ is defined by

$$\rho^{MM'}_{HH'} = \sum_p T^{M}_{Hp}\, T^{M'^*}_{H'p}$$

and the $D^J(\Omega)$ are the rotation functions, C is a normalization constant, and the $F^{1/2}_\nu$ are two decay amplitudes for the weak decay $\Lambda \to p\pi^-$ (the decay amplitudes for the other (strong) decays are constants and are contracted into C).

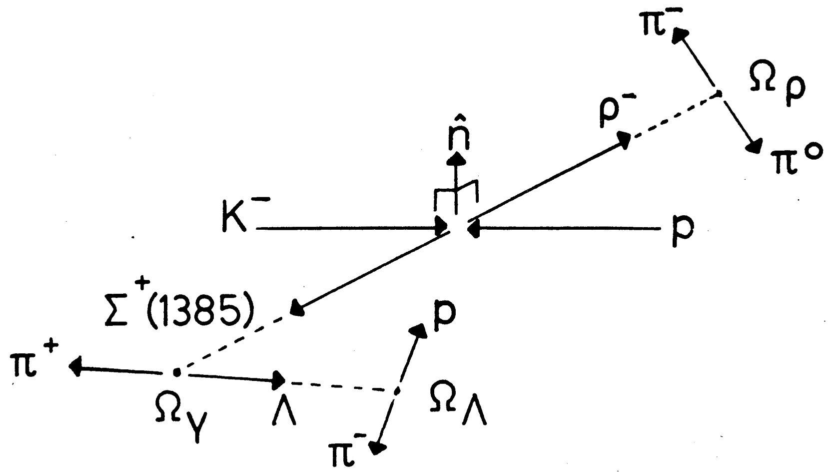

Fig. 3.10.1 The decay angles (Ω_i) which play a role in the amplitude-analysis of the reaction $K^-p \to \rho^-\Sigma^+(1385)$. Dashed lines represent Lorentz transformations to the rest-frame of the corresponding particle.

By fitting the experimental decay distribution with the expression given above, one obtains 22 of the 24 independent parameters which determine the production amplitudes. For the transversity-frame these 22 parameters are the moduli of the 12 transversity amplitudes and 10 relative phases. The two remaining variables are the phase between two groups of amplitudes and the overall phase. The first variable can be measured if a polarized target is used.

Amplitude analyses of this type have been performed in our experiment for the following reactions:

$K^-p \to \pi^{\mp}\Sigma(1385)^{\pm}$

$K^-p \to \rho^o,\omega,\phi\Lambda$

$K^-p \to \rho^o,\phi\Sigma^o$

$K^-p \to \rho^-\Sigma(1385)^+,\phi\Sigma(1385)^o$

As an example fig. 3.10.2 shows the results of the amplitude analysis of the reaction $K^-p \to \omega\Lambda$. The favourable experimental situation (large sample, small background) allows a detailed study of this reaction. The results for the other reactions can be found in references quoted in the tables of this chapter. Some of these results will be used in chapter 4 to test quark model predictions for these amplitudes.

If one studies only the strong decay distribution of one of the outgoing particles, the information obtained about the spin orientation of this particle is usually expressed in terms of spin density matrix elements. For instance the angular decay distribution $\frac{d\sigma}{d\Omega}$ for a meson resonance with spin J decaying into spinless particles can be written as:

$$\frac{d\sigma}{d\Omega} = C' \sum_{MM'} D^{J^*}_{M0}(\Omega)\, D^{J}_{M'0}(\Omega)\, \rho_{MM'}$$

where the density matrix is related to the production amplitudes by

$$\rho_{MM'} = \sum_{H\,p} T^{M}_{Hp}\, T^{M'^*}_{Hp}$$

One can understand from the relation above that not all the matrix-elements are independent. Moreover, as a consequence of the symmetry properties of the $D^J(\Omega)$ functions, some of the independent variables drop out of the $\frac{d\sigma}{d\Omega}$ formula when this is evaluated and thus they can not be measured.

As an example of such orientation measurements the distributions for the 3 measurable density matrix elements of the vector meson are shown in fig. 3.10.2 for the reactions of the $1^-1/2^+$ group. The data are shown for the s-channel helicity frame, which means that the spin quantization axis is along the direction of the vector-meson in the total c.m. frame. The parameter $\rho_{1,1}$ in this figure measures the relative amount of vector mesons produced with spin component (helicity) +1 along this axis. As due to parity conservation the +1 and -1 helicity states are equally populated, the figure shows, that apart from production near $t' = 0$ for the Λ reactions, this parameter is nearly always maximal ($\rho_{11} = 0.5$). The other two parameters are related to the interference between the helicity +1 and helicity -1 amplitudes, and between the helicity 1 and helicity 0 amplitudes respectively. One notes that for forward production ρ_{1-1} is larger on average for the Σ^0 reactions than for the corresponding Λ-reactions. In chapter 4 these measurements will be further discussed.

3.11 Suppression of backward ϕ and f' production.

As shown in the previous sections no backward peaks are observed in the differential cross section distributions

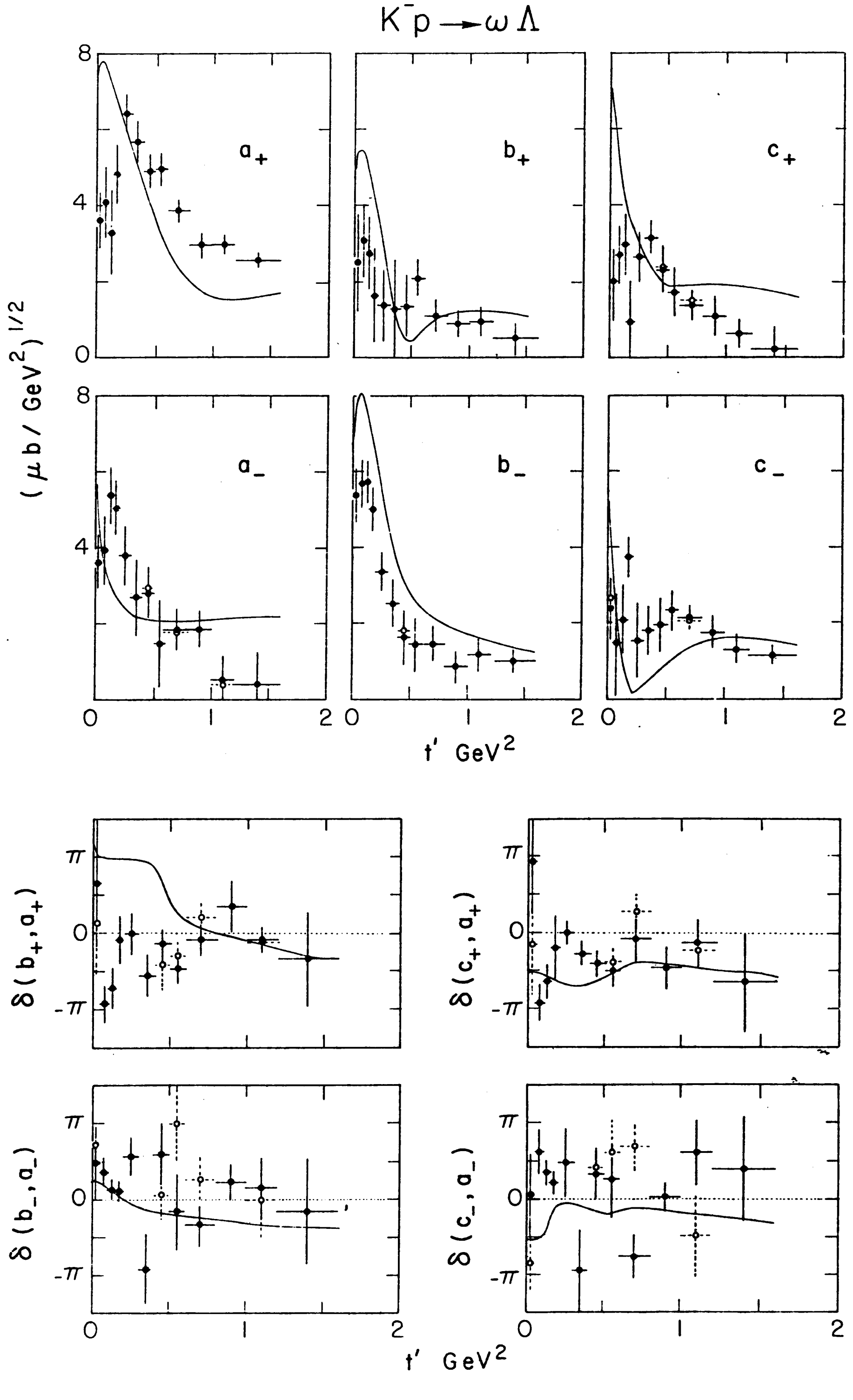

Fig. 3.10.2 Moduli and relative phases of the Byers-Yang amplitudes for the $0^-1/2^+ \to 1^-1/2^+$ reaction $K^-p \to \omega\Lambda$ as functions of t'. These amplitudes are linear combinations of the transversity amplitudes [6] and can be simply interpreted in terms of t-channel exchange mechanisms. The open dots are alternative solutions resulting from the fits and the curves are model prediction described in ref. 6.

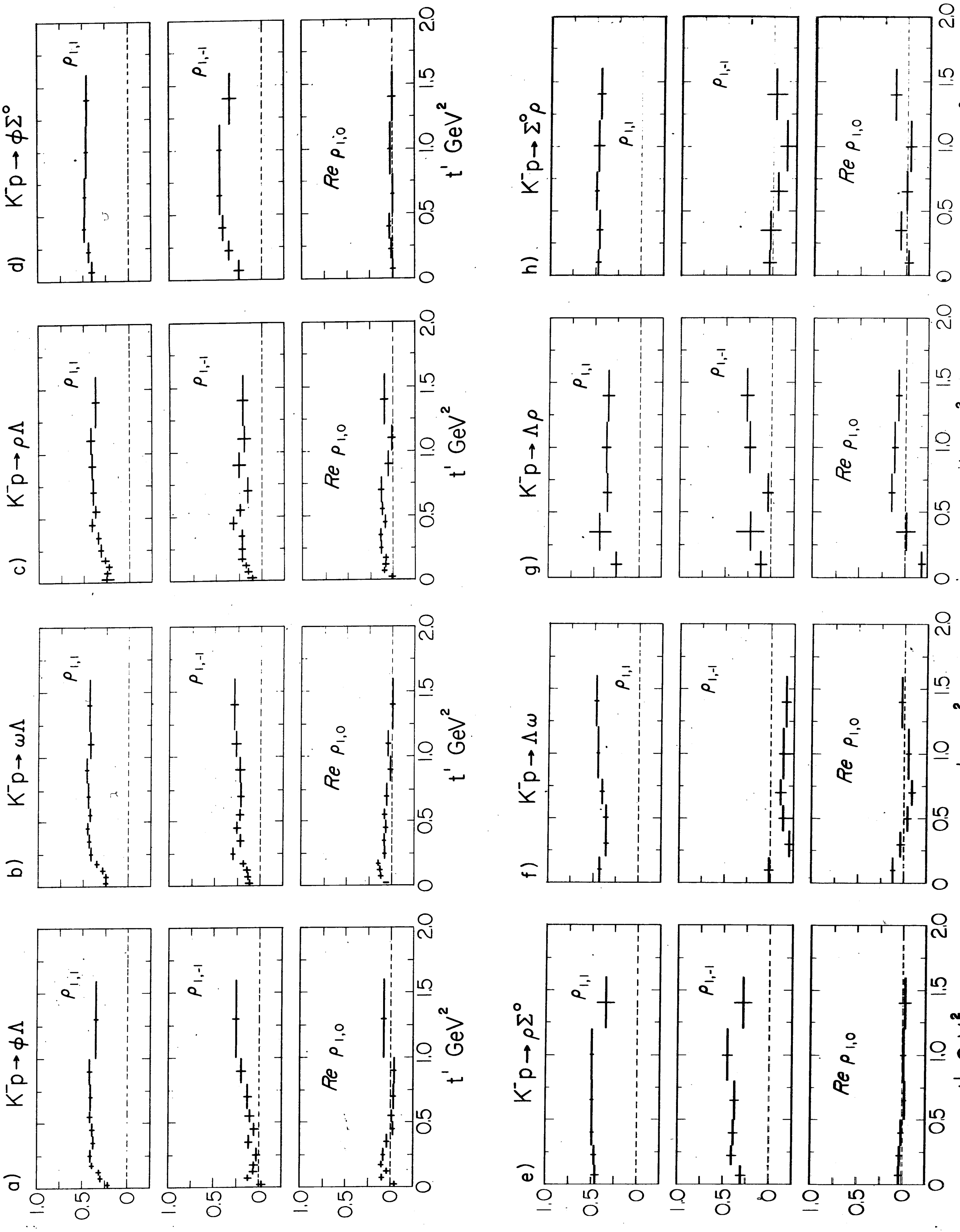

Fig. 3.10.3 Distributions of the spin density matrix elements of the vector-meson for reactions of the type $0^- 1/2^+ \rightarrow 1^- 1/2^+$.

for the reactions producing a ϕ or a f' meson. The u-channel for these reactions is not exotic. It has isospin $I = 1/2$ and strangeness $S = 0$, and thus for instance nucleon (N_α) exchange is possible. The distributions for the corresponding reactions producing an ω, ρ or f meson show substantial backward production. The dips in some of these distributions near $u' = 0.2\ \mathrm{GeV}^2$ may be related to exchange of the N_α Regge trajectory [6].

In the quark model the suppression of ϕ and f' production by baryon exchange can be explained with the Zweig rule [13]. This rule decouples particles with hidden strangeness (i.e. composed of a strange quark and its anti-quark) from states in which no strangeness is involved (e.g. $N\bar{N}$ states). An essential condition for this suppression to occur is ideal mixing, by which the ϕ and the f' meson contain only strange quarks (see also chapter 4, section 6). Assuming the Zweig rule to be exact, we can use our results to give an upper limit for the deviation θ from the ideal value $\theta_{id} = 35.3$ for the mixing angle [14]:

$$\tan^2 \theta = \frac{g^2_{N\bar{N}\phi}}{g^2_{N\bar{N}\omega}} = \frac{\sigma(K^- p \to \phi + \mathrm{Hyperon})_{\mathrm{backw.}}}{\sigma(K^- p \to \omega + \mathrm{Hyperon})_{\mathrm{backw.}}}$$

and correspondingly for the f and f' reactions.

In our experiment the lowest limit for the vector mesons is obtained with the Λ reactions. The cross sections for $u' < 1.0\ \mathrm{GeV}^2$ are $\sigma(K^- p \to \phi\Lambda) < 0.4\ \mu b$ at 95% confidence level, and $\sigma(K^- p \to \omega\Lambda) = 19.0 \pm 0.7\ \mu b$. The cross section ratio corresponds to $\theta \lesssim 8^{\circ}$ for the vector mesons.

For the tensor mesons an upper limit of $\theta \lesssim 7^{\circ}$ (95% confidence level) was obtained with the backward hemisphere cross sections for $K^- p \to f\Lambda$ and $K^- p \to f'\Lambda$ [10].

The small backward cross sections for the ϕ and f' reactions are additional evidence for the absence of significant s-channel mechanisms.

References Chapter 3

1) Review of Particle Properties, Particle Data Group, Rev. Mod. Phys. 48 (1976) No. 2, part II.

2) F. Marzano et al., Nucl. Phys. B123 (1977) 203.

3) G.G.G. Massaro et al., Phys. Lett. 66B (1977) 385.

4) R.J. Hemingway, CERN, Private communication.

5) S.O. Holmgren et al., Nucl. Phys. B119 (1977) 261.

6) M.J. Losty et al., Non-strange vector meson production in K^-p interactions at 4.2 GeV/c, CERN/EP/Phys. 77-45 and submitted for publication.

7) M. Aguilar-Benitez et al., Nucl. Phys. B124 (1977) 189.

8) M. Cerrada et al., Nucl. Phys. B126 (1977) 241.

9) G.G.G. Massaro, The reactions $K^-p \to f\ \Lambda, \Sigma^o$ at 4.2 GeV/c Internal 4.2 report no.89, Zeeman laboratory, Amsterdam.

10) F. Barreiro et al., Nucl. Phys. B121 (1977) 237.

11) S. Barlag et al., The reactions $K^-p \to \pi^o$, η, $\eta'\Lambda(1520)$ at 4.2 GeV/c, ACNO-collaboration, to be published.

12) F. Marzano et al., Phys. Lett. 68B (1977) 292.

13) G. Zweig, CERN report TH 412 (1964).

14) H.J. Lipkin, Phys. Lett. 60B (1976) 371.

Chapter 4.

FORWARD SCATTERING, REGGE-EXCHANGE MODELS, ADDITIVE QUARK MODEL

4.1 Introduction

In this chapter the data on forward (small t') scattering in the reactions

$$K^-p \rightarrow \text{Meson} + \text{Hyperon}$$

is confronted with predictions coming from two different phenomenological approaches, viz. simple Regge-exchange models [1] and the additive quark model [2]. To a certain extent the two approaches are complementary. In the simple Regge-exchange models the s- and t-dependence of the scattering process is determined by the Regge-trajectories which are exchanged in the t-channel. However, the spin dependence of the amplitudes is not easily derived with these models. The additive quark model on the other hand, exploits the idea of reducing the particle - particle scattering amplitudes to quark - quark scattering amplitudes. In this way relations between reactions amplitudes with different particle spin projections can be obtained, but no predictions for the s- and t-dependence are derived.

As was shown in the previous chapter the differential cross section and the polarization distributions for these hypercharge exchange reactions present a large variety of structures. It is therefore not surprising that rather sophisticated Regge exchange models are required in order to reproduce these distributions in detail. Working with these models implies, in general, fitting the data of many reactions with a large number of parameters. Since I have not been involved in such work, only some general predictions of simple Regge-exchange models will be tested in this chapter. The main part of this chapter is devoted to the additive quark model, which is shown to be remarkably succesful, despite its simplicity.

In section 4.2 the separation into natural-parity and unnatural-parity exchange contributions is discussed. In section 4.3 the predictions from simple Regge-exchange models are tested. In section 4.4 the additive quark model is introduced, and in the following sections various predictions from this model are tested. Finally in section 4.8 the conclusions are drawn.

4.2 Natural-parity and unnatural-parity exchange.

Forward production in reactions (1) corresponds to exchange of virtual mesons, which have quantum numbers $I = 1/2$ and $S = 1$ like the K and K* mesons. Sometimes also exotic exchanges with $I = 3/2$ and/or $S = 2$ occur. When discussing exchange mechanisms, it is useful to distinguish between natural-parity and unnatural-parity exchange. The distinction is based on the relation between the exchange spin (J) and parity (P) quantum numbers, which is determined by the sign of the naturality (P^J for meson-exchange). In table 4.2.1 the combinations of (non-exotic) quantum numbers, which can be exchanged in the reactions of type (1), are listed. The names and J^P numbers refer to the leading poles of the corresponding Regge trajectories, and the C-parity refers to the neutral non-strange members of the corresponding SU(3) nonets.

Table 4.2.1

	Name	Naturality	J^P	C-parity
Natural-Parity Exchange	K^*	+	1^-	-
	K^{**}	+	2^+	+
Unnatural-Parity Exchange	K	-	0^-	+
	K_B	-	1^+	-
	K_A	-	1^+	+
	K_Z	-	2^-	-

For reactions in which a 0^- meson is produced only natural-parity exchange is allowed by parity conservation at the meson vertex. For the other reactions one can use the information on the spin orientation of the outgoing meson, to separate the contributions of the two types of exchanges to the differential cross section and the polarization. This will be illustrated for the reactions in which a vector meson ($J^P = 1^-$) is produced.

Using the spin density matrix elements in a helicity frame (see section 3.10) the differential cross section can be separated into the three following contributions [3]:

a) Natural-parity exchange produces only mesons with helicity ±1, and the contribution is given by

$$(\rho_{11} + \rho_{1-1}) \frac{d\sigma}{dt},$$

b) Unnatural-parity exchange with meson helicity 0 contributes

$$\rho_{00}\,\frac{d\sigma}{dt'}\,,\ \text{with}\ \rho_{00} = 1-2\rho_{11}.$$

c) Unnatural-parity exchange with meson helicity ±1 contributes

$$(\rho_{11} - \rho_{1-1})\,\frac{d\sigma}{dt'}.$$

This separation is valid to order 1/s, where s = (total c.m. energy)^2 = 9 GeV^2 in our case. In table 4.2.2 the separated cross sections are listed for the reactions $K^-p \rightarrow$ Vector meson + Hyperon. One notices that for the $1^-1/2^+$ reactions the most important contributions come from natural-parity exchange. This is especially true for the Σ^o reactions, where the unnatural-parity exchange cross sections are much smaller than those for the corresponding Λ reactions. Unnatural-parity exchange is dominant in the reactions with a spin 3/2 hyperon.

The distribution of $\rho_{00}\,\frac{d\sigma}{dt'}$ (related to K exchange) is peaked at small t' values in these reactions. The other distributions are expected to dip near t' = 0 [4]. Indications for these effects can be seen in the distributions of ρ_{11} and ρ_{1-1} plotted in fig. 3.10.3. The $\frac{d\sigma}{dt'}$ distributions for the reactions $K^-p \rightarrow \omega\Lambda$ and $K^-p \rightarrow \phi\Lambda$, separated according to the prescriptions listed above, are shown in fig. 4.3.3.

For tensor meson ($J^P = 2^+$) production one may use similar combinations of density matrix elements to separate the contributions from unnatural- and natural-parity exchange [3]. The results for two reactions of the $2^+1/2^+$ group are also listed in table 4.2.2 (the contributions have been summed over the meson helicity states). Comparing σ_u/σ_n for corresponding $2^+1/2^+$ and $1^-1/2^+$ reactions one notices that for A_2^o and $\rho^o\Lambda$ this ratio is about equal

Table 4.2.2 Forward cross sections ($t' < 1.2$ GeV^2) for natural (σ_n) and unnatural (σ_u) parity exchange. The upper index refers to the helicity of the vector meson. For the tensor meson reactions the partial cross sections have been summed over the helicity states.

J^P Group	Reaction	$\sigma_n^{\pm 1}$	σ_u^{0}	$\sigma_u^{\pm 1}$	[μb]
	$\rho^o\Lambda$	24 ± 3	16 ± 3	6.0 ± 1.7	
	$\omega\Lambda$	30 ± 3	12 ± 2	8.7 ± 1.9	
$1^- 1/2^+$	$\phi\Lambda$	28 ± 3	17 ± 2	16 ± 2	
	$\rho^o\Sigma^o$	14 ± 2	1.1 ± 0.4	2.1 ± 0.6	
	$\phi\Sigma^o$	24 ± 2	2.8 ± 0.7	2.0 ± 0.7	
$1^- 3/2^+$	$\rho^-\Sigma(1385)^+$	10 ± 3	27 ± 3	31 ± 4	
	$\phi\Sigma(1385)^o$	7.3 ± 1.4	8.8 ± 1.5	5.9 ± 1.4	
$1^- 3/2^-$	$\omega\Lambda(1520)$	4.0 ± 1.3	5.9 ± 1.1	11 ± 2	
	$\phi\Lambda(1520)$	13 ± 3	8.5 ± 2.2	12 ± 3	
$2^+ 1/2^+$	$A_2^o\Lambda$	9.5 ± 1.8	13 ± 2		
	$f'\Lambda$	2.6 ± 1.0	10 ± 2		

and near to 1. In contrast it is ~ 4 for $f'\Lambda$, while also ~ 1 for $\phi\Lambda$.

The separation into natural-parity and unnatural-parity exchange is particularly simple for the transversity amplitudes [5]. For the reactions discussed in this thesis the transversity amplitudes T^{M}_{Hp} with $M = \text{even}$ correspond (in the high energy limit) to natural-parity exchange, and those with $M = \text{uneven}$ to unnatural-parity exchange.

4.3 Simple Regge models

The simplest Regge-model one can use to give a general description of the data, is one in which only Regge-poles are exchanged, and the corresponding Regge-trajectories are exchange degenerate [1]. Thus for the reactions of type (1) such a description would use 3 pairs of exchange degenerate trajectories: K^*/K^{**}, K/K_B and K_A/K_Z (see table 4.2.1). Two kinds of exchange degeneracy (EXD) may be distinguished:

a) Weak EXD, in which only the trajectory-functions are equal, i.e. the trajectories lie on top of each other in the Chew-Frautschi plot [1].

b) Strong EXD, in which in addition the residue-functions (i.e. the couplings at the vertices) are equal for a pair of trajectories.

An immediate consequence of strong EXD is that the hyperon polarization should be zero in reactions like $K^-p \to \pi^o\Lambda$ and $K^-p \to \pi^-\Sigma^+$ where only K^*/K^{**} exchange is allowed [1]. As can be seen in fig. 3.2.1 and 2, these reactions have large polarizations and especially for $\pi^o\Lambda$ the prediction is totally violated.

A test of the weak EXD assumption can be made by comparing line-reversed reactions, such as drawn in fig. 4.3.1:

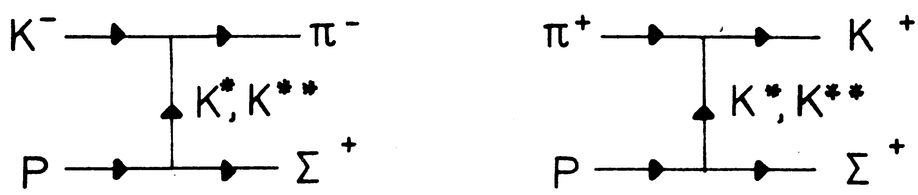

Fig. 4.3.1 Examples of reactions which are related by line-reversal at the upper vertex.

For weak EXD these reactions should have the following relations

$$\frac{d\sigma}{dt}\,(K^-p \to \pi^-\Sigma^+) \;=\; \frac{d\sigma}{dt}\,(\pi^+p \to K^+\Sigma^+)$$

$$P_\Sigma\,(K^-p \to \pi^-\Sigma^+) \;=\; -\,P_\Sigma(\pi^+p \to K^+\Sigma^+)$$

which apply for both Σ^+ and $\Sigma^+(1385)$.

In fig. 4.3.2 the differential cross sections and the Σ^+ polarizations are compared for the Σ^+ reactions. As one can see in this figure the predictions are not in agreement with experiment. A similar comparison using our data for the $\Sigma^+(1385)$ reactions has also shown disagreement between prediction and experiment [6]. Using line-reversal

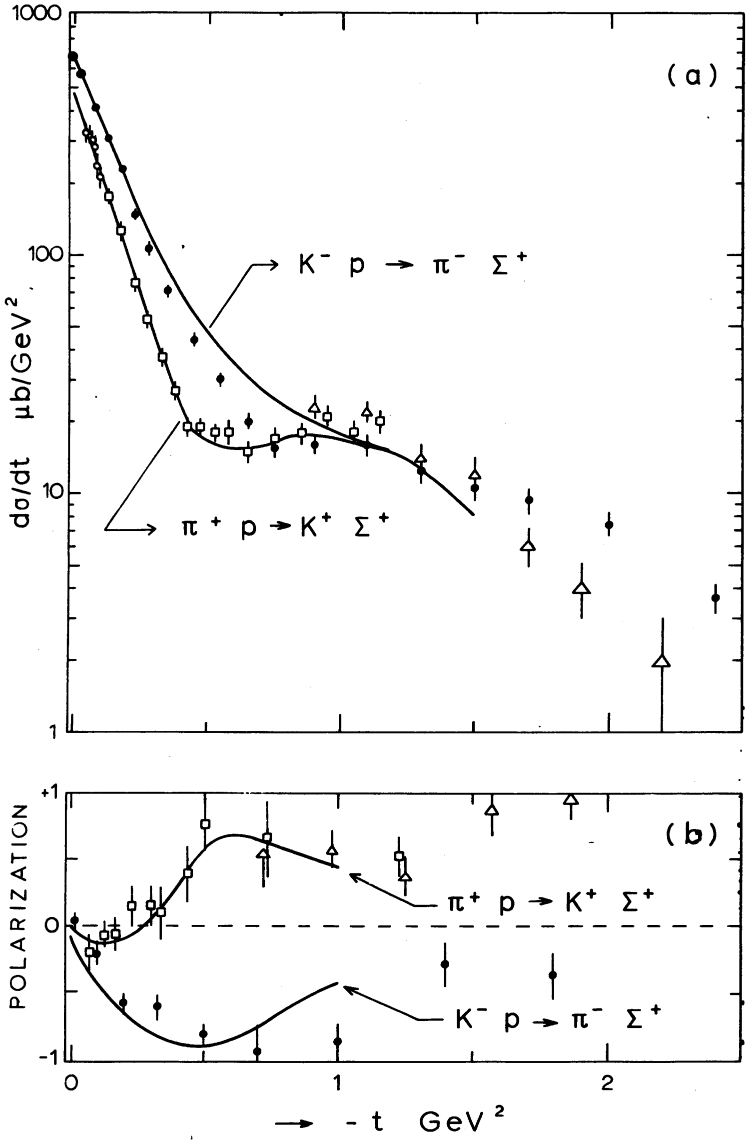

Fig. 4.3.2 Comparison of the differential cross sections and the polarizations for the reaction $K^-p \to \pi^-\Sigma^+$ at 4.15 GeV/c (this experiment) and for the line-reversed reaction $\pi^+p \to K^+\Sigma^+$ at 4.25 GeV/c (ref. [7]), and at 4.0 GeV/c (ref. [8], ref. [9]). The curves are fit-results of the amplitude analysis described in ref. [10].

and isospin conservation one can relate $K^-p \rightarrow \pi^o\Lambda$ with $\pi^-p \rightarrow K^o\Lambda$, and for weak EXD the following relations should hold:

$$2\,\frac{d\sigma}{dt}\,(K^-p \rightarrow \pi^o\Lambda) \;=\; \frac{d\sigma}{dt}\,(\pi^-p \rightarrow K^o\Lambda)$$

$$P\,(K^-p \rightarrow \pi^o\Lambda) \;=\; -\,P\,(\pi^-p \rightarrow K^o\Lambda)$$

In table 4.3.1 forward cross sections *) and average polarizations are compared for these reactions and they show strong disagreement with the predicted 2 : 1 ratio for the cross sections and opposite polarizations. The cross sections for the corresponding $\Lambda(1520)$ reactions are also listed in table 4.3.1 and show the same disagreement.

Table 4.3.1 Comparison of forward cross sections and average polarizations ($t' < 0.8$ GeV).

Beam momentum	4.2 GeV/c	3.9 GeV/c [11]	4.5 GeV/c [12]
Reaction	$K^-p \rightarrow \pi^o\Lambda$	$\pi^-p \rightarrow K^o\Lambda$	
σ	59 ± 3 μb	49 ± 3 μb	49 ± 2 μb
P_Λ	0.49 ± 0.05	0.08 ± 0.13	0.22 ± 0.10
Reaction	$K^-p \rightarrow \pi^o\Lambda(1520)$	$\pi^-p \rightarrow K^o\Lambda(1520)$	
σ	34 ± 2 μb	-	21 ± 3 μb

*) In the comparison of cross sections in this section no corrections have been applied for phase-space differences. These corrections are small and do not change the conclusions.

The predictions listed above involve reactions in which only natural-parity exchange is allowed. The following prediction, which is also a consequence of the weak EXD assumption [4], should be valid both for natural- and unnatural-parity exchange:

$$2\,\frac{d\sigma}{dt}\,(K^-p \to \omega\Lambda) \;=\; \frac{d\sigma}{dt}\,(K^-p \to \phi\Lambda)$$

In fig. 4.3.3 this prediction is tested for the differential cross section, separated into the 3 contributions defined in section 4.2. The figure shows reasonable agreement for unnatural-parity exchange and disagreement for natural-parity exchange. However, if one tests the corresponding prediction for the $\Lambda(1520)$ reactions, the situation is reversed as can be seen in table 4.2.2.

If the EXD assumption is not used, but again only Regge-pole exchanges are considered, the following combinations of the predictions listed above should hold:

$$P_\Sigma\,\frac{d\sigma}{dt}\,(K^-p \to \pi^-\Sigma^+) \;=\; -\,P_\Sigma\,\frac{d\sigma}{dt}\,(\pi^+p \to K^+\Sigma^+)$$

$$2\,P_\Lambda\,\frac{d\sigma}{dt}\,(K^-p \to \pi^o\Lambda) \;=\; -\,P_\Lambda\,\frac{d\sigma}{dt}\,(\pi^-p \to K^o\Lambda)$$

As can be deduced from figure 4.3.2 and table 4.3.1 these predictions are not fulfilled.

It is clear from the examples shown above, that a simple Regge-pole model, even without EXD, will not give satisfactory results in describing the data. In more sophisticated models also the effects of "absorption", i.e. the absorptive rescattering of the particles in the initial and final state of the reactions, are taken into account. This absorption can be parametrized as Regge-cut contributions to the amplitudes. Examples of what can be achieved in this way are given by the curves in fig. 4.3.2, which

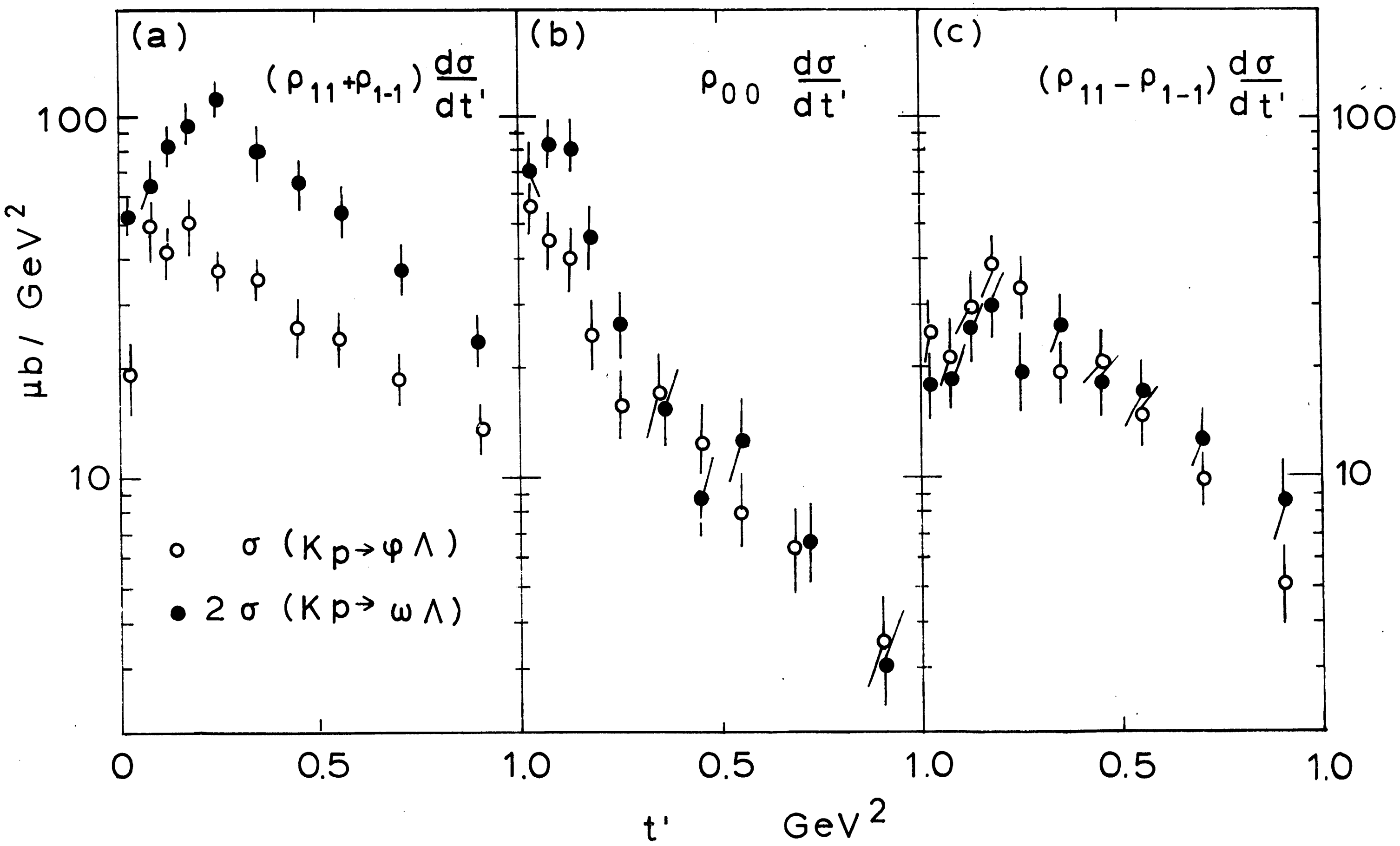

Fig. 4.3.3 Test of the prediction $\frac{d\sigma}{dt'}(K^-p \to \phi\Lambda) = 2\,\frac{d\sigma}{dt'}(K^-p \to \omega\Lambda)$ for natural- (a) and unnatural-parity exchange (b and c). The separation is described in section 4.2.

come from ref. [10] and the curves in fig. 3.10.2, which are explained in ref. [4]. In both cases these curves are the results of model-dependent amplitude fits in which our new data was not used. Although the curves give a reasonable description of the data, the agreement can still be improved. The Oxford group of our collaboration is currently attempting to describe the data with these models. In this thesis the subject will not be further discussed. General information on these models can be found in ref. 1.

4.4 Introduction to the additive quark model.

The two main ideas behind the additive quark model [2] are the following:

I. Mesons are composed of a quark (q) and an antiquark ($\bar{q}$) and baryons are qqq systems. The quantum numbers of the quarks which play a role in the reactions described here are listed in table 4.4. The decomposition of the various mesons and baryons into quarks can be found in ref. [2a].

Table 4.4 Quantum numbers of quarks

Name	J^P	B	I	I_3	S	Q
u	$1/2^+$	1/3	1/2	+1/2	0	2/3
d	$1/2^+$	1/3	1/2	-1/2	0	-1/3
s	$1/2^+$	1/3	0	0	-1	-1/3

II. In the reactions between two hadrons only one quark (or antiquark) of each hadron interacts with only one quark of the other hadron. The other quarks are "spectators" and do not take part in the interaction.

The corresponding diagram is plotted in fig. 4.4.1 for a two-body reaction of the type $K^-p \to$ Meson + Hyperon. The reaction amplitudes are coherent sums of the qq or $q\bar{q}$ amplitudes which can contribute to the corresponding spin states of the particles.

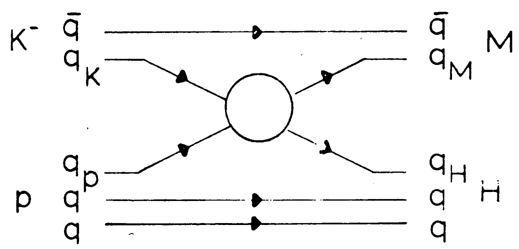

Fig. 4.4.1 Quark diagram for the reaction $K^-p \to M + H$

The relation between the reaction amplitudes and the qq amplitudes may be expressed as:

$$T^{M}_{H\,p} = \sum_{\substack{q_M\, q_K \\ q_H\, q_p}} C(M\,;q_M,q_K)\; C'(H,p\,;q_H,q_p) < q_H\, q_M\, |T|\, q_p\, q_K >$$

The subindices of the quark spin projections q_i refer to the particle to which the interacting quark belongs. The functions C and C' represent the couplings of the active quarks to the hadrons. They do not depend on the qq interaction, and in the comparison of different reaction amplitudes, their t-dependence is assumed to be equal for the corresponding reactions. In the derivation of these relations only the relevant Clebsch-Gordan coefficients are taken into account.

Since the quarks have spin 1/2, and parity is conserved in the qq interactions, there are eight independent qq amplitudes for a given combination of interacting quarks. The following notation will be used for these amplitudes

$$T^{q_M\, q_K}_{q_H\, q_p} \equiv < q_H\, q_M\, |T|\, q_p\, q_K >$$

To distinguish them from the normal reaction amplitudes only the signs of the quark spin projections will be denoted, e.g. T^{++}_{--} etc.

The relations between qq amplitudes and reaction amplitudes are particularly simple if a transversity base is used. (Provided the quarks in the particles have zero orbital angular momentum, the normal to the qq scattering plans coincides with the normal to the reaction plane). The eight non-zero and independent qq transversity amplitudes are

$$T^{++}_{++} \; , \; T^{++}_{--} \; , \; T^{--}_{++} \; , \; T^{--}_{--}$$

$$T^{+-}_{+-} \; , T^{+-}_{-+} \; , \; T^{-+}_{+-} \; , \; T^{-+}_{-+}$$

One notices that in this base quark spin flip or non-flip at the baryon vertex is coupled to quark spin flip or non-flip at the meson vertex. Since the meson transversity is related to the exchange-naturality (see section 4.2) this means that there is a correlation between the type of exchange (natural- or unnatural parity) and the type of qq transversity amplitudes (non-flip or flip) for these reactions.

By reducing the reaction amplitudes to sums of qq amplitudes using the assumptions of the additive quark model, one may predict:

a) the vanishing of reaction amplitudes which cannot be obtained from single qq scattering.
b) spin correlations between amplitudes for the same reaction.
c) relations between amplitudes of different reactions, which correspond to the same qq interaction.

More predictions for the reaction amplitudes can be obtained if one assumes time reversal invariance for the qq amplitudes e.g. $T^{+-}_{-+} = T^{-+}_{+-}$. However, the validity of these so called class B and C relations [13] may depend on the Lorentz frame in which they are tested. The predictions discussed in this thesis are all of class A, for which only the quark additivity assumption is needed.

For the hypercharge exchange $K^-p \rightarrow$ Meson + Hyperon, the model implies only $I = 1/2$ exchange in the t-channel and absence of exotic exchanges. As already indicated by the observation of small $I = 3/2$ exchanges in the reactions $K^-p \rightarrow \pi^+\Sigma^-$ and $K^-p \rightarrow \pi^+\Sigma^-(1385)$, one cannot expect an exact description of two-body reactions from such a simple model. In the following sections a 10 - 20% deviation from the predictions is not considered as evidence against the model, but rather as an indication for a contribution from more complicated processes, e.g. double quark scattering. These sections successively treat predictions concerning the amplitudes of only one reaction, predictions relating reactions with the same baryon vertex, and predictions relating reactions with the same meson vertex.

4.5 Quark model predictions for the amplitudes of one reaction.

Application of the additive quark model to reactions of the type $0^-1/2^+ \rightarrow 0^-3/2^+$ and $0^-1/2^+ \rightarrow 1^-3/2^+$ leads to a substantial reduction in the number of independent amplitudes for these reactions [13]. In this section predictions for the amplitudes of the reactions $K^-p \rightarrow \pi^-\Sigma^+(1385)$ and $K^-p \rightarrow \rho^-\Sigma^+(1385)$ are tested. Deviations from the predictions are discussed in terms of double quark scattering. Finally attention is drawn to the alignment found in the $0^-1/2^+ \rightarrow 0^-3/2^-$ reaction $K^-p \rightarrow \pi^o\Lambda(1520)$.

The reaction

$$K^-p \rightarrow \pi^-\Sigma^+(1385)$$

is of the type $0^-1/2^+ \rightarrow 0^-3/2^+$ and has the following non-zero transversity amplitudes (see section 3.10):

$T_{\frac{1}{2}\frac{1}{2}}$, $T_{-\frac{3}{2}\frac{1}{2}}$, $T_{-\frac{1}{2}-\frac{1}{2}}$, $T_{\frac{3}{2}-\frac{1}{2}}$

The quark line diagram for this reaction is drawn in fig. 4.5.1

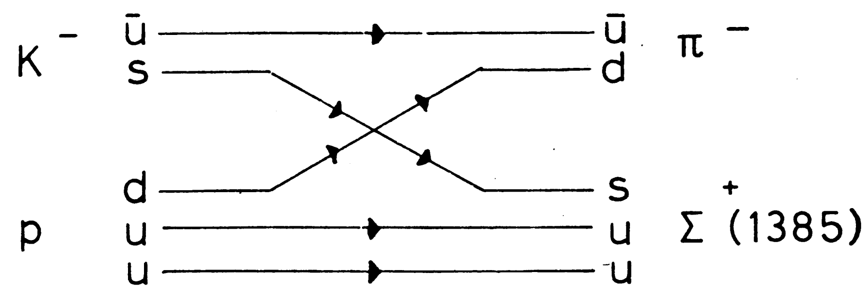

Fig. 4.5.1 Quark-line diagram for the reaction $K^-p \rightarrow \pi^-\Sigma^+(1385)$

As only one quark from the proton and one quark from the $\Sigma^+(1385)$ participate in the interaction, the total quark spin-projection in the baryons can change by at most one unit. Since moreover the quarks in these baryons have no orbital angular momentum, this means that the two amplitudes $T_{-\frac{3}{2}\frac{1}{2}}$ and $T_{\frac{3}{2}-\frac{1}{2}}$, which require a change of 2 units of spin, should be zero. The two remaining transversity amplitudes turn out to be composed of the same sum of qq-amplitudes.

Thus the quark model predictions for the transversity amplitudes of this reaction are:

$$T_{-\frac{3}{2}\frac{1}{2}} = T_{\frac{3}{2}-\frac{1}{2}} = 0 \quad \text{and} \quad T_{\frac{1}{2}\frac{1}{2}} = T_{-\frac{1}{2}-\frac{1}{2}}$$

Fig. 4.5.2 shows the moduli of these amplitudes as functions of t'. The amplitudes in this figure are normalized as $\sum_{Hp} |T_{Hp}|^2 = 1$. One sees that the predictions are very well fulfilled except in the region near t' = 0. In this region especially the double-flip amplitude $T_{\frac{3}{2}-\frac{1}{2}}$ is significantly different from zero.

Forward production in the reaction $K^-p \rightarrow \pi^+\Sigma^-(1385)$ corresponds to exotic t-channel quantum numbers and requires double quark scattering. Białias and Zalewski have proposed a model for such a process [14]. They note that exotic forward cross sections in reactions of the type $0^-1/2^+ \rightarrow 0^-1/2^+$ are much smaller than those in the corresponding reactions of the type $0^-1/2^+ \rightarrow 0^-3/2^+$, e.g. $\sigma_F(K^-p \rightarrow \pi^+\Sigma^-) << \sigma_F(K^-p \rightarrow \pi^+\Sigma^-(1385))$ (see fig. 3.2.2b and 3.3.1b). Therefore they assume that double spin flip amplitudes, which cannot occur in the $0^-1/2^+ \rightarrow 0^-1/2^+$ reactions, dominate in these double quark scattering processes. Furthermore this double quark scattering should also give a charge symmetric contribution to the double flip amplitudes of the non-exotic reaction $K^-p \rightarrow \pi^-\Sigma^+(1385)$. In order to test these predictions we have also performed an amplitude analysis of the exotic reaction in our experiment. This has indeed shown that the largest contribution comes from the double flip amplitude $T_{\frac{3}{2}-\frac{1}{2}}$ for t' < 0.25 GeV^2. Normalizing the amplitudes according to

$$\sum_{JHp} |{}^J T_{Hp}|^2 = \frac{d\sigma}{dt'}$$

where J = 3/2 for the resonance and J = 1/2 for the S-wave background contribution, which was added coherently in the

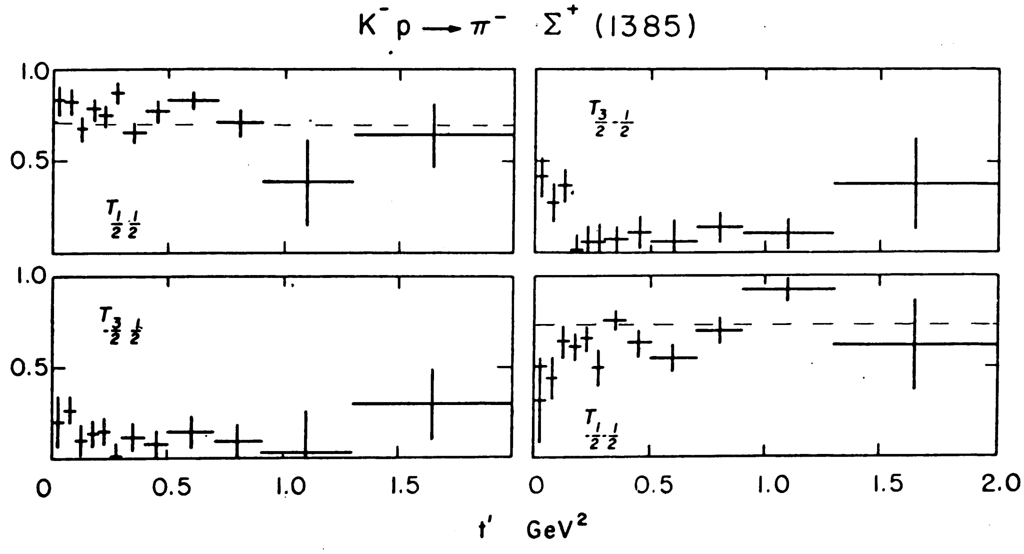

Fig. 4.5.2 Moduli of the transversity amplitudes for the reaction $K^-p \to \pi^-\Sigma^+(1385)$. The normalization is $\sum_{Hp} |T_{Hp}|^2 = 1$. Quark model predictions are $T_{\frac{3}{2}-\frac{1}{2}} = T_{-\frac{3}{2}\frac{1}{2}} = 0$ and $|T_{\frac{1}{2}\frac{1}{2}}| = |T_{-\frac{1}{2}-\frac{1}{2}}| = \frac{1}{\sqrt{2}}$ (indicated by the dotted lines).

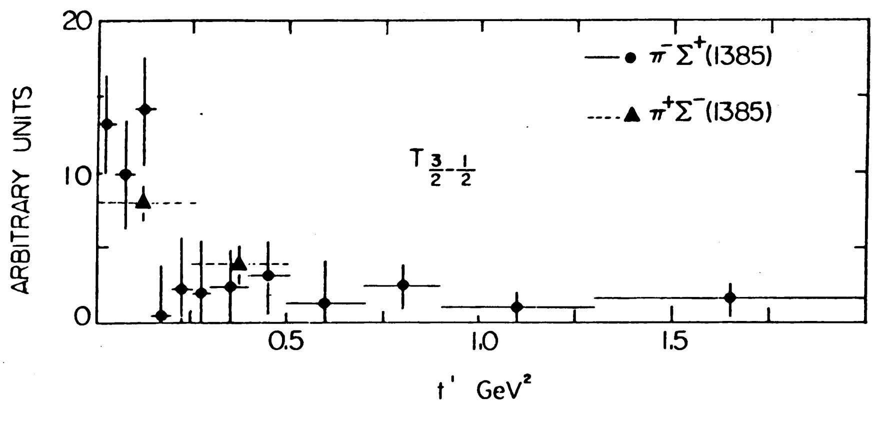

Fig. 4.5.3 Modulus of the transversity amplitude $T_{\frac{3}{2}-\frac{1}{2}}$ for the reactions $K^-p \to \pi^-\Sigma^+(1385)$ and $K^-p \to \pi^+\Sigma^-(1385)$. See text for normalization.

amplitude analyses [6], one may directly compare $T_{\frac{3}{2}-\frac{1}{2}}$ for both reactions. As is shown in fig. 4.5.3 the values are indeed consistent with charge symmetry.

The reaction

$$K^- p \rightarrow \rho^- \Sigma^+(1385)$$

belongs to the type $0^- 1/2^+ \rightarrow 1^- 3/2^+$ and has 12 non-zero transversity amplitudes:

$$T^{0}_{+\frac{1}{2}+\frac{1}{2}},\ T^{0}_{-\frac{3}{2}+\frac{1}{2}},\ T^{1}_{-\frac{1}{2}+\frac{1}{2}},\ T^{1}_{+\frac{3}{2}+\frac{1}{2}},\ T^{-1}_{-\frac{1}{2}+\frac{1}{2}},\ T^{-1}_{+\frac{3}{2}+\frac{1}{2}}$$

$$T^{0}_{-\frac{1}{2}-\frac{1}{2}},\ T^{0}_{+\frac{3}{2}-\frac{1}{2}},\ T^{1}_{+\frac{1}{2}-\frac{1}{2}},\ T^{1}_{-\frac{3}{2}-\frac{1}{2}},\ T^{-1}_{+\frac{1}{2}-\frac{1}{2}},\ T^{-1}_{-\frac{3}{2}-\frac{1}{2}}$$

The quark-line diagram for this reaction is the same as the one sketched in fig. 4.5.1, except that here a ρ^- is produced at the upper vertex. The four amplitudes with meson transversity 0 correspond to natural-parity exchange. For the additive quark model they are completely analoguous to the amplitudes of the reaction $K^- p \rightarrow \pi^- \Sigma^+(1385)$ and thus the same predictions apply. The eight remaining amplitudes correspond to unnatural-parity exchange. When these are decomposed into qq-scattering amplitudes the following relation is found between amplitudes with $\Sigma(1385)$ transversity 1/2 and 3/2 respectively:

$$T^{M}_{3\lambda,\lambda} = \sqrt{3}\ T^{M}_{\lambda,-\lambda} \quad \text{with} \quad M = \pm 1, \text{ and } \lambda = \pm \frac{1}{2}$$

In fig. 4.5.4 the quark model predictions are tested for the moduli of the amplitudes as functions of t'. Again the overall agreement is good. Four of the ten measurable relative phases can be used to test phase relations following from these predictions and they have shown reasonable agreement [15]. Tests and discussions of the class B and C predictions for this reaction can be found in ref. [15].

A similar analysis of the amplitudes for the reaction $K^-p \to \phi\Sigma^0(1385)$ has also shown agreement with the predictions listed above [15,16].

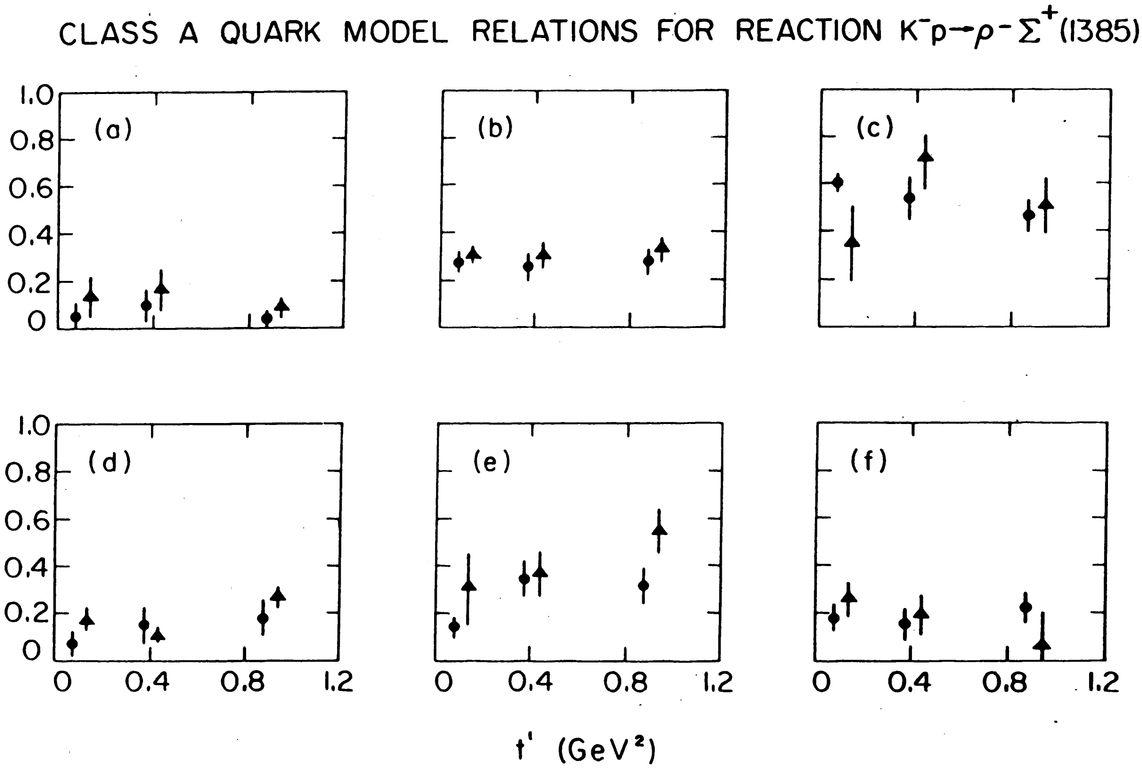

Fig. 4.5.4 Tests of quark model predictions for the moduli of the transversity amplitudes for the reaction $K^-p \to \rho^-\Sigma^+(1385)$. The figures test the relations: $T^{0}_{-\frac{3}{2}\frac{1}{2}} = T^{0}_{\frac{3}{2}-\frac{1}{2}} = 0$ (a), $T^{0}_{\frac{1}{2}\frac{1}{2}} = T^{0}_{-\frac{1}{2}-\frac{1}{2}}$ (b) and $T^{M}_{3Hp} = \sqrt{3}\, T^{M}_{H-p}$ for $M = \pm 1$ and $H = p = \pm\frac{1}{2}$ (c - f).

Contrary to the $0^-1/2^+ \rightarrow 0^-3/2^+$ reactions, the reactions of the type $0^-1/2^+ \rightarrow 0^-3/2^-$ cannot be treated simply in the context of the additive quark model, since the quarks in the final state baryon have orbital angular momentum. To my knowledge no quark model predictions for the amplitudes of these reactions have been published. However, the results obtained for the density matrix elements of the reaction $K^-p \rightarrow \pi^o\Lambda(1520)$ suggest that simple relations exist between the production amplitudes for this reaction. This will be discussed in the context of the vector meson exchange model of Stodolsky and Sakurai [17]. With this model, predictions for the helicity density matrix elements of both the $0^-1/2^+ \rightarrow 0^-3/2^+$ and the $0^-1/2^+ \rightarrow 0^-3/2^-$ reactions have been derived. For the first type of reactions the predictions correspond exactly to those of the additive quark model (which were derived later). In the vector meson exchange model the spin transitions at the baryon vertex of the $3/2^+$ reactions are considered to be of the type $1^-1/2^+ \rightarrow 3/2^+$ e.g. $K^*N \rightarrow \Sigma(1385)$, and they are predicted to be the same as the ones found in the reaction $\gamma N \rightarrow \Delta$. Consequently a M1 transition is expected to dominate and the corresponding values for the ρ parameters in any helicity frame are

$$\rho_{\frac{3}{2}\frac{3}{2}} = \frac{3}{8} \ , \ \mathrm{Re}\ \rho_{\frac{1}{2}\frac{3}{2}} = 0 \quad \text{and} \quad \mathrm{Re}\ \rho_{-\frac{1}{2}\frac{3}{2}} = \frac{\sqrt{3}}{8}$$

In fig. 4.5.5a these observables are plotted as functions of t' for the reaction $K^-p \rightarrow \pi^-\Sigma^+(1385)$ and the predicted values are indicated by dotted lines. The agreement is good, except at small t' values, where small deviations are seen. These correspond to the deviations from the quark model predictions for the amplitudes, which were discussed above.

Similarly Stodolsky and Sakurai derived predictions for the vertex $K^*N\Lambda(1520)$, which is of the type $1^-1/2^+ \rightarrow 3/2^-$. The 3 possible transitions and the corresponding ρ-parameters in the t-channel helicity frame are listed below

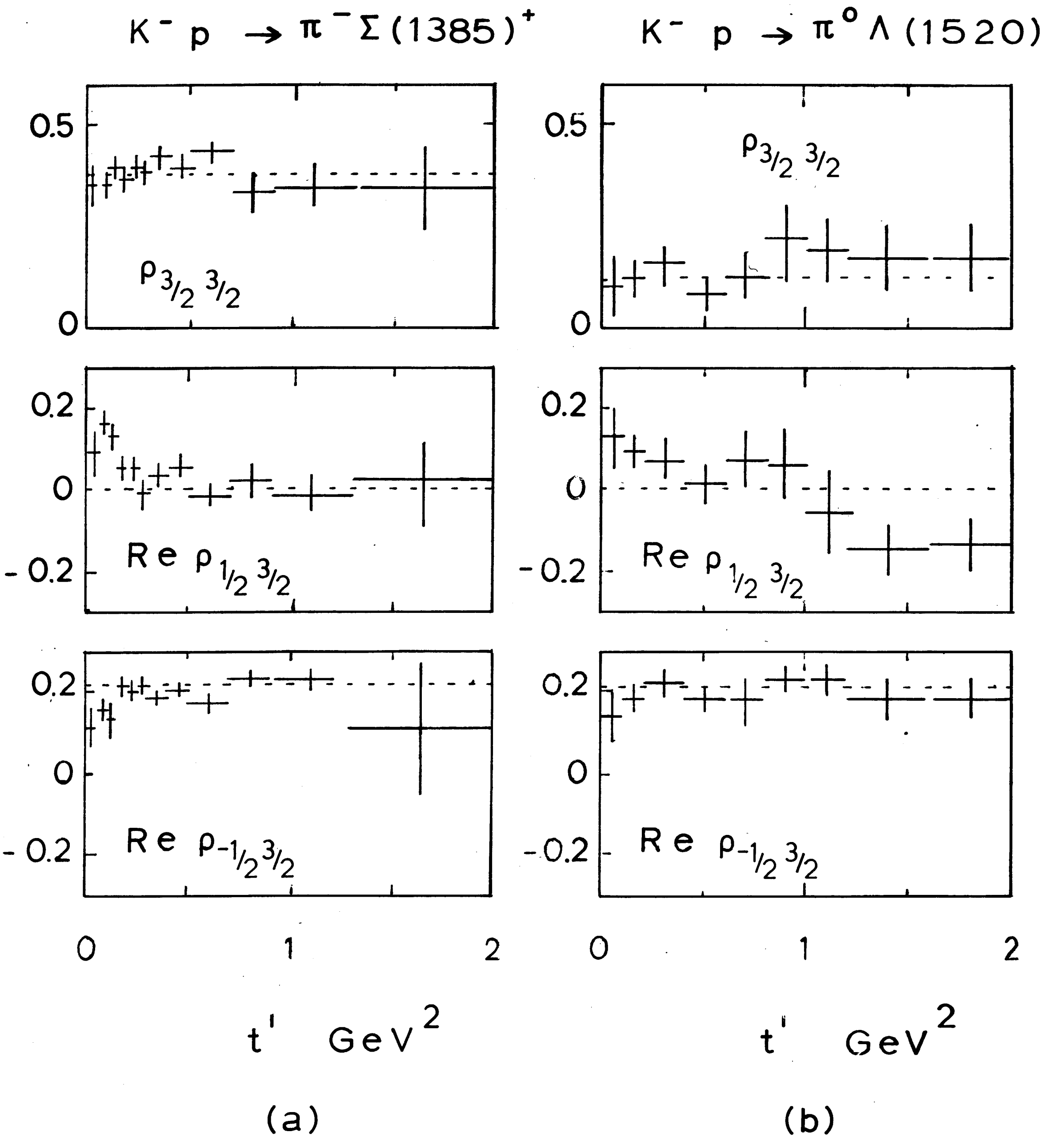

Fig. 4.5.5 Distributions of spin density matrix elements for the $0^-1/2^+ \rightarrow 0^-3/2^+$ reaction $K^-p \rightarrow \pi^-\Sigma(1385)^+$, fig. (a), and for the $0^-1/2^+ \rightarrow 0^-3/2^-$ reaction $K^-p \rightarrow \pi^0\Lambda(1520)$, fig. (b). For fig. (a) the s-channel helicity frame is used, in which the quantization axis is along the direction of the resonance in the total c.m. frame. For fig. (b) the t-channel helicity frame is used, where this exis is along the direction of the incoming proton in the resonance rest frame. The dotted lines correspond to predictions discussed in section 4.5.

Transition	$\rho_{\frac{3}{2}\frac{3}{2}}$	Re $\rho_{\frac{1}{2}\frac{3}{2}}$	Re $\rho_{-\frac{1}{2}\frac{3}{2}}$
E1	3/8	0	$-\sqrt{3}/8$
M2	1/8	0	$\sqrt{3}/8$
L1	0	0	0

As can be seen in fig. 4.5.5b the experimental values for the reaction $K^-p \to \pi^o\Lambda(1520)$ surprisingly correspond to dominance of M2 (indicated by the dotted lines in the figure) rather than E1. It would be worthwile to investigate whether the additive quark model can predict such a result.

4.6 Quark model relations for reactions with the same baryon vertex.

Those reactions of the type $K^-p \to$ Meson + Hyperon which are allowed by the additive quark model can be written as $K^-p \to M^{\bar{o}} + Y^{\overset{+}{o}}$, where Y stands for any hyperon with strangeness $S = -1$. Since pure isospin $I = 1/2$ exchange is implied by the model, the production amplitudes of the reactions which can occur in both charge modes are related in a simple way: $T(K^-p \to M^- + Y^+) = 2T(K^-p \to M^o + Y^o)$. Thus it will be sufficient to consider only the qq-interactions in the reactions of the type

$$K^-p \to M^o + Y^o \tag{1a}$$

The two allowed quark-line diagrams for these reactions are shown in fig. 4.6.1.

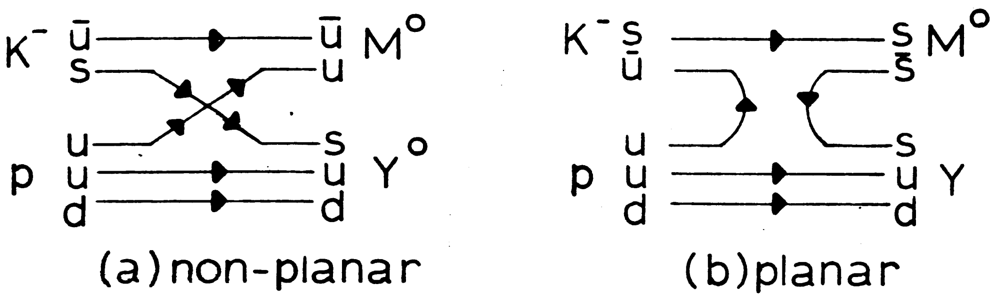

Fig. 4.6.1 Quark-line diagrams for the reactions of the type $K^- p \rightarrow M^o + Y^o$.

The planar diagram corresponds to $q\bar{q}$-annihilation and recreation, and the non-planar diagram to qq-rearrangement. Which (or what mixture) of the two processes contributes to a particular reaction, depends on the $q\bar{q}$ composition of the outgoing meson M^o. The $q\bar{q}$ composition for pure SU(3) singlet and octet states is given below:

SU(3) singlet $\quad M_1^o(I=0) = \frac{1}{\sqrt{3}}(u\bar{u} + d\bar{d} + s\bar{s})$

SU(3) octet
$$M_8^o(I=0) = \frac{1}{\sqrt{6}}(u\bar{u} + d\bar{d} - 2s\bar{s})$$
$$M_8^o(I=1) = \frac{1}{\sqrt{2}}(u\bar{u} - d\bar{d})$$

The physical M $(I=0)$ mesons are mixtures of the $I=0$ pure singlet and octet states. For the $J^P = 1^-$ mesons the mixing is supposed to be "ideal", such that

$$\phi = -s\bar{s}$$

and $\quad \omega = \frac{1}{\sqrt{2}}(u\bar{u} + d\bar{d})$

Thus for the reactions of type (1a), ω production corresponds only to the non-planar diagram, and ϕ productions only to the planar diagram *). Moreover, since $u\bar{u} = \frac{1}{\sqrt{2}}(\rho^o + \omega)$ the additive quark model predicts [18]

$$T(K^-p \rightarrow \omega Y^o) = T(K^-p \rightarrow \rho^o Y^o)$$

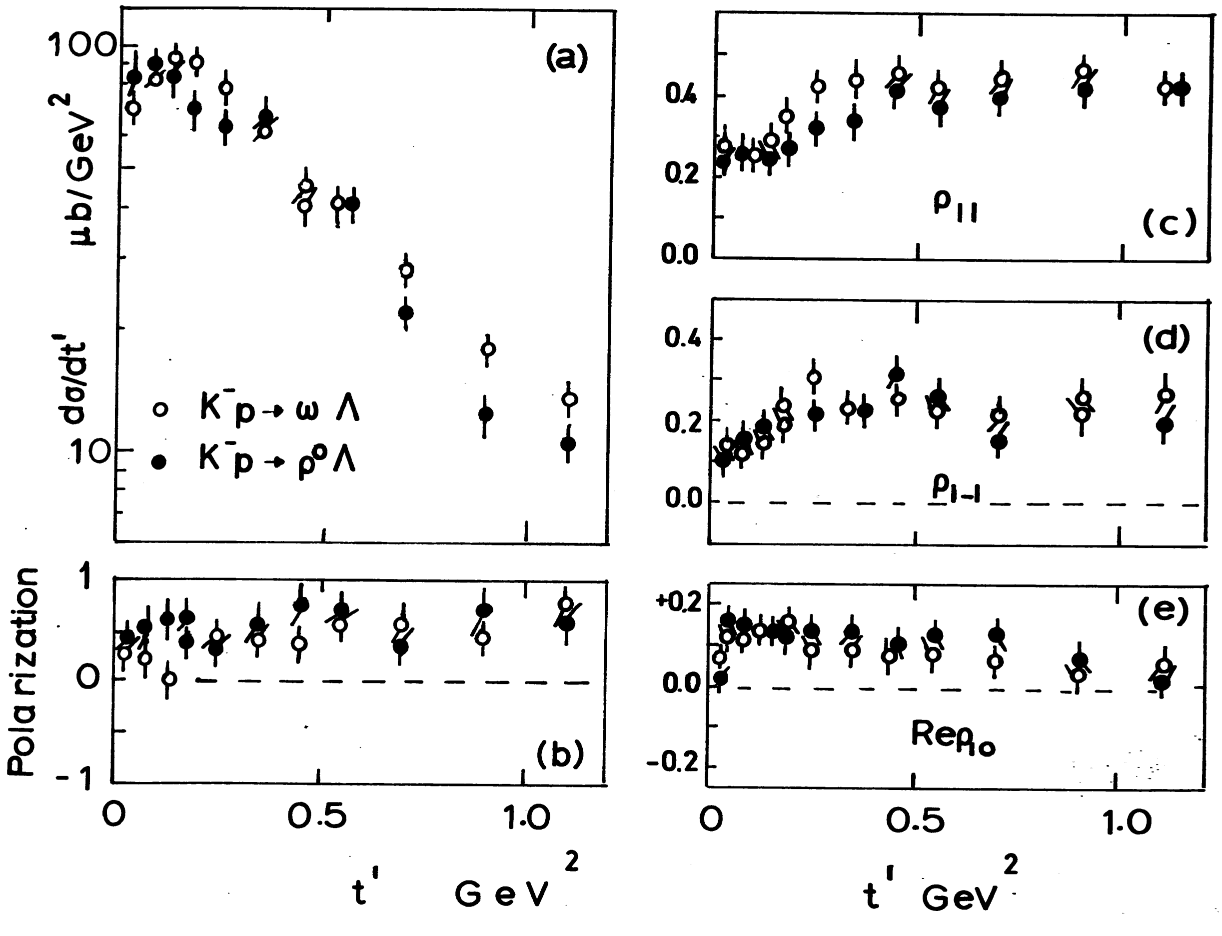

Fig. 4.6.2 Comparison of the $d\sigma/dt'$ (a), the Λ-polarization (b), and the spin density matrix elements of the vector-meson in the s-channel helicity frame (c - e) for the reactions $K^-p \rightarrow \rho^o\Lambda$ and $K^-p \rightarrow \omega\Lambda$.

---

*) Apart from ideal mixing one must also assume that the $u\bar{u}$ and $s\bar{s}$ meson states cannot transform into each other spontaneously. The suppression of this transition is known as the Zweig rule [19].

Table 4.6.1 Comparison of integrated cross section (in μb) for $t' < 1.0$ GeV^2. A 5% error is added to the statistical error in the cross sections. The quark model predictions are: $A + B = C + D$ for the reactions with a 0^- meson, and $A = D$ and $B = C$ for the other reactions. Correcting for phase-space differences between the reactions would not make an appreciable change in the level of agreement or disagreement with the predictions.

	K^-p 4.2 GeV/c			π^-p 3.9 GeV/c [11],[20]	π^-p 4.5 GeV/c [12]
	A	B	C	D	
$0^-1/2^+$	$\eta\Lambda$ 19 ± 2	$\eta'\Lambda$ 44 ± 4	$\pi^0\Lambda$ 62 ± 4	$K^0\Lambda$ 52 ± 5	50 ± 4
$0^-3/2^-$	$\eta\Lambda(1520)$ 7 ± 3	$\eta'\Lambda(1520)$ 12 ± 3	$\pi^0\Lambda(1520)$ 36 ± 3	$K^0\Lambda(1520)$ -	22 ± 4
$1^-1/2^+$	$\phi\Lambda$ 58 ± 3	$\omega\Lambda$ 48 ± 3	$\rho^0\Lambda$ 44 ± 3	$K^*\Lambda$ 49 ± 4	45 ± 4
$1^-1/2^+$	$\phi\Sigma^0$ 27 ± 3	- -	- -	$K^*\Sigma^0$ 31 ± 5	20 ± 3
$1^-3/2^+$	$\phi\Sigma(1385)^0$ 22 ± 4	- -	- -	$K^*\Sigma(1385)^0$ 20 ± 4	-
$2^+1/2^+$	$f'\Lambda$ 13 ± 2	$f\Lambda$ 39 ± 7	$A_2^0\Lambda$ 22 ± 3	$K^{**}\Lambda$ -	16 ± 3

In fig. 4.6.2 this prediction is tested by comparing the differential cross section, the Λ-polarization, and the density matrix elements of the vector-meson for the reactions $K^-p \to \rho^o,\omega\Lambda$. The figure shows good overall agreement. Small deviations can be seen but, since these could originate from the treatment of the large background under the ρ^o, or from the parametrization of the ρ/ω interference [4], it is not clear whether they should be taken seriously. A direct comparison of the transversity amplitudes for these two reactions has shown the same level of agreement [20]. The integrated forward cross sections for these reactions can be compared in table 4.6.1.

If one replaces the spectator s quark in the upperhalf of the planar diagram (fig. 4.6.1b) by a spectator d quark, the diagram corresponds to the reactions of the type $\pi^-p \to K^o, K^{*o}, .. + Y^o$. (Replacing the spectator quark in the other diagram does not lead to reactions which are accessible to experiment). Since the $q\bar{q}$ amplitudes are the same, the production amplitudes for these reactions are related to those for the reactions corresponding with the original diagram and the following prediction can be obtained [18]:

$$T(K^-p \to \phi Y^o) \quad = \quad -T(\pi^-p \to K^{*o}Y^o)$$

In fig, 4.6.3 and 4.6.4 this prediction is tested by comparing observables for the reactions $K^-p \to \phi\Lambda,\Sigma^o$ with those for the corresponding π^-p reactions at 3.9 GeV/c [20]. In each case there is good agreement. A similar comparison for the reactions with $Y = \Sigma(1385)^o$ has also shown good [15] agreement. The integrated forward cross sections for the reactions used in these tests are listed in table 4.7.1.

Assuming ideal mixing for the tensor mesons ($J^P = 2^+$) leads to similar predictions:

$$T(K^-p \to A_2^oY^o) \quad = \quad T(K^-p \to fY^o)$$

$$T(K^-p \to f'Y^o) \quad = \quad -T(\pi^-p \to K^{**}Y^o)$$

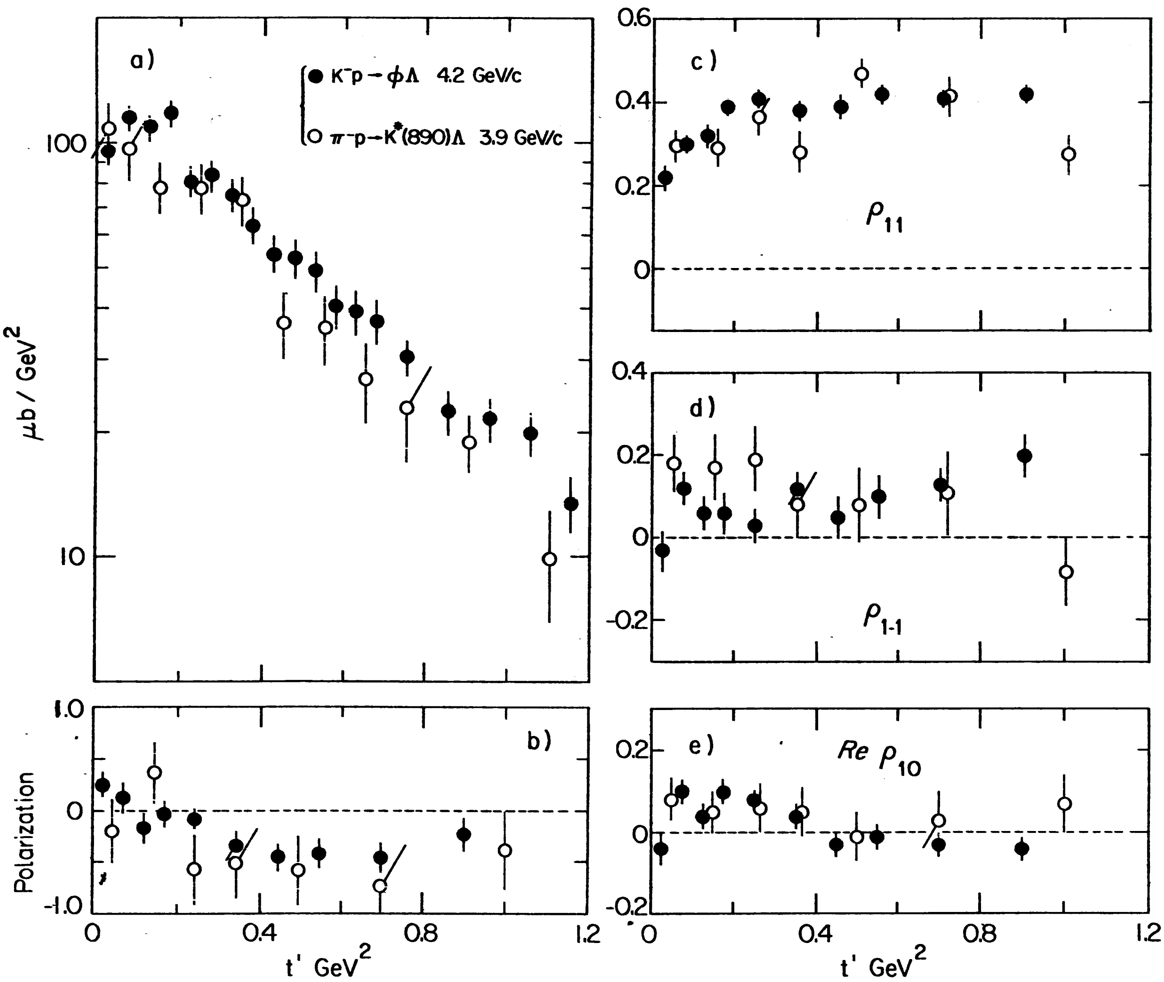

Fig. 4.6.3 Comparison of the $d\sigma/dt'$ (a), the Λ-polarization (b), and the spin density matrix elements of the vector-meson in the s-channel helicity frame (c - e) for the reaction $K^-p \to \phi\Lambda$ at 4.2 GeV/c and the reaction $\pi^-p \to K^{*o}\Lambda$ at 3.9 GeV/c [20].

The first prediction can be tested by comparing the $d\sigma/dt'$ and P_Λ distributions for the reactions $K^-p \to A_2^o, f\Lambda$ shown in fig. 3.6.1a and b. For the cross sections the agreement is not good, but the errors are large and the discrepancy is of the order of 2 standard deviations. The integrated cross sections listed in table 4.6.1 for the reactions $K^-p \to f'\Lambda$ and $\pi^-p \to K^{**}\Lambda$ are in good agreement with the second prediction.

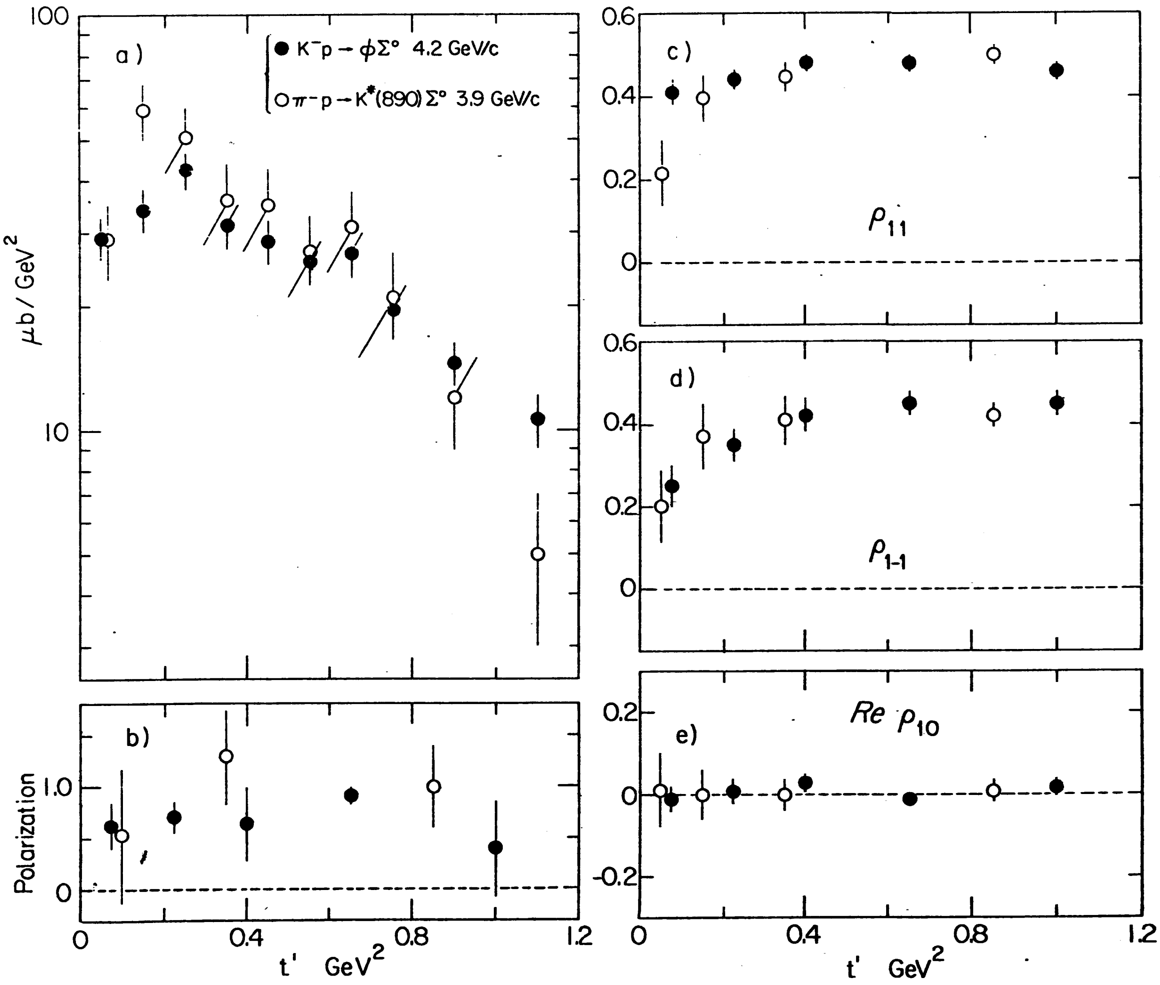

Fig. 4.6.4 Comparison of the $d\sigma/dt'$ (a), the Σ^o-polarization (b), and the spin density matrix elements of the vector-meson in the s-channel helicity frame (c - e) for the reaction $K^-p \to \phi\Sigma^o$ at 4.2 GeV/c and the reaction $\pi^-p \to K^{*o}\Sigma$ at 3.9 GeV/c [20].

For the $J^P = 0^-$ mesons the mixing angle is far from the ideal value. Consequently both diagrams contribute to each of the reactions of the type $K^-p \to \eta Y^o$ and $K^-p \to \eta' Y^o$. Therefore one cannot derive separate predictions for η or η' production in these reactions, but the following sum-rule should be obeyed [18]:

$$\frac{d\sigma}{dt}(K^-p \to \eta Y^o) + \frac{d\sigma}{dt}(K^-p \to \eta' Y^o) = \frac{d\sigma}{dt}(K^-p \to \pi^o Y^o) + \frac{d\sigma}{dt}(\pi^-p \to K^o Y^o)$$

In fig. 4.6.5 this prediction is tested for the Λ reactions. The π^-p data has been interpolated at 4.2 GeV/c from the data of ref. [11] at 3.9 GeV/c, and of ref. [12] at 4.5 GeV/c. The figure shows clearly that the sum-rule is violated at all t values and also that the violation is t-dependent. The integrated cross sections listed in table 4.6.1 also show how serious the disagreement is. The discrepancy is even worse for the $\Lambda(1520)$ reactions, as can be seen in the same table.

Summarizing one may conclude that the quark model relations of this section are correct for vector mesons, and probably also for tensor mesons, but fail in the case of pseudoscalar mesons. As also in other aspects the description of the pseudoscalar mesons meets with problems, we attribute this failure to complications in the pseudoscalar octet rather than to the additive quark model.

4.7 Quark model relations for reactions with the same meson vertex.

In this section the additive quark model is used to relate the amplitudes of reactions with the same meson vertex. We consider only those reactions of type (1a) in which the hyperon is a state with zero orbital angular momentum between the quarks. Thus we select the reactions of the type:

$$K^-p \to M^o + \Lambda, \Sigma^o, \Sigma(1385)^o \qquad (1b)$$

For each choice of M^o the three reactions in the set correspond to the same (mixture of) quark-line diagram(s) plotted in fig. 4.6.1a and b. The only difference between the reactions is the spin and isospin structure of the diquark spectator system at the baryon vertex. If one uses the SU(6) baryon wave functions for this structure the following prediction can be derived [21]:

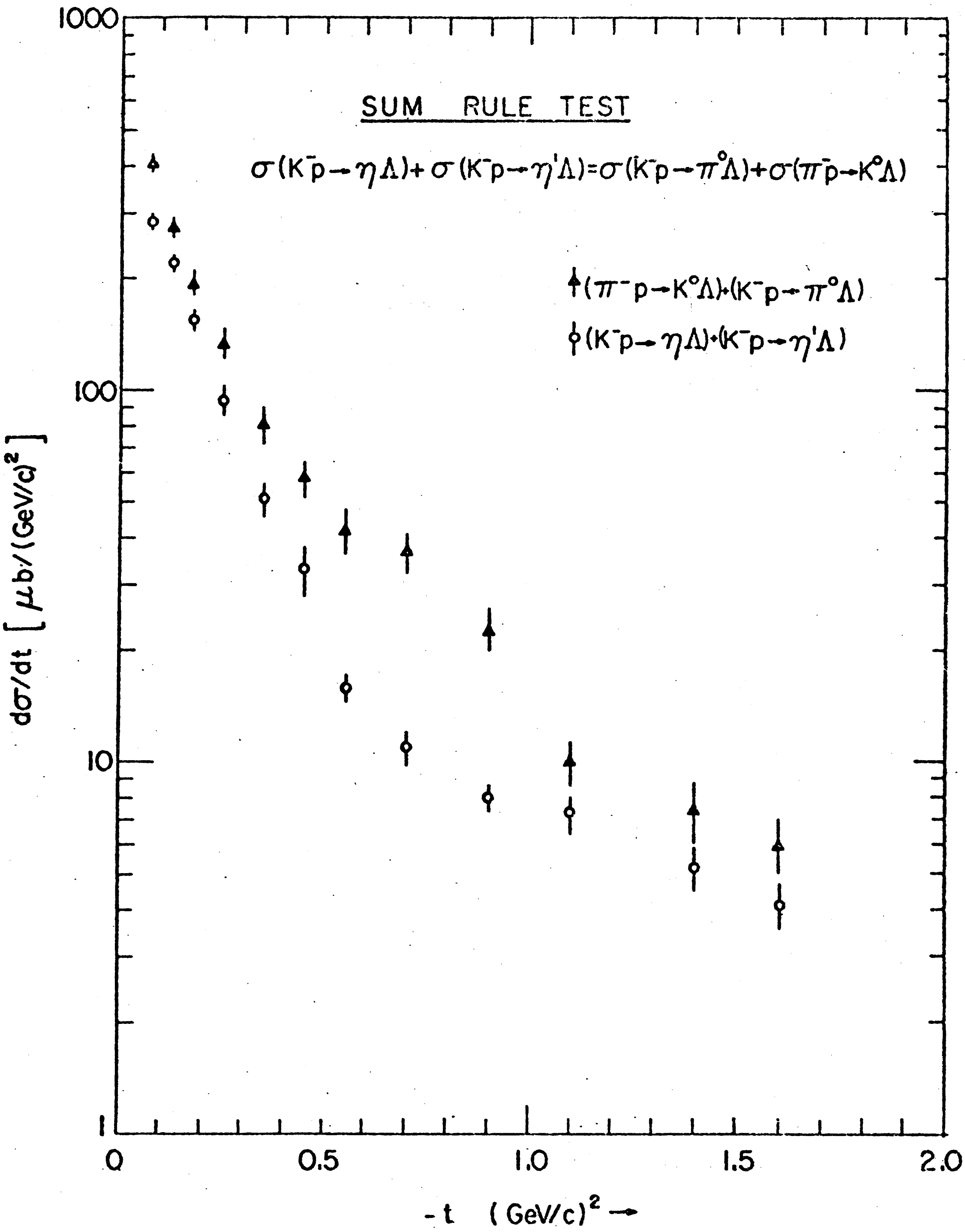

Fig. 4.6.5 Test of the quark model prediction for the differential cross sections of $0^- 1/2^+ \rightarrow 0^- 1/2^+$ reactions.

$$\sigma(\Lambda) = 3[\sigma(\Sigma) + \sigma(Y)] \qquad \text{(I)}$$

where the notation used is $\sigma(\Lambda) \equiv \frac{d\sigma}{dt}(K^-p \rightarrow M^o + \Lambda)$ etc. In this section $Y \equiv \Sigma(1385)$ and the hyperons are neutral, if the charge is not indicated. Prediction (I) is known to be in strong disagreement with experiment (ref [22] contains a list of references to experimental tests of this prediction). Using our data this can be shown for the reactions with $M^o = \pi^o, \rho^o$ or ϕ. Integrated forward cross sections ($t' < 1.0$ GeV) are listed in table 4.7.1 for the corresponding sets of reactions. In this table the relation $\sigma(K^-p \rightarrow M^-\Sigma^+, Y^+) = 4(K^-p \rightarrow M^o\Sigma^o, Y^o)$ is used if the data on the M^o reaction is not available. As remarked previously, this is allowed in the context of the additive quark model. The mass differences between the hyperons have been taken into account by using the corrected cross sections

$$\bar{\sigma}(\Sigma,Y) = \frac{P_{\Lambda}^{cm}}{P_{\Sigma,Y}^{cm}}\,\sigma(\Sigma,Y)$$ where the P_i^{cm}'s are the c.m.s. momenta in the final state of the reactions. The corrections are < 5% for $\sigma(\Sigma)$, and < 20% for $\sigma(Y)$. As prediction (I) can be derived for both exchange-naturalities also the separated cross sections are listed. By comparing the cross sections in the first and the last column of this table one sees that they are all inconsistent with the ratio 3 : 1. This does not mean however that the additive quark model is totally useless for relating the reactions of type (1b), as will be shown in the rest of this section.

To begin with, one may observe that the cross sections in the first and last column of table 4.7.1 are nearly equal for every set of reactions. This can also be shown for the integrated cross sections obtained from other K^-p experiments (at beam momenta between 3 and 14 GeV/c), and even for the cross sections of corresponding reactions in π^-p, $\bar{p}p$ and γp experiments [22]. All these cross sections are within 20% consistent with the ratio $\bar{\sigma}(\Lambda)/[\bar{\sigma}(\Sigma) + \bar{\sigma}(Y)] = 1.1$.

Table 4.7.1 Comparison of forward cross sections ($t' < 1.0$ GeV^2) for reactions of the type $K^-p \rightarrow M^o + \Lambda, \Sigma^o, \Sigma^o(1385)$.

Reactions used	$\bar{\sigma}(\Lambda)$	$\bar{\sigma}(\Sigma)$	$\bar{\sigma}(Y)$	$\bar{\sigma}(\Sigma) + \bar{\sigma}(Y)$
$\pi^o\Lambda, \pi^-\Sigma^+, \pi^-Y^+$	61 ± 3	31 ± 2	20 ± 1	51 ± 3
$\rho^o\Lambda, \rho^o\Sigma^o, \rho^-Y^+$	46 ± 3	18 ± 2	20 ± 2	38 ± 3
idem $\bar{\sigma}_n$	24 ± 2	16 ± 1	4 ± 1	20 ± 2
idem $\bar{\sigma}_u$	22 ± 2	3 ± 1	16 ± 2	19 ± 2
$\phi\Lambda, \phi\Sigma^o, \phi Y^o$	59 ± 3	27 ± 2	26 ± 2	53 ± 3
idem $\bar{\sigma}_n$	27 ± 3	23 ± 2	8 ± 1	31 ± 2
idem $\bar{\sigma}_u$	32 ± 3	4 ± 2	18 ± 2	22 ± 2

Moreover a comparison of the differential cross sections in our experiment shows the same near equality of $\bar{\sigma}(\Lambda)$ and $\bar{\sigma}(\Sigma) + \bar{\sigma}(Y)$ as a function of t'. This can be seen in fig. 4.7.1 for the π^o reactions, and in fig. 4.7.2 for the ρ^o and the ϕ reactions, both also separated into $\bar{\sigma}_n$ and $\bar{\sigma}$. Considering that the reactions have rather different $d\sigma/dt'$ distributions, this experimental observation is not trivial, and therefore points to the existence of simple relations between the amplitudes of the reactions. The additive quark model can provide such simple relations, but the SU(6) symmetry requirements for the baryon wave functions lead to the wrong predictions. In the following I will discuss these quark model relations in more detail, and also discuss the possibilities of obtaining better predictions for the observables.

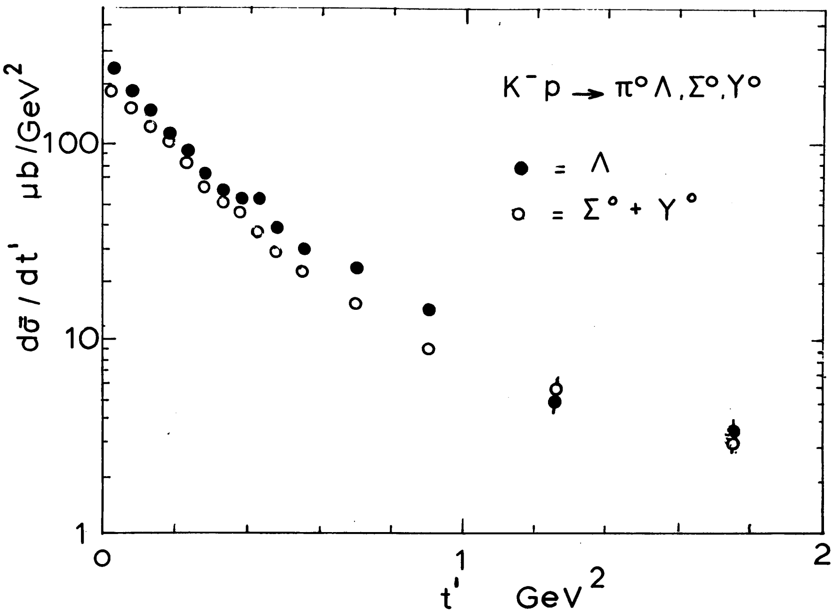

Fig. 4.7.1 Comparison of the differential cross sections $\frac{d\bar\sigma}{dt'}(K^- p \to \pi^o \Lambda)$ and $\frac{1}{4}\left[\frac{d\bar\sigma}{dt'}(K^- p \to \pi^- \Sigma^+) + \frac{d\bar\sigma}{dt'}(K^- p \to \pi^- \Sigma^+(1385)\right]$

The quark model relations are most easily derived if one expresses the production amplitudes T^M_{Hp} for the reactions of type (1b) in meson-quark scattering amplitudes $T^M_{q_H\, q_p}$, which by themselves are linear combinations of the actual quark-quark scattering amplitudes:

$$T^M_{q_H\, q_p} = \sum_{q_M\, q_K} C^M_{q_M\, q_K} \langle q_H\, q_M |T| q_p\, q_K \rangle$$

The sub-indices of the q's refer to the particle to which the interacting quark belongs. In the transversity frame the allowed meson-quark amplitudes are all independent, and the relations are simple. Moreover in this frame there is a direct connection between the meson transversity M and the exchange-naturality. In table 4.7.2 the relations between the $T^M_{H\,p}$ and the $T^M_{q_H\, q_p}$ are listed for the reactions in which M^o is a pseudoscalar or a vector meson. In this

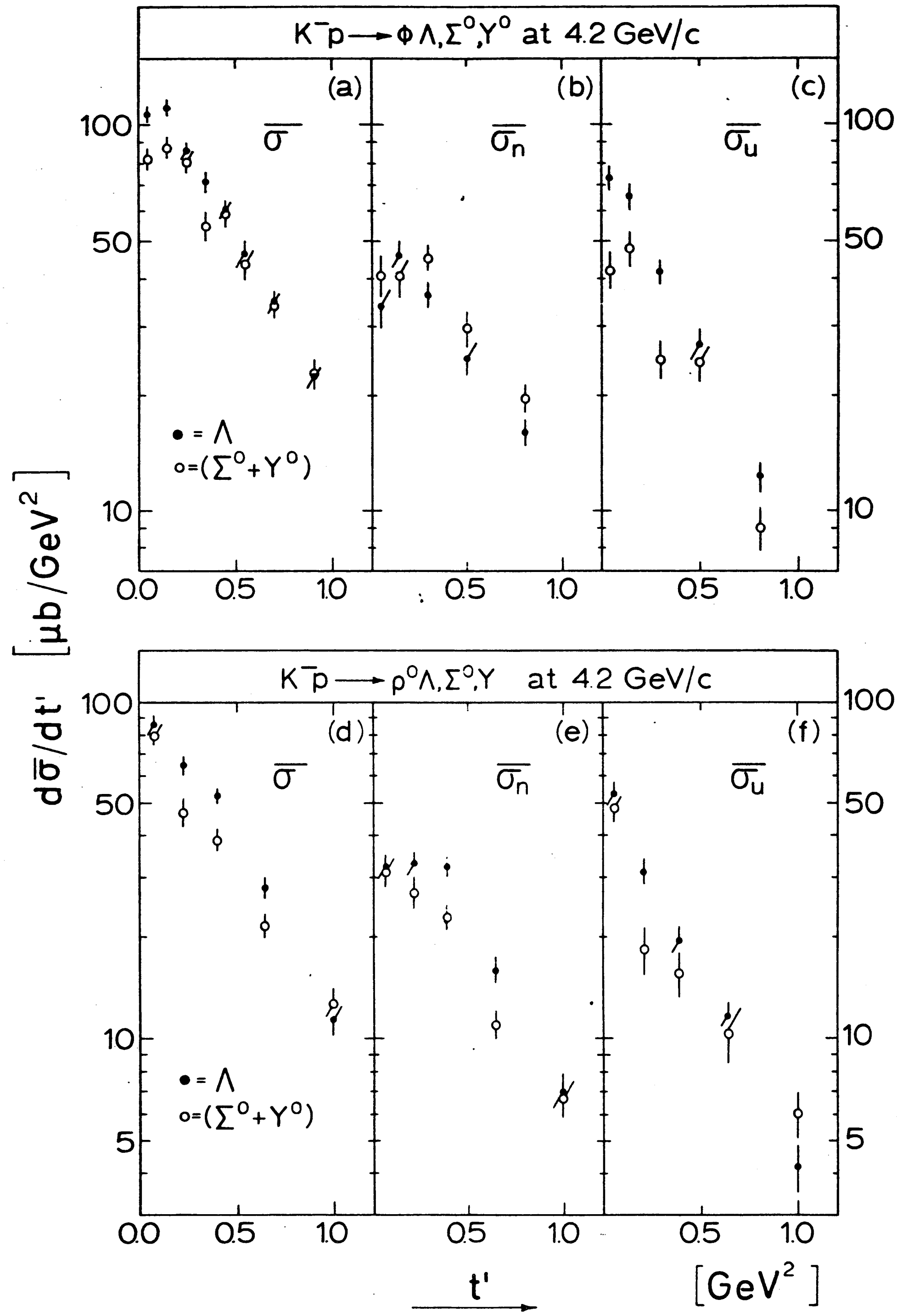

Fig. 4.7.2 Comparison of differential cross sections. In fig. (a) $\frac{d\bar{\sigma}}{dt'}(K^-p \to \phi\Lambda)$ is compared with $\frac{d\bar{\sigma}}{dt'}(K^-p \to \phi\Sigma^o) + \frac{d\bar{\sigma}}{dt'}(K^-p \to \phi\Sigma^o(1385))$. In fig. (d) $\frac{d\bar{\sigma}}{dt'}(K^-p \to \rho^o\Lambda)$ is compared with $\frac{d\bar{\sigma}}{dt'}(K^-p \to \rho^o\Sigma^o) + \frac{1}{4}\frac{d\bar{\sigma}}{dt'}(K^-p \to \rho^-\Sigma^+(1385))$. In fig. (b) and (e) the corresponding natural-parity exchange parts, and in fig. (c) and (f) the unnatural-parity exchange parts are compared.

Table 4.7.2 Relations between the transversity amplitudes T^{M}_{Hp} for the reactions $K^{-}p \rightarrow M^{o} + \Lambda,\Sigma,Y$ and the meson-quark transversity amplitudes $T^{M}_{q_H\, q_p}$ (see text). The relations apply to the reactions where M^{o} has $J^{P} = 0^{-}$ (only natural-parity exchange), or $J^{P} = 1^{-}$.

Hyperon	natural-parity exchange	unnatural-parity exchange
Λ	$T^{0}_{\frac{1}{2}\frac{1}{2}} = T^{0}_{++}$ $T^{0}_{-\frac{1}{2}-\frac{1}{2}} = T^{0}_{--}$	$T^{\pm 1}_{-\frac{1}{2}\frac{1}{2}} = T^{\pm 1}_{-+}$ $T^{\pm 1}_{\frac{1}{2}-\frac{1}{2}} = -C\ T^{\pm 1}_{+-}$
Σ	$T^{o}_{\frac{1}{2}\frac{1}{2}} = C_{\Sigma}(T^{0}_{++} + 2T^{0}_{--})$ $T^{0}_{-\frac{1}{2}-\frac{1}{2}} = C_{\Sigma}(2T^{0}_{++} + T^{0}_{--})$	$T^{\pm 1}_{-\frac{1}{2}\frac{1}{2}} = -C_{\Sigma}T^{\pm 1}_{+-}$ $T^{\pm 1}_{\frac{1}{2}-\frac{1}{2}} = -C_{\Sigma}T^{\pm 1}_{+-}$
Y	$T^{0}_{\frac{1}{2}\frac{1}{2}} = C_{Y}(-T^{0}_{++} + T^{0}_{--})$ $T^{0}_{-\frac{1}{2}-\frac{1}{2}} = C_{Y}(-T^{0}_{++} + T^{0}_{--})$	$T^{\pm 1}_{\frac{3}{2}\frac{1}{2}} = \sqrt{3}\ T^{\pm 1}_{\frac{1}{2}-\frac{1}{2}} = \sqrt{3}\ C_{Y}T^{\pm 1}_{+-}$ $T^{\pm 1}_{-\frac{3}{2}-\frac{1}{2}} = \sqrt{3}\ T^{\pm 1}_{-\frac{1}{2}\frac{1}{2}} = \sqrt{3}\ C_{Y}T^{\pm 1}_{-+}$
SU(6) : $C_{\Sigma} = 1/\sqrt{27}$, $C_{Y} = \sqrt{2/27}$		

notation the distinction between the two sorts of amplitudes is made by only denoting the sign of the quark transversities in the meson-quark amplitudes. The normalization is such that

$$\sum_{M\, q_H\, q_p} |T^{M}_{q_H\, q_p}| = \sigma(\Lambda)$$

and the SU(6) branching ratios are absorbed into the coefficients C_Σ and C_Y.

The differential cross sections and the polarization of the hyperon (with spin J = 1/2 or 3/2) are expressed in the reaction transversity amplitudes as:

$$\frac{d\sigma}{dt} = \sum_{MHp} |T^{M}_{Hp}|^2 \quad \text{and} \quad P\,\frac{d\sigma}{dt} = \frac{1}{J} \sum_{MHp} p\,|T^{M}_{Hp}|^2$$

Using table 4.7.2 one obtains the following predictions for these observables:

for natural-parity exchange

$$\sigma_n(\Lambda) = \frac{1}{9}\left[\frac{\sigma_n(\Sigma)}{C_\Sigma^2} + 2\,\frac{\sigma_n(Y)}{C_Y^2}\right] \overset{SU(6)}{=} 3\left[\sigma_n(\Sigma) + \sigma_n(Y)\right] \qquad \text{(NI)}$$

$$P_n(\Lambda)\sigma_n(\Lambda) = -\,\frac{P_n(\Sigma)\sigma_n(\Sigma)}{3C_\Sigma^2} \overset{SU(6)}{=} -9\;P_n(\sigma)\sigma_n(\Sigma) \qquad \text{(NII)}$$

$$P_n(Y) = 0 \qquad \text{(NIII)}$$

for unnatural-parity exchange:

$$\sigma_u(\Lambda) = \frac{\sigma_u(\Sigma)}{C_\Sigma^2} = \frac{\sigma_u(Y)}{4C_Y^2} \overset{SU(6)}{=} 27\;\sigma_n(\Sigma) = \frac{27}{8}\;\sigma_n(Y) \qquad \text{(UI)}$$

(UI) implies

$$\sigma_u(\Lambda) = \frac{1}{9}\left[\frac{\sigma_u(\Sigma)}{C_\Sigma^2} + \frac{\sigma_u(Y)}{C_Y^2}\right] \overset{SU(6)}{=} 3\left[\sigma_u(\Sigma) + \sigma_u(Y)\right] \qquad \text{(UII)}$$

$$P_u(\Lambda) = P_u(\Sigma) = \frac{6}{5}\,P_u(Y) \qquad \text{(UIII)}$$

The polarization predictions (NIII) and (UIII) do not depend on the coefficients C_Σ and C_Y. The first one is implied by the predictions for the amplitudes tested in section 4.5. It is in good agreement with experiment except near $t' = 0$, where possibly small $I = 3/2$ exchange amplitudes are present. The second prediction, although satisfied by the data, cannot be used as a sensitive test of the model in our case, since the P_u values observed for the ρ^o and ϕ reactions are small and the measurement errors are large.

The other predictions are found to disagree with experiment in the sense that the SU(6) values for C_Σ and C_Y lead to factors in front of $\sigma(\Sigma)$ and $\sigma(Y)$ which are about 3 times too big. For the predictions (NI) and (UII) this discrepancy was already shown at the beginning of this section. For the prediction (UI) this can be checked in table 4.7.1, where the σ_u values are in reasonable agreement with the relation $\sigma_u(\Lambda) = 9\ \sigma_u(\Sigma) = \frac{9}{8}\ \sigma_u(Y)$. And also for the prediction (NII) a similar factor 3 discrepancy has been observed [16].

One can now make the following ad-hoc assumption:
the relations between the production amplitudes for the reactions of type (1b) following from table 4.7.2 are correct, but one should use $C_\Sigma = \frac{1}{3}$ and $C_Y = \frac{\sqrt{2}}{3}$ instead of the SU(6) values.

For natural-parity exchange this assumption has been tested in detail by fitting the 5 observables $\sigma_n(\Lambda)$, $\sigma_n(\Sigma)$, $\sigma_n(Y)$, $P_n(\Lambda)$ and $P_n(\Sigma)$ with the 3 parameters $|T^o_{++}|$, $|T^o_{--}|$ and $\cos\delta$, where δ is the relative phase between the two quark-meson amplitudes. For the π^o-reactions such fits have been performed at 15 different t' values between 0 and 2 GeV^2 and the results are shown in fig. 4.7.3. The fitted values for the observables at each t' are connected by drawn lines in this figure. These fits show that the relations of table 4.7.2 are well satisfied when the new values for C_Σ and C_Y

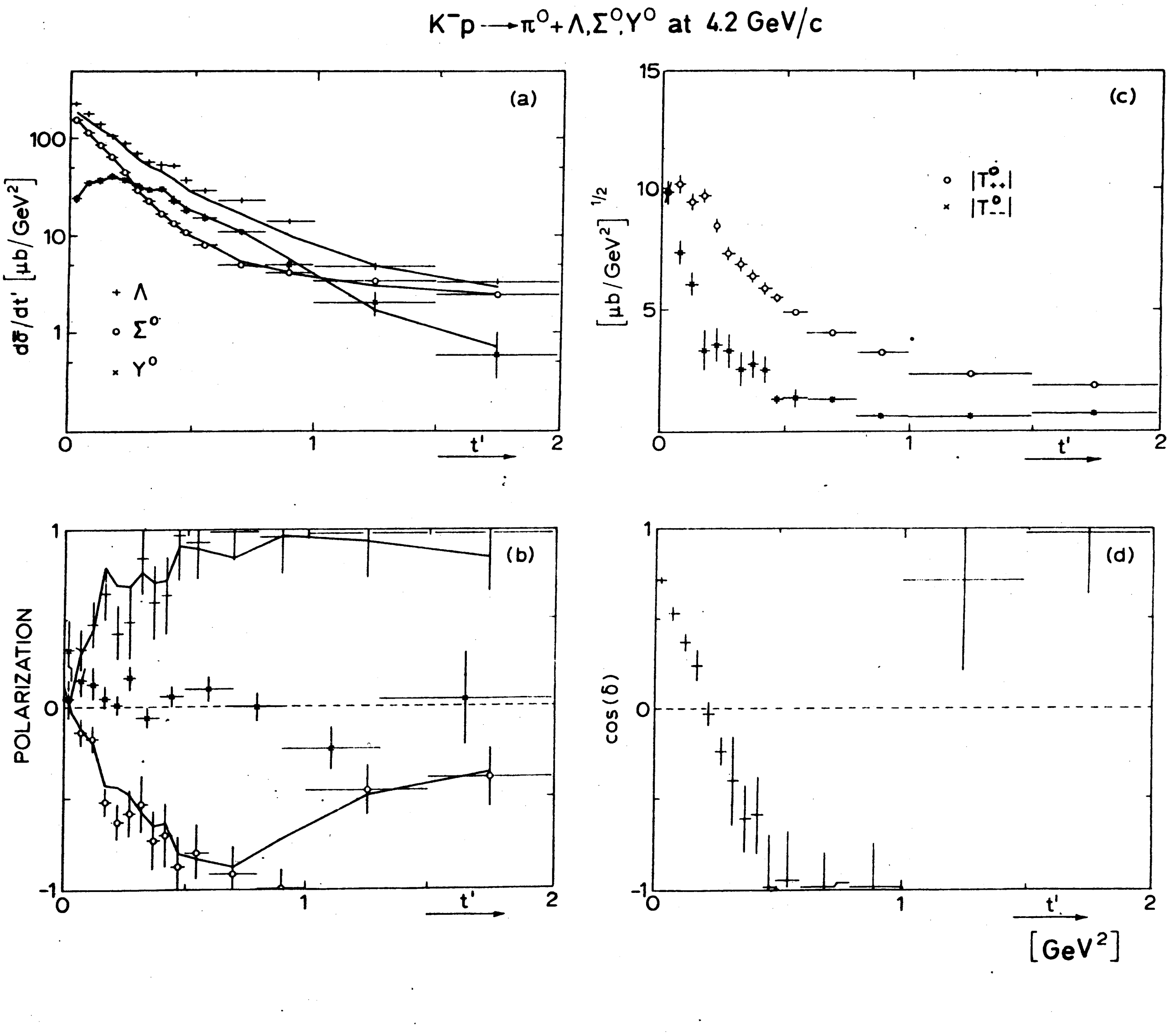

Fig. 4.7.3 Observables and fit-results for the reactions $K^-p \to \pi^0 + \Lambda, \Sigma, Y$.

(a) The corrected differential cross sections. The fitted $d\bar{\sigma}/dt'$ values are connected by drawn lines.

(b) The hyperons polarizations. The Y-polarization is not used in the fits, it is predicted to be zero.

(c) Moduli of the meson-quark amplitudes T^0_{++} and T^0_{--}.

(d) The cosine of the phase between these amplitudes.

are used. The corresponding values for $|T^{o}_{++}|$, $|T^{o}_{--}|$ and $\cos\delta$ are smooth functions of t', which also indicates that the ad-hoc assumption makes sense. The natural-parity exchange data for the ρ^{o} and the ϕ reactions have also been fitted in this way and the results are shown in fig. 4.7.4 and 4.7.5. Again a reasonable description of the observables can be obtained with the three variables and the relations following from the ad-hoc assumption.

The alternative values proposed for C_{Σ} and C_{Y} and used in the fits were chosen on the basis of the approximate factor of 3 discrepancy between the data and the SU(6) predictions. However, one cannot arbitrarily deviate from the SU(6) values for these coefficients and still use the normal 3 quark structure for the baryons to derive the relations in table 4.7.2, without also breaking SU(3) symmetry. This problem can be avoided by using baryon wave functions which correspond to non-symmetric three quark states. Such wave functions have been proposed by Pavković [23] and Carroll et al. [24]. If for example the diquark spectator system in these reactions is not considered as just the combination of the two quarks which do not take part in the interactions, but as a distinguishable bound state, the symmetry requirements can be relaxed.

It can be shown [25] that with the use of such a quark-diquark model for baryons and the additivity assumption, one can derive the same relations as listed in table 4.7.2. Moreover, in that case the coefficients C_{Σ} and C_{Y} can be expressed as functions of a mixing angle Γ in such a way as to assure the conservation of SU(3) symmetry. On the basis of our experimental value for the ratio $\sigma_u(Y)/\sigma_u(\Lambda)$ in the ρ^{o} reactions a value of $\Gamma \approx 53^{o}$ has been proposed. This value corresponds to $C_{\Sigma} \approx 0.34$ and $C_{Y} \approx 0.43$, which is very close to the values $C = \frac{1}{3}$ and $C = \frac{\sqrt{2}}{3}$ used in the fits described above. A publication containing tests and discussions of this model is being prepared by the Nijmegen group of our collaboration [25].

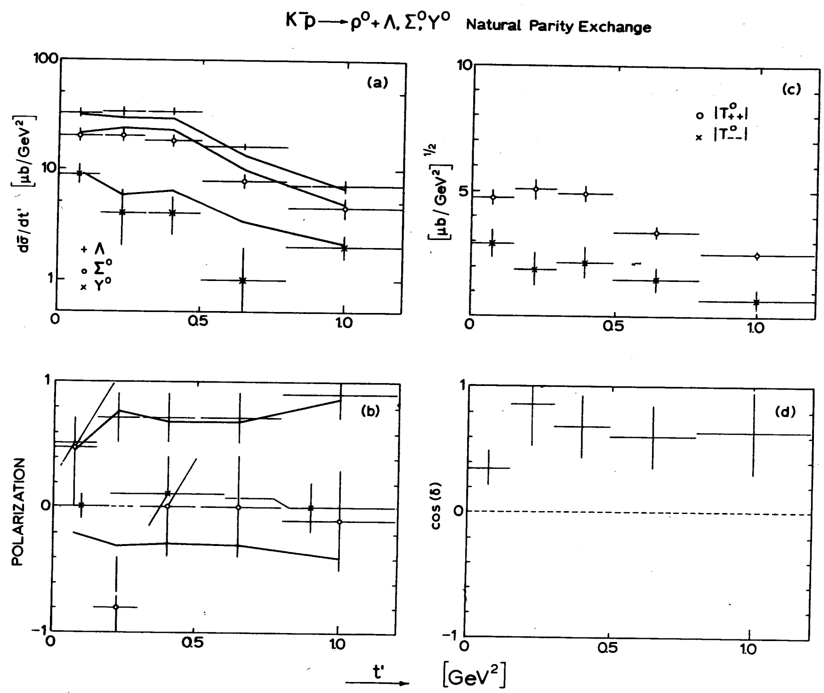

Fig. 4.7.4 Observables and fit-results for natural-parity exchange in the reactions $K^-p \to \rho^0 + \Lambda,\Sigma,$ Y, see caption of fig. 4.7.3.

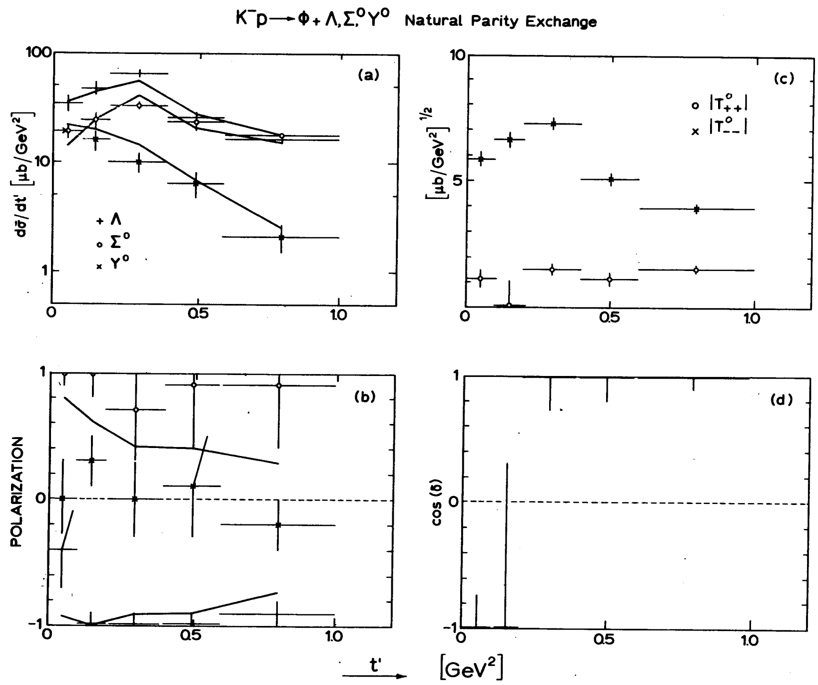

Fig. 4.7.5 Observables and fit results for natural-parity exchange in the reactions $K^-p \to \phi + \Lambda,\Sigma,$ Y, see caption of fig. 4.7.3.

4.8 Conclusions.

In this chapter two phenomenological models which attempt to describe forward scattering in two-body hypercharge exchange reactions have been confronted with the data of our experiment. The high statistical sensitivity allows more detailed tests of the predictions (especially those for the hyperon polarizations) than was previously possible.

The observed large polarizations and the deviations from line-reversal predictions for these reactions have clearly shown that simple Regge-exchange models without absorption are not useful. The precision and variety of our new data should be helpful in the evaluation of more complicated exchange models.

The predictions coming from the additive quark model are in much better agreement with our data. Apart from small deviations which can be expected for such a simple model, two effects have been observed which have more serious consequences:

a) The sum-rule predicted for pseudoscalar meson production in these reactions is not at all satisfied, moreover the deviation appears to depend on momentum-transfer.
b) The relations between the amplitudes of the reactions $K^-p \rightarrow M^o + \Lambda, \Sigma^o, \Sigma^o(1385)$ which can be derived with quark-additivity are well satisfied if SU(6) symmetry for the baryons is abandoned.

Many of the quark model predictions tested in this chapter may in principle also be obtained with an exchange model especially if one introduces symmetries like SU(3) and SU(6), and special assumptions like ideal mixing and the Zweig rule into the Regge-exchange description. However, in most cases one also needs other simplifying assumptions (e.g. exchange-degeneracy) which imply the wrong predictions for line-reversed reactions and/or the hyperon polarizations. The additive quark model, on the other hand, does not suffer from problems with line-reversed reactions. In this model they correspond to different quark-line diagrams (planar and non-planar respectively) and the reaction amplitudes are not directly related. Another example which shows the difference between the two models is given by the polarization data for the reactions $K^- p \to \pi^o \Lambda$ and $K^- p \to \pi^- \Sigma^+(1385)$. Strong exchange-degeneracy in a Regge-model predicts zero polarizations for both reactions. For $\pi^o \Lambda$ the data disagrees totally with the prediction, for $\pi^- \Sigma^+(1385)$ there is good agreement. The additive quark model predicts zero polarization only for the second reaction. In this model the polarization in $\pi^o \Lambda$ involves four independent qq amplitudes, and without further assumptions on these amplitudes there is no evident restriction on the polarization. Thus one may conclude that the quark model explanation for relations which work in both models, seems to be more attractive.

References Chapter 4

1) Introductions to and reviews of Regge and absorption models:

a) V. Barger, D.B. Cline, "Phenomenological Theories of High Energy Scattering", Benjamin, New York, 1969.

b) G.C. Fox, C. Quigg, Ann. Rev. Nucl. Sc. 23 (1973) 219.

c) F. Schrempp, B. Schrempp, Proc. E.P.S. Conference, Palermo, 1975, 682.

d) G.L. Kane, A. Seidl, Rev. Mod. Phys. 48 (1976) 309.

e) A.C. Irving, R.P. Worden, "Regge Phenomenology", to be published in Physics Reports.

2) Introductions to and reviews of the quark model:

a) J.J.J. Kokkedee, "The Quark Model", Benjamin, New York, 1969.

b) H.J. Lipkin, Phys. Rev. 8C (1973) 173.

3) J.P. Ader et al., Nuovo Cimento 56A (1968) 952.

4) M.J. Losty et al., "Non-strange vector meson production in K^-p interactions at 4.2 GeV/c", CERN/EP/PHYS 77-45, and to be published.

5) A. Kotanski, Acta Phys. Polon. 30 (1966) 629.

6) S.O. Holmgren et al., Nucl. Phys. B119 (1977) 261.

7) A. Bashian et al., Phys. Rev. D4 (1971) 2667.

8) S.M. Pruss et al., Phys. Rev. Lett. 23 (1969) 189.

9) K.S. Han et al., Phys. Rev. Lett. 24 (1970) 1353.

10) H. Navelet, P.R. Stevens, Nucl. Phys. B104 (1976) 171.

11) M. Abramovich et al., Nucl. Phys. B27 (1971) 477.

12) D. Crennell et al., Phys. Rev. D6 (1972)1220.

13) A. Białias, K. Zalewski, Nucl. Phys. B6 (1968) 449, 463, 478.

14) A. Białias, K. Zalewski, Phys. Lett. 30B (1969) 109.

15) M. Aguilar-Benitez et al., Nucl. Phys. B124 (1977) 189.

16) G.G.G. Massaro, "The reactions $K^-p \to \rho^o, \varphi + \Lambda, \Sigma^o, \Sigma^o(1385)$ and Quark Model Predictions", 4.2 report 85, Zeeman-laboratory, Amsterdam, 1977.

17) L. Stodolsky, J.J. Sakurai, Phys. Rev. Lett. 17 (1966) 412.

18) G. Alexander et al., Phys. Rev. Lett. 17 (1966) 412.

19) S. Okubo, Phys. Lett. 5 (1963) 165.
G. Zweig, "Symmetries in Elementary Particle Physics", Academic Press, New York, 1965, 192.
J. Iizuka, Suppl. to Progr. of Theor. Phys. 37-38 (1966) 21.

20) D. Yaffe et al., Nucl. Phys. B75 (1974) 365.

21) H.J. Lipkin, F. Scheck, Phys. Rev. Lett. 18 (1976) 347.

22) J.C. Kluyver et al., "On quark model relations for hypercharge exchange reactions", Preprint ACNO collab., Amsterdam,1977

23) M.I, Pavkovič, Phys. Rev. D13 (1976) 2128 and D14 (1976) 3186.

24) J. Carroll et al., Phys. Rev. 174 (1968) 1681.

25) M. Zrałek et al., "Test of an additive diquark spectator model for meson-baryon quasi-two-body reactions", Preprint ACNO collab., Nijmegen, 1977.

Table A1 K^-p two-body reaction kinematics

The number between brackets is the particle mass in MeV, the other quantities are in GeV[2].

Beam - $K^-(494)$ Target - $p(938)$ p_{lab} - 4.15

E_{cm} - 2.99 p_{cm}^{in} - 1.30

Reaction	p_{cm}^{fin}	t_{max}	u_{max}	$t'_{max}-u'_{max}$
K (496) N (939)	1.30	-.00	.05	6.76
π (135) Λ (1116)	1.29	.01	.10	6.69
η (549) Λ (1116)	1.22	-.00	.06	6.36
ρ^0 (770) Λ (1116)	1.16	-.02	.03	6.01
ω (785) Λ (1116)	1.15	-.02	.02	5.98
η' (958) Λ (1116)	1.08	-.05	-.02	5.61
Φ (1020) Λ (1116)	1.05	-.06	-.04	5.46
f (1270) Λ (1116)	.90	-.13	-.16	4.70
A_2 (1310) Λ (1116)	.88	-.15	-.18	4.56
f' (1514) Λ (1116)	.71	-.27	-.34	3.69
π (140) Σ (1193)	1.26	.01	.11	6.53
ρ (770) Σ (1192)	1.12	-.03	.03	5.82
Φ (1020) Σ (1192)	1.01	-.08	-.06	5.24
f (1270) Σ (1192)	.85	-.18	-.20	4.43
K (496) Ξ (1318)	1.15	-.00	.10	5.96
π (140) Σ (1385)	1.17	.03	.16	6.10
ρ (770) Σ (1385)	1.02	-.07	.03	5.29
Φ (1020) Σ (1385)	.89	-.17	-.11	4.61
π (135) Λ (1520)	1.11	.04	.20	5.75
η (549) Λ (1520)	1.02	-.02	.12	5.33
ω (785) Λ (1520)	.93	-.11	.01	4.82
η' (958) Λ (1520)	.83	-.21	-.11	4.29
Φ (1020) Λ (1520)	.78	-.26	-.17	4.07
K (494) Ξ^* (1530)	1.04	-.01	.14	5.39

Table A2 Cross-sections and Polarizations of $0^-1/2^+$ reactions

$\pi^0\Lambda$

t' GeV^2	$d\sigma/dt'$ μb/GeV^2
.000 - .025	263. ± 14.
.025 - .050	206. ± 13.
.050 - .075	187. ± 12.
.075 - .100	177. ± 12.
.100 - .125	148. ± 11.
.125 - .150	136. ± 10.
.150 - .200	107. ± 6.
.200 - .250	89. ± 6.
.250 - .300	70. ± 5.
.300 - .350	57. ± 5.
.350 - .400	53. ± 6.
.400 - .450	52. ± 4.
.450 - .500	37. ± 3.
.500 - .600	28. ± 2.
.600 - .700	26. ± 2.
.700 - .800	20. ± 2.
.80 - 1.00	14. ± 1.
1.00 - 1.25	5.8 ± 1.0
1.25 - 1.50	4.4 ± .8
1.50 - 2.00	3.3 ± .4
2.00 - 3.33	.9 ± .2

t' GeV^2	Polarization
.000 - .050	.05 ± .11
.050 - .100	.33 ± .12
.100 - .150	.47 ± .13
.150 - .200	.64 ± .15
.200 - .250	.42 ± .16
.250 - .300	.48 ± .19
.300 - .350	.84 ± .21
.350 - .400	.59 ± .21
.400 - .450	.63 ± .22
.450 - .500	.97 ± .26
.500 - .600	.93 ± .21
.600 - .800	.99 ± .17
.80 - 1.00	.96 ± .21
1.00 - 1.50	.98 ± .26
1.50 - 2.00	.98 ± .33
2.00 - 3.30	.95 ± .39

u' GeV^2	$d\sigma/du'$ μb/GeV^2
.000 - .100	12. ± 2.
.100 - .300	3.7 ± 1.3
.300 - .700	5.0 ± .7
.70 - 1.10	4.5 ± .9
1.10 - 1.50	2.8 ± .7
1.50 - 2.00	2.3 ± .5
2.00 - 3.30	.5 ± .2

u' GeV^2	Polarization
.000 - .100	.36 ± .39
.100 - .700	-.81 ± .25
.70 - 2.00	-.75 ± .21
2.00 - 3.30	.07 ± .51

$\eta\Lambda$

t' GeV^2	$d\sigma/dt'$ μb/GeV^2
.000 - .025	155. ± 13.
.025 - .050	121. ± 12.
.050 - .100	73. ± 6.
.100 - .150	52. ± 5.
.150 - .300	12. ± 2.
.300 - .600	3.2 ± .6
.60 - 1.00	6.7 ± .6
1.00 - 1.40	4.5 ± .8
1.40 - 2.20	1.6 ± .3
2.20 - 3.20	.7 ± .2

t' GeV^2	Polarization
.000 - .050	-.04 ± .10
.050 - .300	-.17 ± .09
.30 - 1.00	.32 ± .17
1.00 - 3.20	.17 ± .34

u' GeV^2	$d\sigma/du'$ μb/GeV^2
.000 - .500	1.2 ± .5
.50 - 1.50	.7 ± .3
1.50 - 3.15	.3 ± .1

u' GeV^2	Polarization
0.00 - 3.20	.39 ± .35

$\eta'\Lambda$

t' GeV^2	$d\sigma/dt'$ μb/GeV^2
.000 - .050	211. ± 14.
.050 - .100	170. ± 12.
.100 - .150	130. ± 11.
.150 - .200	94. ± 9.
.200 - .250	79. ± 8.
.250 - .300	53. ± 7.
.300 - .350	41. ± 6.
.350 - .400	33. ± 5.
.400 - .600	12. ± 2.
.60 - 1.00	2.6 ± .5
1.00 - 1.50	2.1 ± .5
1.50 - 2.00	1.7 ± .4
2.00 - 2.80	1.2 ± .3

t' GeV^2	Polarization
.000 - .050	0.00 ± .17
.050 - .100	.30 ± .19
.100 - .150	.31 ± .22
.150 - .300	.40 ± .16
.300 - .600	.41 ± .22
.60 - 2.80	.24 ± .25

u' GeV^2	$d\sigma/du'$ μb/GeV^2
.000 - .500	2.2 ± .9
.50 - 1.50	1.1 ± .6
1.50 - 2.80	.5 ± .3

u' GeV^2	Polarization
0.00 - 2.80	.56 ± .69

Table A2 (Continued)

$\pi^-\Sigma^+$

t' GeV²	dσ/dt μb/GeV²
0.00 - .05	620. ± 20.
.05 - .10	449. ± 16.
.10 - .15	329. ± 13.
.15 - .20	249. ± 10.
.20 - .25	173. ± 9.
.25 - .30	114. ± 7.
.30 - .35	88. ± 6.
.35 - .40	65. ± 5.
.40 - .45	52. ± 4.
.45 - .50	42. ± 4.
.50 - .60	31. ± 2.
.60 - .70	24. ± 2.
.70 - .80	15. ± 2.
.80 - 1.00	16. ± 1.
1.00 - 1.20	16. ± 2.
1.20 - 1.60	12. ± 1.
1.60 - 2.00	8.6 ± .8
2.00 - 2.40	5.7 ± .7
2.40 - 2.80	2.7 ± .5
2.80 - 3.25	1.5 ± .3

t' GeV²	Polarization
0.00 - .05	.06 ± .07
.05 - .10	-.13 ± .08
.10 - .15	-.17 ± .08
.15 - .20	-.52 ± .08
.20 - .25	-.63 ± .10
.25 - .30	-.58 ± .13
.30 - .35	-.53 ± .16
.35 - .40	-.73 ± .17
.40 - .45	-.70 ± .18
.45 - .50	-.88 ± .17
.50 - .60	-.80 ± .16
.60 - .70	-.90 ± .17
.70 - .80	-.96 ± .16
.80 - 1.00	-.99 ± .11
1.00 - 1.20	-.64 ± .19
1.20 - 1.60	-.22 ± .18
1.60 - 2.00	-.44 ± .20
2.00 - 2.40	-.26 ± .27
2.40 - 3.25	-.62 ± .33

u' GeV²	dσ/du μb/GeV²
0.00 - .10	17. ± 3.
.10 - .20	16. ± 2.
.20 - .40	11. ± 1.
.40 - .60	6.3 ± 1.1
.60 - .80	3.0 ± .7
.80 - 1.00	2.6 ± .7
1.00 - 1.20	3.5 ± .8
1.20 - 1.60	2.8 ± .5
1.60 - 2.00	4.1 ± .6
2.00 - 2.40	5.5 ± .7
2.40 - 2.80	3.9 ± .6
2.80 - 3.25	2.0 ± .4

u' GeV²	Polarization
0.00 - .20	-.12 ± .32
.20 - .60	-.38 ± .24
.60 - 1.60	.63 ± .28
1.60 - 2.40	.93 ± .20
2.40 - 3.25	.69 ± .29

$\pi^+\Sigma^-$

t' GeV²	dσ/dt μb/GeV²
0.00 - .20	1.0 ± .3
.20 - .60	.4 ± .1
.60 - 1.00	.5 ± .1
1.00 - 2.00	.2 ± .1
2.00 - 2.40	.2 ± .1
2.40 - 2.80	.4 ± .1
2.80 - 3.25	.6 ± .1

u' GeV²	dσ/du μb/GeV²
0.00 - .05	34. ± 3.
.05 - .10	32. ± 3.
.10 - .15	23. ± 3.
.15 - .20	12. ± 2.
.20 - .30	9.2 ± 1.2
.30 - .40	3.8 ± .8
.40 - .60	1.3 ± .3
.60 - .80	1.3 ± .3
.80 - 1.00	1.8 ± .4
1.00 - 1.20	2.1 ± .4
1.20 - 1.60	1.2 ± .2
1.60 - 2.00	.4 ± .1
2.00 - 2.40	.4 ± .1
2.40 - 2.80	.7 ± .2
2.80 - 3.25	.7 ± .2

Table A2 (Continued)

$K^+\Xi^-$

t' GeV²	dσ/dt' μb/GeV²
0.00 - .50	.5 ± .1
.50 - 1.00	.6 ± .1
1.00 - 1.50	.5 ± .2
1.50 - 2.00	.3 ± .1
2.00 - 2.50	.5 ± .1
2.50 - 3.00	.4 ± .1

t' GeV²	Polarization
0.00 - 3.00	.64 ± .37

u' GeV²	dσ/du' μb/GeV²
0.00 - .10	24. ± 2.
.10 - .20	19. ± 2.
.20 - .30	12. ± 1.
.30 - .40	10. ± 1.
.40 - .50	9.7 ± 1.2
.50 - .60	8.5 ± 1.0
.60 - .70	6.5 ± 1.0
.70 - .80	5.9 ± .9
.80 - .90	3.6 ± .7
.90 - 1.00	3.2 ± .7
1.00 - 1.20	3.2 ± .5
1.20 - 1.40	2.7 ± .5
1.40 - 1.60	2.1 ± .4
1.60 - 1.80	1.1 ± .3
1.80 - 2.00	2.0 ± .4
2.00 - 2.50	.8 ± .2
2.50 - 3.00	.8 ± .2

u' GeV²	Polarization
0.00 - .10	-.56 ± .30
.10 - .20	-.33 ± .33
.20 - .40	-.91 ± .27
.40 - .60	-.65 ± .34
.60 - 1.00	-.25 ± .34
1.00 - 1.50	-.54 ± .36
1.50 - 3.00	-.64 ± .34

$K^0\Xi^0$

u' GeV²	dσ/du' μb/GeV²
0.00 - .10	27. ± 5.
.10 - .20	6.5 ± 2.1
.20 - .30	7.5 ± 2.8
.30 - .40	7.5 ± 2.8
.40 - .60	1.6 ± .9
.60 - .80	1.8 ± .9
.80 - 1.00	2.1 ± 1.0

Table A3 Cross-sections and Polarizations of $0^-3/2^+$ reactions

$\pi^+\Sigma(1385)^-$

t' GeV²	dσ/dt μb/GeV²
0.00 - .05	13. ± 2.
.05 - .10	11. ± 2.
.10 - .20	8.0 ± 1.0
.20 - .35	3.0 ± .5
.35 - .50	1.5 ± .3
.50 - 3.00	.3 ± .2

u' GeV²	dσ/du μb/GeV²
0.00 - .10	10. ± 2.
.10 - .20	12. ± 2.
.20 - .30	11. ± 2.
.30 - .40	10. ± 2.
.40 - .55	8.0 ± 1.0
.55 - .80	3.4 ± .6
.80 - 1.10	2.7 ± .5
1.10 - 1.35	3.2 ± .6
1.35 - 1.65	2.7 ± .5
1.65 - 2.10	2.1 ± .4
2.10 - 3.00	.6 ± .1

u' GeV²	Polarization
0.00 - .25	-.01 ± .25
.25 - .50	.08 ± .14
.50 - 1.00	-.17 ± .33
1.00 - 2.00	-.48 ± .39

$\pi^-\Sigma(1385)^+$

t' GeV²	dσ/dt μb/GeV²	t' GeV²	Polarization	u' GeV²	Polarization
0.00 - .05	83. ± 7.	0.00 - .05	.33 ± .17	0.00 - .50	.22 ± .33
.05 - .10	120. ± 8.	.05 - .10	.16 ± .09	.50 - 1.00	.11 ± .24
.10 - .15	127. ± 9.	.10 - .15	.14 ± .10	1.00 - 1.50	-.17 ± .29
.15 - .20	140. ± 9.	.15 - .20	.06 ± .07	1.50 - 2.00	.23 ± .32
.20 - .25	130. ± 9.	.20 - .25	.02 ± .08	2.00 - 3.08	-.24 ± .13
.25 - .30	113. ± 8.	.25 - .30	.17 ± .07		
.30 - .35	102. ± 8.	.30 - .40	-.05 ± .06		
.35 - .40	104. ± 8.	.40 - .50	.07 ± .06		
.40 - .45	78. ± 7.	.50 - .70	.11 ± .07		
.45 - .50	62. ± 6.	.70 - .90	.01 ± .08		
.50 - .55	61. ± 6.	.90 - 1.30	-.22 ± .12		
.55 - .60	46. ± 5.	1.30 - 2.00	.08 ± .26		
.60 - .65	43. ± 5.				
.65 - .70	37. ± 5.				
.70 - .75	37. ± 5.				
.75 - .80	34. ± 4.				
.80 - .85	21. ± 3.				
.85 - .90	16. ± 3.				
.90 - .95	14. ± 3.				
.95 - 1.00	17. ± 3.				
1.00 - 1.10	10. ± 2.				
1.10 - 1.20	10. ± 2.				
1.20 - 1.40	4.5 ± .8				
1.40 - 1.65	3.1 ± .6				
1.65 - 2.00	1.8 ± .4				
2.00 - 2.40	1.6 ± .3				
2.40 - 3.00	1.4 ± .2				

u' GeV²	dσ/du μb/GeV²
0.00 - .15	2.3 ± .4
.15 - .40	1.2 ± .2
.40 - .55	2.2 ± .4
.55 - .70	2.7 ± .5
.70 - .85	2.4 ± .5
.85 - 1.00	3.4 ± .7
1.00 - 1.15	3.3 ± .7
1.15 - 1.35	2.8 ± .5
1.35 - 1.60	2.5 ± .4
1.60 - 1.90	1.7 ± .3
1.90 - 2.10	2.4 ± .5
2.10 - 2.30	2.6 ± .5
2.30 - 2.55	1.8 ± .3
2.55 - 2.75	1.7 ± .3
2.75 - 3.00	1.4 ± .3

$K^+\Xi(1530)^-$

u' GeV²	dσ/du' μb/GeV²
0.00 - .10	4.2 ± 1.3
.10 - .20	3.7 ± 1.2
.20 - .40	1.3 ± .5
.40 - .60	2.2 ± .7
.60 - .80	1.0 ± .4
.80 - 1.00	.4 ± .3
1.00 - 2.00	.1 ± .1

Table A4 Cross-sections and Polarizations of $1^-1/2^+$ reactions

$\omega\Lambda$

t'	dσ/dt'	t'	Polari-	1.30 - 1.40	12. ± 2.
GeV²	μb/GeV²	GeV²	zation	1.40 - 1.60	7.0 ± .9
0.00 - .05	70. ± 6.	0.00 - .05	.35 ± .20	1.60 - 1.80	6.0 ± .9
.05 - .10	83. ± 6.	.05 - .10	.22 ± .19	1.80 - 2.00	4.6 ± .8
.10 - .15	93. ± 6.	.10 - .15	.03 ± .17	2.00 - 2.20	5.6 ± .8
.15 - .20	92. ± 6.	.15 - .20	.36 ± .14	2.20 - 2.40	3.9 ± .7
.20 - .25	75. ± 6.	.20 - .30	.40 ± .14	2.40 - 2.60	4.2 ± .7
.25 - .30	76. ± 6.	.30 - .40	.38 ± .16	2.60 - 2.80	3.6 ± .6
.30 - .35	69. ± 5.	.40 - .50	.34 ± .17	2.80 - 3.00	3.7 ± .7
.35 - .40	56. ± 5.	.50 - .60	.55 ± .17	u'	Polari-
.40 - .45	47. ± 4.	.60 - .80	.54 ± .15	GeV²	zation
.45 - .50	37. ± 4.	.80 - 1.00	.40 ± .18	0.00 - .20	-.21 ± .21
.50 - .55	45. ± 4.	1.00 - 1.20	.77 ± .13	.20 - .40	-.41 ± .21
.55 - .60	38. ± 4.	1.20 - 1.60	.90 ± .14	.40 - .60	-.15 ± .20
.60 - .65	33. ± 4.	1.60 - 2.20	.20 ± .21	.60 - .80	-.41 ± .18
.65 - .70	30. ± 4.	2.20 - 3.00	-.19 ± .20	.80 - 1.20	-.61 ± .11
.70 - .80	23. ± 2.	u'	dσ/du'	1.20 - 1.60	-.53 ± .18
.80 - .90	16. ± 2.	GeV²	μb/GeV²	1.60 - 2.20	-.21 ± .21
.90 - 1.00	19. ± 2.	0.00 - .10	27. ± 3.	2.20 - 3.00	.52 ± .20
1.00 - 1.10	15. ± 2.	.10 - .20	17. ± 2.		
1.10 - 1.20	11. ± 2.	.20 - .30	17. ± 2.		
1.20 - 1.40	10. ± 1.	.30 - .40	17. ± 2.		
1.40 - 1.60	7.5 ± .9	.40 - .50	22. ± 2.		
1.60 - 1.80	4.5 ± .7	.50 - .60	23. ± 2.		
1.80 - 2.00	6.3 ± .8	.60 - .70	20. ± 2.		
2.00 - 2.20	3.9 ± .7	.70 - .80	19. ± 2.		
2.20 - 2.40	2.8 ± .6	.80 - .90	12. ± 2.		
2.40 - 2.60	3.8 ± .7	.90 - 1.00	17. ± 2.		
2.60 - 2.80	4.6 ± .7	1.00 - 1.10	13. ± 2.		
2.80 - 3.00	4.6 ± .7	1.10 - 1.20	11. ± 2.		
		1.20 - 1.30	9.4 ± 1.4		

Table A4 (Continued)

$\rho^0\Lambda$

t'	$d\sigma/dt$	2.30 - 3.00	.22 ± .28
GeV^2	μb/GeV^2	u'	$d\sigma/du$
0.00 - .05	83. ± 15.	GeV^2	μb/GeV^2
.05 - .10	88. ± 9.	0.00 - .20	16. ± 4.
.10 - .15	83. ± 10.	.20 - .50	5.5 ± 2.0
.15 - .20	69. ± 8.	.50 - .80	15.0 ± 2.0
.20 - .30	63. ± 6.	.80 - 1.20	12.0 ± 2.0
.30 - .40	65. ± 5.	1.20 - 1.60	9.5 ± 2.0
.40 - .50	40. ± 4.	1.60 - 2.30	5.5 ± .8
.50 - .60	40. ± 4.	2.30 - 3.00	4.1 ± .7
.60 - .80	22. ± 2.	u'	Polari-
.80 - 1.00	12. ± 2.	GeV^2	zation
1.00 - 1.20	10. ± 1.	0.00 - .20	.36 ± .22
1.20 - 1.60	7.8 ± 1.1	.20 - .50	.13 ± .48
1.60 - 2.30	7.7 ± .8	.50 - .80	-.62 ± .18
2.30 - 3.00	4.1 ± .7	.80 - 1.20	-.29 ± .30
t'	Polari-	1.20 - 1.60	-.47 ± .23
GeV^2	zation	1.60 - 2.30	-.20 ± .17
0.00 - .05	.41 ± .18	2.30 - 3.00	.28 ± .31
.05 - .10	.53 ± .21		
.10 - .15	.59 ± .22		
.15 - .20	.63 ± .18		
.20 - .30	.32 ± .18		
.30 - .40	.55 ± .24		
.40 - .50	.79 ± .15		
.50 - .60	.60 ± .19		
.60 - .80	.29 ± .19		
.80 - 1.00	.67 ± .23		
1.00 - 1.20	.57 ± .21		
1.20 - 1.60	.21 ± .24		
1.60 - 2.30	.55 ± .17		

$\phi\Lambda$

t'	$d\sigma/dt$	.20 - .30	-.08 ± .10
GeV^2	μb/GeV^2	.30 - .40	-.34 ± .14
0.00 - .05	95. ± 8.	.40 - .50	-.45 ± .14
.05 - .10	114. ± 8.	.50 - .60	-.41 ± .15
.10 - .15	109. ± 8.	.60 - .80	-.45 ± .14
.15 - .20	118. ± 9.	.80 - 1.00	-.22 ± .17
.20 - .25	81. ± 7.	1.00 - 1.60	-.20 ± .17
.25 - .30	83. ± 7.	1.60 - 2.75	-.05 ± .36
.30 - .35	75. ± 7.	u'	$d\sigma/du$
.35 - .40	63. ± 6.	GeV^2	μb/GeV^2
.40 - .45	54. ± 6.	0.00 - 1.00	$<$ .4
.45 - .50	53. ± 6.	1.00 - 2.75	.2 ± .1
.50 - .55	49. ± 5.		
.55 - .60	40. ± 5.		
.60 - .65	39. ± 5.		
.65 - .70	37. ± 5.		
.70 - .80	31. ± 3.		
.80 - .90	22. ± 3.		
.90 - 1.00	22. ± 3.		
1.00 - 1.10	20. ± 2.		
1.10 - 1.20	13. ± 2.		
1.20 - 1.40	7.5 ± 1.0		
1.40 - 1.60	5.7 ± .9		
1.60 - 1.80	2.9 ± .7		
1.80 - 2.75	.8 ± .2		
t'	Polari-		
GeV^2	zation		
0.00 - .05	.25 ± .13		
.05 - .10	.13 ± .15		
.10 - .15	-.17 ± .15		
.15 - .20	-.03 ± .14		

Table A4 (Continued)

$\rho^0\Sigma^0$				$\phi\Sigma^0$	
t' GeV²	dσ/dt' μb/GeV²	u' GeV²	Polarization	t' GeV²	dσ/dt' μb/GeV²
0.00 - .15	26. ± 4.	0.00 - .20	-.84 ± .18	0.00 - .10	29. ± 3.
.15 - .30	23. ± 3.	.20 - .50	.81 ± .31	.10 - .20	34. ± 4.
.30 - .50	19. ± 2.	.50 - .80	.88 ± .32	.20 - .30	42. ± 4.
.50 - .80	9.5 ± 1.0	.80 - 1.20	.29 ± .48	.30 - .40	31. ± 4.
.80 - 1.20	5.4 ± .9	1.20 - 1.60	-.34 ± .48	.40 - .50	29. ± 4.
1.20 - 1.60	2.8 ± 1.0	1.60 - 2.30	.10 ± .41	.50 - .60	25. ± 3.
1.60 - 2.30	1.6 ± .4	2.30 - 3.00	.02 ± .48	.60 - .70	27. ± 3.
2.30 - 3.00	1.2 ± .3			.70 - .80	19. ± 3.
t'	Polari-			.80 - 1.00	15. ± 2.
GeV²	zation			1.00 - 1.20	11. ± 2.
0.00 - .15	.37 ± .37			1.20 - 1.40	7.5 ± 1.2
.15 - .30	-.66 ± .34			1.40 - 1.60	6.0 ± 1.1
.30 - .50	-.02 ± .33			1.60 - 1.80	5.6 ± 1.1
.50 - .80	-.07 ± .41			1.80 - 2.70	.9 ± .2
.80 - 1.20	.08 ± .37			t'	Polari-
1.20 - 1.60	-.44 ± .61			GeV²	zation
1.60 - 2.30	-.62 ± .24			0.00 - .15	.62 ± .22
2.30 - 3.00	-.55 ± .62			.15 - .30	.71 ± .15
u'	dσ/du'			.30 - .50	.64 ± .36
GeV²	μb/GeV²			.50 - .80	.91 ± .08
0.00 - .20	13. ± 2.			.80 - 1.20	.40 ± .47
.20 - .50	4.7 ± 1.6			1.20 - 1.60	.77 ± .25
.50 - .80	4.2 ± .8			1.60 - 2.70	.69 ± .64
.80 - 1.20	4.1 ± .7			u'	dσ/du'
1.20 - 1.60	2.5 ± .6			GeV²	μb/GeV²
1.60 - 2.30	1.9 ± .6			0.00 - 1.00	< .4
2.30 - 3.00	2.4 ± .5			1.00 - 2.70	.1 ± .1

Table A5 Cross-sections and Polarizations of $1^-3/2^+$ reactions

$\rho^-\Sigma(1385)^+$

t' GeV^2	$d\sigma/dt'$ μb/GeV^2	u' GeV^2	$d\sigma/du'$ μb/GeV^2
0.00 - .05	238. ± 32.	0.00 - .20	15. ± 5.
.05 - .10	146. ± 26.	.20 - .60	3.4 ± 3.6
.10 - .15	138. ± 24.	.60 - 1.00	6.4 ± 3.2
.15 - .20	106. ± 22.	1.00 - 1.40	2.0 ± 3.4
.20 - .30	46. ± 14.	1.40 - 1.60	3.3 ± 2.8
.30 - .40	46. ± 13.	1.60 - 2.20	4.6 ± 2.4
.40 - .50	67. ± 12.	2.20 - 2.60	.60 ± 2.00
.50 - .60	64. ± 11.		
.60 - .80	23. ± 6.		
.80 - 1.00	28. ± 6.		
1.00 - 1.20	26. ± 5.		
1.20 - 1.60	5.0 ± 2.8		
1.60 - 2.00	3.3 ± 2.6		
2.00 - 2.60	4.2 ± 1.8		

t' GeV^2	Polarization
0.00 - .05	.26 ± .12
.05 - .10	-.03 ± .13
.10 - .15	-.10 ± .13
.15 - .20	-.13 ± .18
.20 - .30	.30 ± .14
.30 - .40	-.08 ± .17
.40 - .50	.41 ± .12
.50 - .60	.35 ± .18
.60 - .80	.08 ± .13
.80 - 1.00	-.09 ± .16
1.00 - 1.20	.31 ± .18

$\Phi\Sigma(1385)^0$

t' GeV^2	$d\sigma/dt'$ μb/GeV^2
0.00 - .10	38. ± 8.
.10 - .20	36. ± 8.
.20 - .40	20. ± 4.
.40 - .60	20. ± 4.
.60 - .80	12. ± 3.
.80 - 1.20	7.8 ± 1.7
1.20 - 2.00	1.6 ± .5

t' GeV^2	Polarization
0.00 - .40	.24 ± .07
.40 - 1.20	-.22 ± .16

u' GeV^2	$d\sigma/du'$ μb/GeV^2
0.00 - 2.20	$<$ .5

Table A6 Cross-sections and Polarizations of $2^+1/2^+$ reactions

$A_2^0 \Lambda$	
t' GeV²	dσ/dt' μb/GeV²
0.00 - .10	44. ± 9.
.10 - .20	43. ± 9.
.20 - .40	32. ± 6.
.40 - .60	22. ± 5.
.60 - .90	12. ± 4.
t' GeV²	Polarization
0.00 - .10	.45 ± .25
.10 - .20	.47 ± .25
.20 - .40	.62 ± .20
.40 - .60	.40 ± .20
.60 - .90	.08 ± .20

$f\Lambda$	
t' GeV²	dσ/dt' μb/GeV²
0.00 - .20	58. ± 22.
.20 - .40	61. ± 17.
.4 - 1.0	30. ± 11.
1.0 - 2.4	7.9 ± 2.7
t' GeV²	Polarization
0.00 - .20	.68 ± .28
.20 - .40	.43 ± .25
.4 - 1.0	.30 ± .27
1.0 - 2.4	-.26 ± .30
u' GeV²	dσ/du' μb/GeV²
0.00 - .30	40. ± 8.
.30 - .50	21. ± 7.
.50 - .80	30. ± 7.
.8 - 1.2	25. ± 6.
1.2 - 2.4	6.6 ± 2.6
u' GeV²	Polarization
0.00 - .30	-.20 ± .19
.30 - .50	-.30 ± .40
.50 - .80	-.02 ± .22
.8 - 1.2	-.60 ± .20
1.2 - 2.4	.05 ± .35

$f'\Lambda$	
t' GeV²	dσ/dt' μb/GeV²
0.00 - .20	24. ± 4.
.20 - .40	19. ± 4.
.40 - .80	10. ± 2.
.8 - 1.5	1.2 ± .6
t' GeV²	Polarization
0.00 - .30	.05 ± .42
.3 - 1.0	.20 ± .48
u' GeV²	dσ/du' μb/GeV²
0.0 - 2.2	.05 ± .15

$f\Sigma^0$	
t' GeV²	dσ/dt' μb/GeV²
0.00 - .20	26. ± 12.
.20 - .50	27. ± 8.
.5 - 1.0	12. ± 4.
1.0 - 2.2	1.1 ± 2.0
t' GeV²	Polarization
0.0 - 2.2	.10 ± .32
u' GeV²	dσ/du' μb/GeV²
0.00 - .20	10. ± 5.
.2 - 2.2	4.0 ± 2.0
u' GeV²	Polarization
0.0 - 2.2	-.38 ± .58

Table A7 Cross-sections and Polarizations of $0^-3/2^-$ reactions

$\pi^0\Lambda(1520)$			
t' GeV²	$d\sigma/dt'$ μb/GeV²	u' GeV²	$d\sigma/du'$ μb/GeV²
0.00 - .10	55. ± 11.	0.00 - .10	51. ± 6.
.10 - .20	67. ± 11.	.10 - .20	43. ± 6.
.20 - .40	50. ± 5.	.20 - .40	16. ± 4.
.40 - .60	33. ± 4.	.40 - .60	15. ± 3.
.60 - .80	25. ± 4.	.60 - .80	7.4 ± 2.1
.8 - 1.0	12. ± 3.	.8 - 1.0	13.0 ± 2.0
1.0 - 1.2	14. ± 3.	1.0 - 1.2	13.0 ± 3.0
1.2 - 1.6	10. ± 2.	1.2 - 1.6	13.0 ± 2.0
1.6 - 2.0	7.5 ± 1.5	1.6 - 2.0	7.4 ± 1.4
2.0 - 2.6	3.6 ± .9	2.0 - 2.6	2.4 ± 1.2
2.6 - 3.2	4.2 ± .9		

$\eta\Lambda(1520)$		$\eta'\Lambda(1520)$	
t' GeV²	$d\sigma/dt'$ μb/GeV²	t' GeV²	$d\sigma/dt'$ μb/GeV²
0.00 - .50	12. ± 5.	0.00 - .50	22. ± 5.
.5 - 1.0	2.7 ± 2.7	.5 - 1.0	1.6 ± 1.2
1.0 - 2.7	1.2 ± 1.2	1.0 - 2.2	1.1 ± .8
u' GeV²	$d\sigma/du'$ μb/GeV²	u' GeV²	$d\sigma/du'$ μb/GeV²
0.0 - 1.0	2.0 ± 1.5	0.00 - .50	2.7 ± 1.2
1.0 - 2.7	2.0 ± 1.4	.5 - 1.0	1.6 ± 1.2
		1.0 - 2.2	1.3 ± .9

Table A8 Cross-sections and Polarizations of $1^-3/2^-$ reactions

$\omega\Lambda(1520)$			
t' GeV²	$d\sigma/dt'$ μb/GeV²	u' GeV²	$d\sigma/du'$ μb/GeV²
0.00 - .10	46. ± 9.	0.00 - .10	28. ± 6.
.10 - .20	29. ± 7.	.10 - .20	24. ± 6.
.20 - .40	25. ± 4.	.20 - .40	21. ± 4.
.40 - .60	14. ± 3.	.40 - .60	22. ± 4.
.60 - .90	12. ± 3.	.60 - .90	15. ± 3.
.9 - 1.2	7.7 ± 2.0	.9 - 1.2	12. ± 3.
1.2 - 1.8	6.4 ± 1.3	1.2 - 1.8	6.9 ± 1.3
1.8 - 2.4	3.9 ± .9	1.8 - 2.4	4.8 ± 1.0

$\Phi\Lambda(1520)$			
t' GeV²	$d\sigma/dt'$ μb/GeV²	u' GeV²	$d\sigma/du'$ μb/GeV²
0.00 - .10	59. ± 12.	0.0 - 2.6	< .50
.10 - .20	60. ± 12.		
.20 - .30	38. ± 9.		
.30 - .40	22. ± 6.		
.40 - .50	34. ± 9.		
.50 - .60	25. ± 7.		
.60 - .70	20. ± 6.		
.70 - .80	19. ± 6.		
.8 - 1.0	12. ± 3.		
1.0 - 1.2	11. ± 3.		
1.2 - 1.4	2.3 ± 1.1		

Table A9 The elastic scattering and the charge exchange reaction

$K^-p \rightarrow K^-p$

t' GeV²	dσ/dt' μb/GeV²
.10 - .12	14530. ± 490.
.12 - .14	12520. ± 430.
.14 - .16	10860. ± 530.
.16 - .18	9260. ± 470.
.18 - .20	7790. ± 410.
.20 - .22	6930. ± 340.
.22 - .24	6000. ± 310.
.24 - .26	5450. ± 290.
.26 - .28	4390. ± 250.
.28 - .30	3600. ± 210.
.30 - .35	2970. ± 130.
.35 - .40	2030. ± 100.
.40 - .45	1430. ± 77.
.45 - .50	873. ± 60.
.50 - .55	703. ± 54.
.55 - .60	468. ± 44.
.60 - .65	277. ± 34.
.65 - .70	240. ± 32.
.70 - .75	207. ± 29.
.75 - .80	157. ± 26.
.80 - .85	91. ± 19.
.85 - .90	66. ± 17.
.90 - .95	124. ± 23.
.95 - 1.00	83. ± 19.
1.00 - 1.10	112. ± 15.
1.10 - 1.20	101. ± 15.
1.20 - 1.30	73. ± 12.
1.30 - 1.40	65. ± 13.
1.40 - 1.50	41. ± 9.
1.50 - 1.75	36. ± 6.
1.75 - 2.00	23. ± 4.
2.00 - 2.25	15. ± 4.
2.25 - 2.50	9.1 ± 2.7
2.50 - 2.75	10.6 ± 3.0
2.75 - 3.00	5.0 ± 2.0
3.00 - 3.50	2.5 ± 1.4

u' GeV²	dσ/du' μb/GeV²
0.00 - 1.80	< .27
1.80 - 2.80	.20 ± .20
2.80 - 3.30	1.20 ± .70

$K^-p \rightarrow \overline{K}^0n$

t' GeV²	dσ/dt' μb/GeV²
0.00 - .02	488. ± 35.
.02 - .04	575. ± 42.
.04 - .06	664. ± 41.
.06 - .08	619. ± 40.
.08 - .10	619. ± 38.
.10 - .12	578. ± 37.
.12 - .14	567. ± 38.
.14 - .16	511. ± 37.
.16 - .18	483. ± 35.
.18 - .20	475. ± 35.
.20 - .22	444. ± 33.
.22 - .24	412. ± 31.
.24 - .26	402. ± 34.
.26 - .28	379. ± 30.
.28 - .30	320. ± 28.
.30 - .35	321. ± 16.
.35 - .40	242. ± 14.
.40 - .45	187. ± 13.
.45 - .50	164. ± 12.
.50 - .55	137. ± 11.
.55 - .60	114. ± 9.
.60 - .65	80. ± 9.
.65 - .70	78. ± 8.
.70 - .75	72. ± 8.
.75 - .80	59. ± 8.
.80 - .85	62. ± 7.
.85 - .90	51. ± 8.
.90 - .95	53. ± 7.
.95 - 1.00	41. ± 6.
1.00 - 1.10	31. ± 4.
1.10 - 1.20	35. ± 4.
1.20 - 1.30	32. ± 4.
1.30 - 1.40	31. ± 4.
1.40 - 1.50	28. ± 4.
1.50 - 1.75	23. ± 2.
1.75 - 2.00	15. ± 2.
2.00 - 2.25	10. ± 1.
2.25 - 2.50	7.2 ± 1.0
2.50 - 2.75	4.0 ± 1.0
2.75 - 3.00	2.4 ± .6
3.00 - 3.50	2.2 ± .4

u' GeV²	dσ/du' μb/GeV²
0.00 - .80	< .15
.80 - 1.80	.09 ± .06
1.80 - 2.80	.19 ± .12
2.80 - 3.30	.24 ± .10

Table A10 Summary of the cross sections
(see footnotes to table 3.2B on page 31).

J^P Group	Reaction	σ_T	σ_F	σ_B
	$\pi^o\Lambda$	74.5 ± 4.2	66.0 ± 4.1	8.5 ± 0.7
	$\eta\Lambda$	24.8 ± 1.3	22.9 ± 1.2	1.9 ± 0.4
	$\eta'\Lambda$	50.5 ± 2.9	47.6 ± 2.8	2.9 ± 0.8
$0^-1/2^+$	$\pi^-\Sigma^+$	154 ± 8	137 ± 7	16.0 ± 1.0
	$\pi^+\Sigma^-$	10.4 ± 0.7	1.3 ± 0.2	9.0 ± 0.6
	$K^+\Xi^-$	14.5 ± 1.0	1.4 ± 0.2	13.2 ± 1.0
	$K^o\Xi^o$	-	-	6.1 ± 0.8
				(u' < 1.0)
	$\pi^-\Sigma(1385)^+$	81 ± 4	75 ± 4	6.6 ± 0.6
$0^-3/2^+$	$\pi^+\Sigma(1385)^-$	12.0 ± 1.6	3.0 ± 0.7	9.0 ± 1.1
	$K^+\Xi(1530)^-$	-	-	1.9 ± 0.4
				(u' < 2.0)
	$\rho^o\Lambda$	82 ± 8	57 ± 5	25 ± 3
	$\omega\Lambda$	91 ± 8	60 ± 5	31 ± 3
$1^-1/2^+$	$\phi\Lambda$	66 ± 4	66 ± 4	0.4 ± 0.2
	$\rho^o\Sigma$	30 ± 3	19 ± 2	11 ± 1
	$\phi\Sigma$	34 ± 3	33 ± 3	0.3 ± 0.2
$1^-3/2^+$	$\rho^-\Sigma(1385)^+$	88 ± 6	74 ± 6	14 ± 3
	$\phi\Sigma(1385)^o$	22 ± 4	21 ± 4	0.6 ± 0.3
	$A_2^o\Lambda$	-	22 ± 3	-
			(t' < 1.0)	
	$f\Lambda$	89 ±10	47 ± 7	41 ± 7
$2^+1/2^+$	$f'\Lambda$	13 ± 2	13 ± 2	0.1 ± 0.3
	$f\Sigma^o$	33 ± 7	23 ± 6	10 ± 5
	$f'\Sigma^o$	5.0 ± 1.1	-	-

Table A10 (continued)

J^P	Reaction	σ_T	σ_F	σ_B
	$\pi^o\Lambda(1520)$	82 ± 8	50 ± 6	32 ± 5
$0^-3/2^-$	$\eta\ \Lambda(1520)$	15 ± 5	9.4 ± 3.5	5.4 ± 2.8
	$\eta'\Lambda(1520)$	17 ± 3	13 ± 3	3.7 ± 1.4
	$\omega\Lambda(1520)$	57 ± 6	27 ± 4	29 ± 4
$1^-3/2^-$	$\phi\Lambda(1520)$	31 ± 9	31 ± 9	0.5 ± 0.4
	K^-p	4500 ± 240	4500 ± 240	0.85 ± 0.23
$0^-1/2^+$	$\bar{K}^on$	266 ± 11	266 ± 11	0.40 ± 0.15

SUMMARY

In this thesis results are presented of a study of two-body reactions in a K^-p bubble chamber experiment at 4.2 GeV/c incoming momentum. The outstanding feature of the experiment is the high level of statistical significance (130 events/μb), acquired through the analysis of 3.1 million bubble chamber pictures. The experiment was carried out by a collaboration of physicists from the Universiteit van Amsterdam, from CERN in Geneva, from the Universiteit van Nijmegen, and from Oxford University respectively. The subject of this thesis covers only part of the experimental data obtained with this experiment.

The thesis summarizes the results of the detailed analyses of two-body hypercharge exchange reactions, performed in the 4.2 experiment. Most of these results have been published in separate papers, and the thesis tries to present an overall view of the data.

In chapter 1 the type of reactions studied are introduced and the special suitability of this experiment for these studies is discussed. Also a short historical review of the experiment is given and the plan of the thesis is outlined.

In chapter 2 the experimental details relevant to the analysis of two-body reactions are discussed. The procedures used to separate the samples of events belonging to the reactions of interest are described. The background problems and systematic losses are discussed and illustrated with some examples.

In chapter 3 the results of the measurements are presented in the form of total and differential cross sections and polarization distributions. For each reaction the presentation is accompanied by some remarks on specific features observed in the distributions. The measurements of other observables are discussed separately, together with the model independent amplitude analyses of these reactions.

In chapter 4 predictions from two complementary phenomenological models for forward (small momentum-transfer) scattering in these reactions are tested. Large deviations are observed from the predictions which follow from simplifying assumptions in a Regge-exchange model. This emphasizes that the composition of the t-channel amplitudes in term of Regge-exchanges has to be complicated, and many parameters are needed for a satisfactory description of the data. The predictions coming from the additive quark model, on the other hand, turn out to be remarkably successful for such a simplistic approach. Serious disagreement with the data has only been observed for the reactions involving the η and η' mesons. The amplitude relations following from the application of the quark spectator idea to the baryon vertex, are in good agreement with experiment if one allows breaking of SU(6) symmetry for the baryon wave functions.

SAMENVATTING.

In dit proefschrift worden resultaten gepresenteerd van de bestudering van twee-deeltjes reacties in een K^-p bellenvat experiment bij 4.2 GeV/c inkomende impuls. Het bijzondere van dit experiment is de hoge statistische gevoeligheid van 130 gebeurtenissen per microbarn, verkregen door de analyse van 3.1 miljoen bellenvatfoto's. Het experiment werd uitgevoerd door een collaboratie van fysici verbonden met de Universiteit van Amsterdam, met CERN in Genève, met de Universiteit van Nijmegen en met Oxford University. Dit proefschrift behandelt slechts een gedeelte van de resultaten van dit experiment.

Met het proefschrift wordt getracht een samenvattend beeld te geven van de analyse van twee-deeltjes reacties met hyperladingsruil die in dit experiment zijn uitgevoerd en waarvan de meeste resultaten in aparte publicaties zijn verschenen.

In hoofdstuk 1 worden de hier beschreven reacties geïntroduceerd en de speciale geschiktheid van het experiment voor de bestudering daarvan besproken. Verder wordt een kort historisch overzicht van het experiment gegeven en de indeling van het proefschrift geschetst.

In hoofdstuk 2 wordt aandacht geschonken aan de experimentele details die van belang zijn voor de analyse van twee-deeltjes reacties. Aan de hand van enkele voorbeelden worden de problemen behandeld die in verband staan met het afzonderen van de gebeurtenissen die tot een bepaalde reactie behoren.

In hoofdstuk 3 worden per reactie de resultaten gepresenteerd van de metingen van de totale en de differentiële werkzame doorsnede en van de hyperon polarizatie. Eventuele andere meetbare grootheden in deze reacties worden in dit hoofdstuk apart behandeld, evenals de model-onafhankelijke amplitude-analyses die daarmee mogelijk zijn.

In hoofdstuk 4 worden voorspellingen getest afkomstig van twee complementaire fenomenologische modellen voor voorwaartse (kleine impuls-overdracht) verstrooiing in tweedeeltjes reacties. Het toepassen van vereenvoudigende veronderstellingen in een Regge-uitwisselings model leidt tot voorspellingen die zeer veel afwijken van het experiment. Dit benadrukt, dat voor een bevredigende beschrijving van de resultaten, de formulering van de t-kanaal amplitudes in termen van Regge uitwisselingen gecompliceerd moet zijn en vele vrije parameters bevat. Daarentegen blijken de voorspellingen die uit het simplistische verstrooiingsbeeld van het additieve quark model voortkomen, verrassend goed met de resultaten overeen te stemmen. Slechts bij de reacties met η en η' mesonen worden belangrijke afwijkingen aangetroffen. De amplitude relaties die volgen uit de toepassing van het quark spectator principe aan het baryon vertex zijn in goede overeenstemming met het experiment, als van SU(6) symmetrie voor de baryon golffuncties wordt afgeweken.

ACKNOWLEDGEMENTS

I am grateful for having had the opportunity to participate in this extraordinary bubble chamber experiment. It has been a special experience to work with a data sample which grew almost by itself to unequalled proportions. This seemingly effortless growth was the result of the work of many people. I want to thank the constructors of the beam, the operating crews of the CERN PS and 2 m HBC, and the scanning, measuring, and computing staffs at each of the participating laboratories for their contribution to this result.

I should certainly express my gratitude for the pleasant and instructive collaboration that I have experienced with my colleagues from all four laboratories. Among my fellow members and former members of the K^- group at the Zeeman-laboratorium, I especially want to thank S. Barlag, R. Blokzijl, A.J. de Groot, W. Hoogland, B. Jongejans and G.F. Wolters, for their share of this collaboration. As our group leader, J.C. Kluyver has always been a promotor of doing good physics in a pleasant atmosphere. I have had the good fortune to profit also from his qualities as promotor of Ph.D. students, for which I am much indebted.

I want to thank my fellow collaboration members at the other laboratories for their hospitality during my visits. I particularly want to mention the co-operation that I enjoyed with R.J. Hemingway, S.O. Holmgren and M.J. Losty, who has also been responsible for many improvements in this thesis.

I want to thank H.R. Schans and H.W.A. Schuijlenburg for their assistance in preparing the drawings for this thesis, and M. Vermeulen for her excellent typing-work.

Finally I want to thank A.N. Diddens for his interest and co-operation during the completion of this thesis.